**Aalborg Universitet**

AALBORG UNIVERSITY
DENMARK

# The Wave Dragon

*evaluation of a wave energy converter*

Nielsen, Anders; Kofoed, Jens Peter

*Publication date:*
1997

*Document Version*
Publisher's PDF, also known as Version of record

Link to publication from Aalborg University

*Citation for published version (APA):*
Nielsen, A., & Kofoed, J. P. (1997). *The Wave Dragon: evaluation of a wave energy converter*. Hydraulics & Coastal Engineering Laboratory, Department of Civil Engineering, Aalborg University.

**General rights**
Copyright and moral rights for the publications made accessible in the public portal are retained by the authors and/or other copyright owners and it is a condition of accessing publications that users recognise and abide by the legal requirements associated with these rights.

- Users may download and print one copy of any publication from the public portal for the purpose of private study or research.
- You may not further distribute the material or use it for any profit-making activity or commercial gain
- You may freely distribute the URL identifying the publication in the public portal -

**Take down policy**
If you believe that this document breaches copyright please contact us at vbn@aub.aau.dk providing details, and we will remove access to the work immediately and investigate your claim.

Downloaded from vbn.aau.dk on: April 24, 2024

# The Wave Dragon

## - evaluation of a wave energy converter

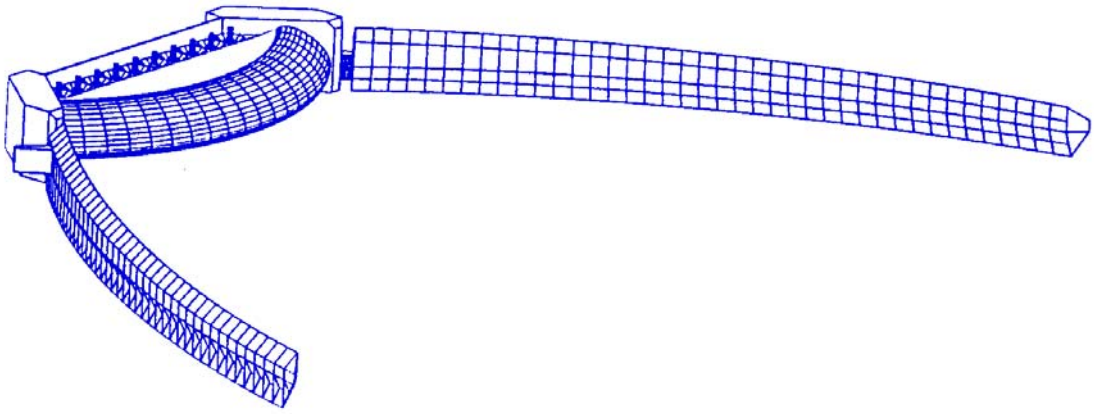

by

Anders Nielsen
Jens Peter Kofoed

M. Sc. graduate report
in Civil Engineering

1997

AALBORG UNIVERSITY
Department of Civil Engineering
Sohngaardsholmsvej 57
DK-9000 Aalborg

# Preface

The present report, "The Wave Dragon – evaluation of a wave energy converter" constitutes the work towards attaining the Master degree in structural engineering. The work has been accomplished from April to August 1997 at the Department of Civil Engineering, Aalborg University, Denmark.

The target group of the report is the designer of the Wave Dragon, Erik Friis-Madsen and other interested wave energy pioneers. Though, some knowledge of fundamental engineering is required of the reader.

The supervisors P. Frigaard and M. Brorsen are acknowledged for their advice and guidance. Furthermore a special thanks is expressed to the technicians N. Drustrup and J. S. Sørensen of the Coastal Engineering Laboratory at Aalborg University for their competent efforts in making the laboratory models of the Wave Dragon. Finally Erik Friis-Madsen and Hans Christian Sørensen are thanked for their constructive collaboration.

Enclosed in the report is an appendix. It contains supplementary derivations, comments and/or elaborations on the main text.

Throughout the report the comma is used as decimal symbol while the full stop is used as a digit grouping symbol. This is according to the Danish standard.

A list of symbols, designations and abbreviations is found after the table of contents. Occasionally the symbols are also explained in the text.

References are given by name(s) of author or publisher and year of publishing. In the end of the main report a complete reference list is found.

Although the technical contents of this report is considered reliable it should be noted that legal and financial responsibilities of any kind are disclaimed. Using results or conclusions from the report are at own risk.

Aalborg, August 27th 1997

Jens Peter Kofoed

Anders Nielsen

# Table Of Contents

## Main report

# Appendix

# List of symbols, designations and abbreviations

## Symbols

$A$ area [$m^2$].

$a$ overtopping coefficient, Van der Meer's formula [ - ].

$b$ overtopping coefficient, Van der Meer's formula [ - ].

$c$ velocity of wave propagation, phase velocity [m/s].

$c_d$ design overtopping coefficient [m].

$c_g$ wave group velocity [m/s].

$c_s$ shifted power constant [m].

$D$ displacement [$m^3$].

$d$ distance from MWL [m].

$E$ total energy density [$J/m^2$].

$E_f$ mean energy flux [J/m/s].

$E_{f,d}$ mean energy flux above the level $d$ [J/m/s].

$E_{kin}$ kinetic energy [J].

$E_{pot}$ potential energy [J].

$E_{tot}$ energy per unit time [J/s]

$f_P$ peak frequency [Hz].

$g$ acceleration of gravity 9,82 $m/s^2$ [$m/s^2$]

$h$ water depth [m].

$H$ wave height [m].

$H_{m0}$ 4 times the square root of the variance of the surface elevation [m].

$h_r$ height of the wave reflectors over MWL [m].

$H_S$ significant wave height [m]. Estimated as $H_{m0}$. Exact for Rayleigh distributed wave heights.

$h_{toe}$ water depth at the toe of the ramp [m].

$I$ moment of inertia of the cross section area in the waterplane [$m^4$].

$I_m$ mass moment of inertia [kg $m^2$].

$k$ wave number, $2\pi/L$ [$m^{-1}$].

$K_{r,E}$ reflection coefficient with respect to energy [ - ].

$K_{r,H}$ reflection coefficient with respect to wave height [ - ].

$L$ Lagrangian function [J].

$L$ wavelength [m].

$M$ mass [kg].

$m_1$ metacenter distance [m].

$P$ sponge layer power factor [ - ].

$p^+$ excess pressure [N].

$Q$ dimensionless flow (overtopping) [ - ]

$q$ flow (overtopping) [$m^3/s/m$]

$r$ rim height, distance from MWL in the basin to the crest freeboard [m].

$R^2$ coefficient of determination from the method of least squares [ - ].

$R_c$ crest freeboard [m].

$R_{c,opt}$ optimal crest freeboard [m].

$R_H$ wave height ratio [ - ]. Defined as the ratio between the significant wave height at the opening and at the exit line of the wave reflectors.

$R_w$ opening ratio [ - ]. See sketch below.

$S$ spectral density [$m^2 \cdot s$]

$S_{op}$ wave steepness parameter [ - ].

$t$ time [s].

$T_0$ natural period [s].

$T_P$ wave peak period [s].

$u$ horizontal particle velocity (in direction of wave propagation) [m/s].

$v$ horizontal particle velocity [m/s].

$\underline{v}$ particle velocities ($u$, $v$, $w$) [m/s].

$w$ vertical particle velocity [m/s].

$w$ width [m].

$x$ horizontal coordinate (in direction of wave propagation).

$y$ horizontal coordinate (perpendicular to the wave propagation).

$z$ vertical coordinate (positive direction is up).

$\alpha$ slope angle of the ramp [ ° ].

$\beta$ angle of wave attack [ ° ]. Perpendicular attack $\beta = 0°$.

$\gamma$ reduction factor [ - ].

$\gamma_P$ peak enhancement factor [ - ].

$\zeta$ sponge layer factor.

$\eta$ wave elevation [m].

$\theta$ angle of propagation with generation line.

$\xi_{op}$ wave breaker parameter [ - ].

$\rho_w$ density of water, $10^3$ kg/$m^3$.

$\Phi$ velocity potential.

$\omega$ cyclic frequency, $2\pi/T$ [$s^{-1}$].

$\underline{\nabla}$ gradient operator ($\partial/\partial x$, $\partial/\partial y$, $\partial/\partial z$).

# Designations

| | |
|---|---|
| composite system | system consisting of both wave reflectors, ramp and basin. |
| net efficiency | efficiency after conversion to electricity. |
| overall efficiency | efficiency distributed over long time. |
| time average mean energy flux | the mean energy flux over all wave conditions (long time). |

The sketch below shows the wave reflectors marking some of the designations used in the text.

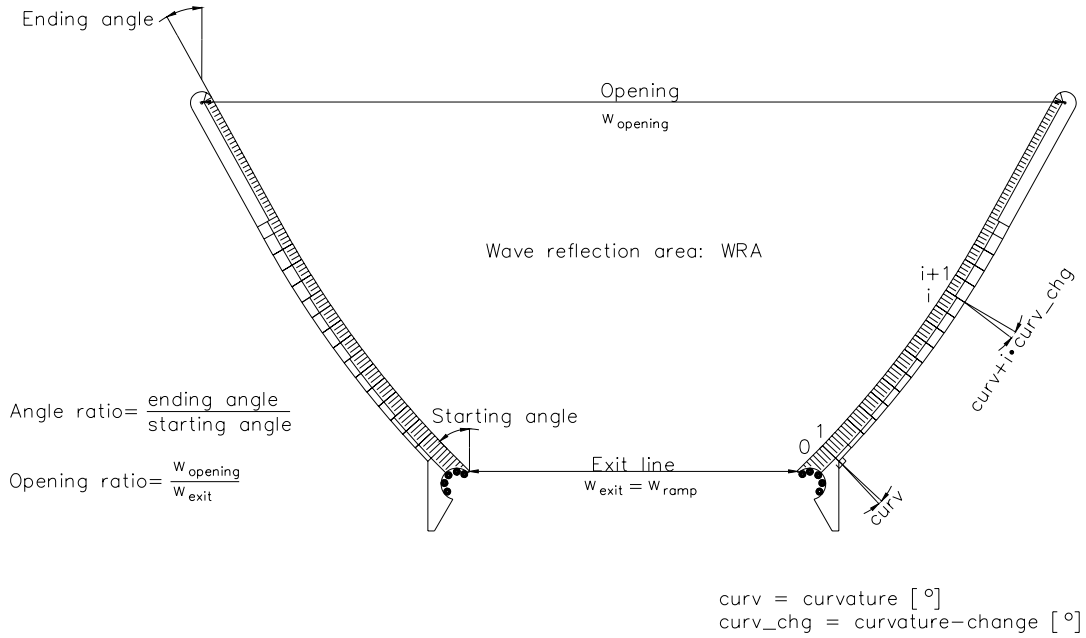


# Abbreviations

AAU Aalborg University.

BC Boundary condition

BVP Boundary value problem

DHI Danish Hydraulic Institute.

DMI Danish Maritime Institute.

DTU Danish Technical University.

EFM Erik Friis-Madsen, Löwenmark, designer of the Wave Dragon.

EMU Energy & Environmental Consultancy.

EU The European Union.

MWL Mean water level.

OSPREY Ocean Swell Powered Renewable energy.

WEC Wave energy converter.

# 1. Introduction

Principles for the utilization of wave energy have been investigated for more than two hundred years, but today the research is still at a relatively immature stage. During the oil crisis in the 1970's the interest in wave energy was heavily increased thereafter, however, the engagement in the area has not been significant. Today wave energy is gradually brought into focus, among other things through the European Union (EU) under the JOULE-THERMIE research and development program for supporting non-nuclear energy projects. However it was not until 1992 that the JOULE-THERMIE program even included wave energy as an area of consideration.

## 1.1 A review of wave energy devices

Wave energy devices can roughly be categorized into 3 main groups, namely:

- Point absorbers
- Backbone absorbers
- Overtopping converters

A review of each of these is presented in the following.

### *1.1.1 Point absorbers*

Although there are many different kinds of point absorbers, the basic principle is mainly the same. The wave energy is converted into energy in an oscillating system, which interacts with the waves. This system can be a water column in a tube or a floating buoy. From this the energy must be converted into useful mechanical energy by means of hydraulic or pneumatic turbines or pumps. Hereby the energy can be converted to electricity by using a generator. A large variety of this type of system has been developed, both for placement near shore and in open sea.

The principle of point absorbers using a floating buoy is most useful for systems with a low energy requirement, e.g. navigation buoys and pumps, as the plants normally have a maximum effect of 50 – 150 kW (1 kW pr. $m^3$ volume of the buoy) //Ingeniøren, 1997//. Since 1965 more than 1.000 wave energy driven navigation buoys have been produced from a point absorber principle developed by the Japanese Yoshio Masuda //NYTEK//. **Figure 1.1** shows 4 different kinds of point absorbers using a floating buoy.

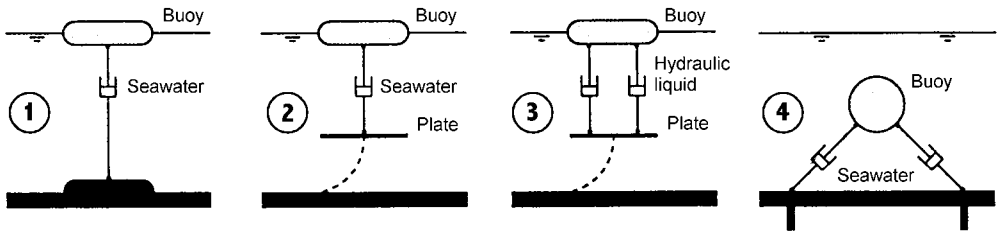


***Figure 1.1:*** *Different point absorbers using a floating buoy. Plant number 1 and 2 are similar, both working from the vertical movement of the buoy caused by the waves, but while number 1 is acting directly against the seabed, number 2 is acting against a moving but counteracting structure. Number 3 is similar to number 2, but has two pumps and thereby also makes use of the pitch (defined as rotation around an axis parallel to the wave fronts) on the buoy. Number 4 is fully submerged and can make use of both vertical and horizontal movement //NYTEK//.*

In Denmark the company Danish Wave Power Aps has developed a point absorber consisting of a buoy connected to a piston secured at the sea bottom. The principle of the absorber corresponds to device number 1 in **Figure 1.1**. The system has been tested twice 2,5 km off the coast of Hanstholm at a water depth of 25 m //Waveλength, 1995//. The first system did not survive the first storm. The development of

the absorber is, until now, the only wave energy system in Denmark financially supported by the government //Ingeniøren, 1997//.

If the point absorber instead uses an oscillating water column, the effect can become much higher. A Scottish engineering company has successfully applied for EU subsidy in making a gravity anchored, near shore, wave power plant called OSPREY (Ocean Swell Powered Renewable Energy). An OSPREY test plant wrecked during installation at 18 m water depth //EMU, 1997//. The expected electrical production rating is 2 MW //Wavelength, 1995//. **Figure 1.2** shows 3 kinds of point absorber using an oscillating water column. The principle used in the Scottish absorber corresponds to plant number 6.

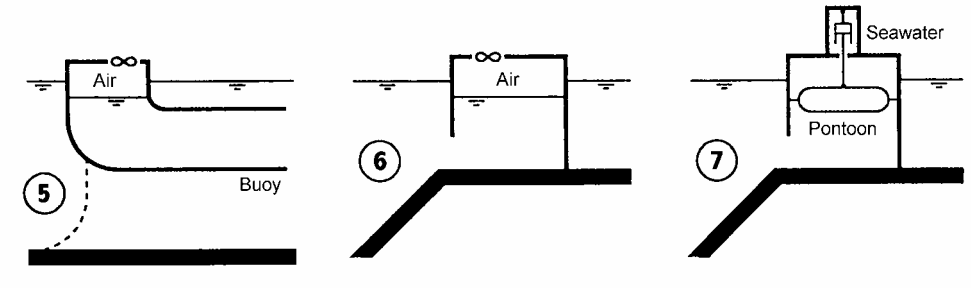


***Figure 1.2:*** *Different point absorbers using an oscillating water column. In plant number 5 and 6 the air is driven through a turbine (∞), while number 7 moves a pontoon connected to a pump. Plant 6 and 7 are secured on a firm platform and thus make use of vertical oscillation, while plant 5 is a free moving buoy, which makes it possible to use both vertical and rotational oscillation. All plants make use of difference in pressure, due to waves, for moving the water column //NYTEK//.*

### 1.1.2 Backbone absorbers

Backbone absorbers differ from point absorbers as they consist of a large row of similar point absorbers connected to a "backbone". Exposing the system to short crested waves will cause a number of single point absorbers to act using the rest of the backbone as counteraction. Thus this action is used to absorb energy with a turbine or pump. Usually the length of the backbone must be more than a typical wavelength, in order to give sufficient reaction force. **Figure 1.3** shows 2 kinds of backbone absorbers.

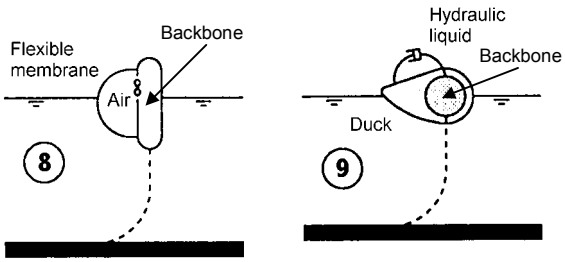


***Figure 1.3:*** *Different backbone absorbers. Plant number 8 uses the horizontal force from the waves for driving air through a turbine (∞), while plant number 9 makes use of the vertical force to pitch a "duck" //NYTEK//.*

### 1.1.3 Overtopping converters

Overtopping converters are relatively new inventions, but the fundamental principle is similar to power utilization in dams. Research was begun in 1985 //Löwenmark, 1997//. They are, unlike point absorbers and backbone absorbers, not based on an oscillating system. Instead the potential and kinetic energy of the waves is converted to potential energy in a basin, which wave energy pioneers expect done with a relatively high efficiency.

The principle consists of a turbine connected to a water basin above mean water level (MWL). By the use of a ramp incoming waves are led from the sea to the basin. Thus the turbines are driven as the elevated

water is led back into the sea. Hereby the problem of an unsteady electricity production, as a consequence of an unsteady oscillation, is reduced because the basin functions as energy storage.

The plants can be placed on shore using the natural surroundings as part of the basin. **Figure 1.4** shows the principle of overtopping converters.

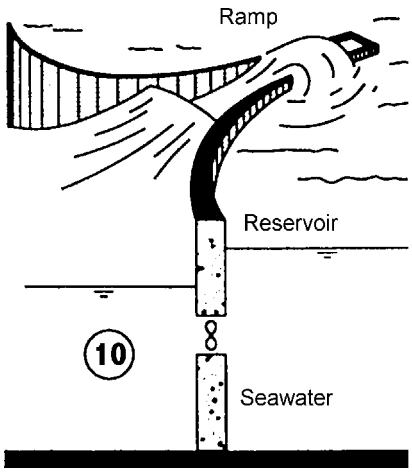


***Figure 1.4:*** *Overtopping converter near the shore. As water fills the reservoir by overtopping the difference in water level between the sea and the reservoir drives a turbine (∞) //NYTEK//.*

Today most of the overtopping power plants are still in the experimental stage. Only the TAPCHAN plant installed on the Norwegian West Coast is fully functional. It has an effect of 350 kW, but using the same principle, the company behind TAPCHAN is building a 1,1 MW plant in Indonesia //Ingeniøren, 1997//.

Furthermore during recent years a Swedish company called Sea Power AB has developed a floating offshore wave energy converter (WEC) also based on the overtopping principle. Sea Power AB built a test plant in 1991 and has on this background estimated an output in the range of 70 – 170 kW and a net efficiency of 20 % //Sea Power, 1992//.

Using the overtopping principle Erik Friis-Madsen (EFM) from the Danish engineering company Löwenmark has designed another floating WEC for use at open sea. The design is still in the development phase, but the offshore placement gives a number of advantages compared to a plant on firm foundation. This floating plant is called Wave Dragon.

### *1.1.4 The overtopping converter, The Wave Dragon*

The experiences from the TAPCHAN-project showed promising results, but for obvious reasons there are problems, which are taken into consideration in the development of the Wave Dragon as well as the WEC developed by Sea Power. They are the major arguments for making a floating offshore construction based on the overtopping principle. The advantages compared to the onshore fixed construction TAPCHAN are:

- No loss of energy due to wave breaking as a consequence of reduced water depth since the WEC is placed offshore.
- The energy production is independent of the tidal variations since the WEC is floating.
- The WEC is constructed with a possibility of controlling the draught and hereby adjusting the level so it fits the occurring wave situation.

The Wave Dragon is, contrary to the Sea Power WEC, equipped with floating “pontoons” (wave reflectors) that focus the waves towards the basin. Furthermore the Wave Dragon is anchored in one single point. Neglecting the influence of currents this will cause the Wave Dragon to sway towards the propagating waves.

## 1.2 Specifications of the Wave Dragon

The Wave Dragon has been developed over the past 10 years by EFM in association with Danish Hydraulic Institute (DHI), Danish Maritime Institute (DMI), Rasmussen & Schiøtz East A/S and others. The developer has applied for patent on the basic principles of the Wave Dragon in both Denmark and most of the European countries with suitable coastal regions. The scope of this report is the development of the Wave Dragon.

The design and specifications of the Wave Dragon given by the developer are described in the following.

### *1.2.1 Construction parts*

The Wave Dragon is primarily constructed of reinforced concrete. The lifetime expectancy of the construction is at least 50 years, without major maintenance costs //Löwenmark, 1997//.

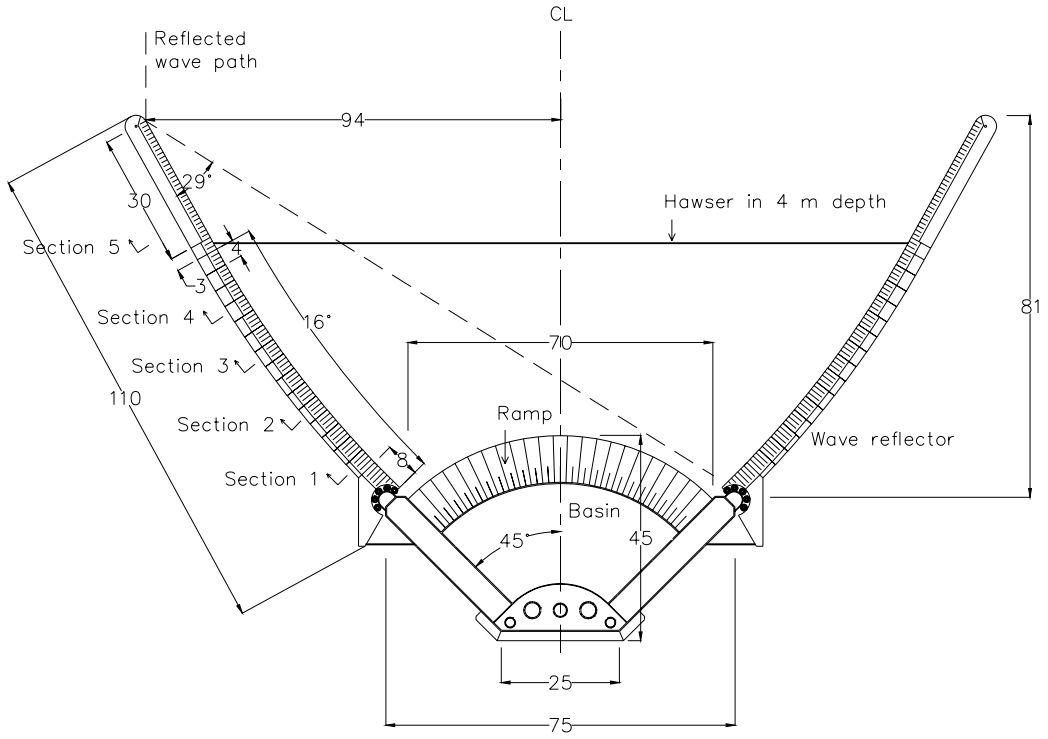


***Figure 1.5:*** *Plan view of the Wave Dragon as proposed by EFM. All measures are in m. The cross sections 1 – 5 are shown in* ***Figure 1.6****. An elevation of a wave reflector is shown in* ***Figure 1.7****.*

As shown in **Figure 1.5** the platform is equipped with 2 floating wave reflectors. Although they have a limited draught, they will focus much of the incoming energy toward the basin, i.e. increase the wave height at the ramp and thus the amount of water caught in the basin. The wave reflectors are stiff and self-stabilizing. During heavy storm conditions the reflectors can be closed together for protection of the reflectors themselves and the platform.

EFM has proposed that 15 equal straight elements constitute the main part of each of the wave reflectors. In addition a longer element with less draught is attached at the end. Transition elements are connecting the basin and the main part as well as the main and the ending part of the wave reflectors.

Curvature of the wave reflectors is obtained by having a constant angle between the elements. Thus in the following the curvature is described by this angle. Furthermore the change in the angle between the elements, starting with the element closest to the ramp, is called the curvature-change. Thus the angle between the $n^{th}$ and the $(n + 1)^{th}$ element is: curvature + $n \cdot$ curvature-change. For the design proposed by EFM the curvature is constantly 1,0°.

The cross sections marked in **Figure 1.5** are shown in **Figure 1.6**. The lower parts of the reflectors are made of reinforced concrete, while the upper parts are made of a steel shell filled with gas concrete. Besides the height and draught of the reflectors, the build up has not been subject to any investigations in this report.

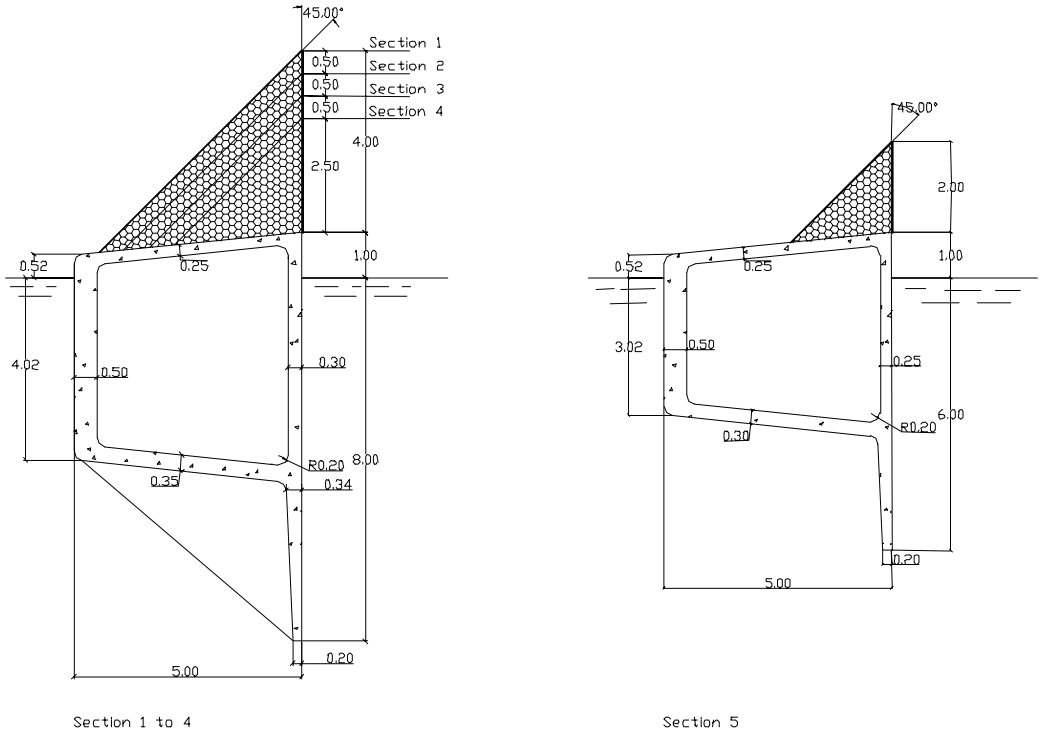


***Figure 1.6:*** *Cross sections 1 to 5 of the wave reflectors shown in* ***Figure 1.5****. All measures are in m.*

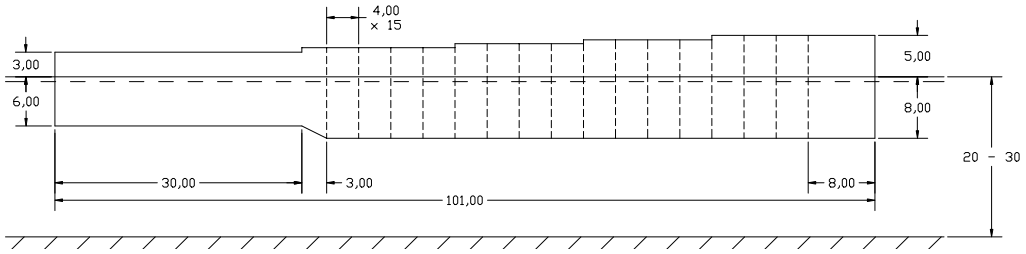


***Figure 1.7:*** *Elevation of the wave reflector shown in* ***Figure 1.5****. All measures are in m.*

The connection between reflectors and the basin is shown in **Figure 1.8**. The connection is designed to allow vertical movements for adjusting the draught of the basin. Rotational movements are partly hindered by the fenders.

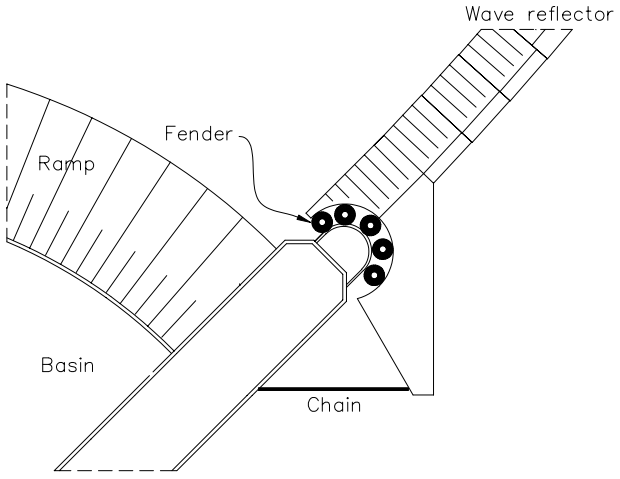


***Figure 1.8:*** *The connection between reflector and basin (cf.* ***Figure 1.5****).*

The functionality of the connection has not been subject of investigation in this report.

The ramp and basin are made of reinforced concrete. A cross section of the basin part is shown in **Figure 1.9**. It is able to hold 1.000 $m^3$ water //EFM, 1997//.

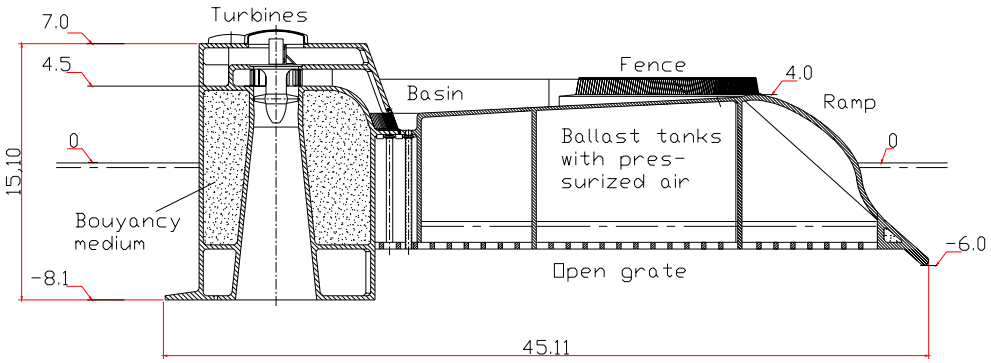


***Figure 1.9**: Cross section of the basin part of the Wave Dragon. All measures are in m.*

The bottom of the platform is an open grate allowing water to enter the body. The draught is thus adjusted by a pressurized air system. The Wave Dragon is designed to float even though the ballast tanks are filled with water.

The Wave Dragon will presumably be gravity anchored, however, other systems such as pile foundation or suction anchors are under consideration. A number of hawsers are fastened to the wave reflectors and the basin and joined at a buoy, which is connected to an anchoring system at the sea bottom.

The weights of the different parts of the Wave Dragon are presented in **Table 1.1**.

| | Basin | Water in basin | Wave reflectors | Total |
|---|---|---|---|---|
| Approximate weight | 6.000 tons | 1.000 tons | 2.000 tons each | 11.000 tons |

***Table 1.1:** Weight of the different parts of the Wave Dragon //EFM, 1997//.*

### *1.2.2 Construction costs*

Altogether it is expected that the total construction costs are 60 million dkr. Furthermore in the development phase the expected costs are approximately 3 million dkr. //Löwenmark, 1997//

### *1.2.3 Functionality of the Wave Dragon*

**Figure 1.10** shows an overview sketch of the Wave Dragon with mounted windmills and a cross section sketch of the platform. The way the waves go through the system is drawn on the cross section sketch. The incoming waves run up the ramp, and are caught in a reservoir slightly elevated over MWL. This insures a relatively steady flow to the turbines and thus a steady energy production. The hereby obtained potential energy is converted into electricity by a number of turbines through which the water is lead back into the sea.

The highest amount of stored potential energy is obtained if the water level of the basin always is close to the rim of the ramp. As the basin is of relatively limited size it can only be supplied with a certain amount of water at the time. Thus the basin can smooth out the energy admission but the amount of overtopping should still be relatively steady.

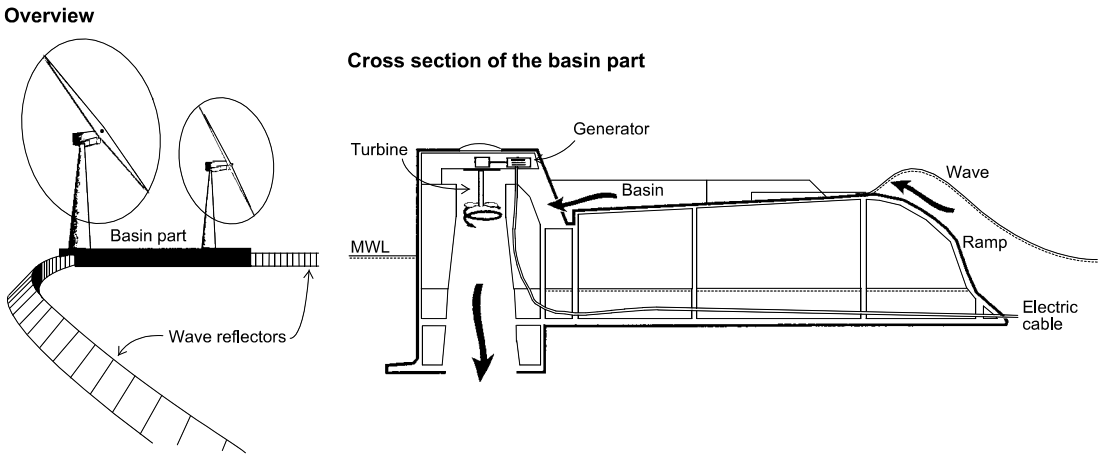


***Figure 1.10:*** *Overview and cross section sketches of the Wave Dragon. The way the waves go through the Wave Dragon is shown on the cross section sketch.*

The platform is furthermore equipped with two windmills. It might prove to be advantageous to share the effect of the windmills out on separate electricity generators and pumps for lifting water into the reservoir. Hereby the electricity peak effect from the combined system is reduced. In return the time of use is increased because the combined electricity production is more constant //Ingeniøren, 1997//.

### *1.2.4 Location of the Wave Dragon*

The principle of the Wave Dragon is not designed for a specific location. However, the size must be adjusted according to the wave climate. The dimensions shown in **Figure 1.5** are designed for placement in the North Sea at a position characterized by //Löwenmark, 1995//:

- Close to shore (less than 20 km).
- Water depth of 20 – 30 m.
- Average mean energy flux of 15 kW/m.

These values correspond to the wave parameters of for instance a wave peak period of about 7 s and a significant wave height of about 2 m.

### *1.2.5 Overall expected efficiencies*

In the basin of the Wave Dragon 5 turbo hydro-turbines are placed. They can either be of the Kaplan type for a high hydraulic head or the Ossberger crossflow type for a low head (down to 0,75 m) //Löwenmark, 1995//. Their mean efficiency is estimated to be between 80 – 85 % //Löwenmark, 1997//.

Specifically for placement in the North Sea the expected efficiency is approximately 25 % //Löwenmark, 1997//. With an average mean energy flux of 15 kW/m this is equivalent to an average output of 700 kW. It is expected that an optimal placement will give an average output of 3 MW //Löwenmark, 1997//.

The electricity price is dependent of the number of Wave Dragons that are build, and varies from 0,87 dkr/kWh for one prototype and 0,45 dkr/kWh for 33 units of Wave Dragons //Ingeniøren, 1997//.

## 1.3 Scheduled phases in the development of the Wave Dragon

EFM has divided the development of the Wave Dragon project into 5 phases, covering aspects from composition of the main idea to testing of a full-scale demonstration model. These 5 phases are considered necessary before construction of a fleet of 25 to 150 Wave Dragon units. The schedule is updated July 1st 1997.

### Phase 1

Phase 1 was completed during 1987 to 1996. EFM conducted the activities, financially supported by Erhvervsfremme Styrelsen (the Danish Agency of Trade and Industry) for preliminary studies on international cooperation. In 1995 and 1996 students from Engineering College Copenhagen made graduate reports where they, among other things, verified parts of the financial aspects. The phase consisted of:

- Formulation of the idea/concept of the Wave Dragon.
- Financial considerations.
- Application for patent and financial support.

### Phase 2

This phase is presently being accomplished. New participants are DMI, DHI, EMU and AAU. The activities are in progress until the year 1998. DHI and DMI contemplate the construction of a 1:40 scale model made at DMI with tests to be carried out at DHI. Hereby it is expected to acquire knowledge of the behavior of the Wave Dragon under influence of waves, forces on the anchor and a magnitude of the efficiency. The present project at AAU is worked out during the same time (cf. below). After conducting the model tests EFM and EMU will adjust the design for use in the next phase. The second phase consists of:

- Elaboration of the Wave Dragon by calculations.
- Production of scale model and testing in wave tank.
- Adjustment of model with reference to phase 3.

### Phase 3

New participants in phase 3 are expected to be University College Cork (Ireland), Danish Technical University (DTU), ELSAM-P, Ossberger-Turbinenfabrik GmbH + Co (Germany) and Technomare (Italy). The activities are to be conducted in the period from 1998 to 2000. University College Cork will conduct model tests to establish design parameters of important parts. From these results DTU and AAU will be capable of making a more precise computer simulation of the dynamic behavior. Ossberger-Turbinenfabrik GmbH + Co is the supplier of the turbines, and from the information of the model test they will optimize the power unit techniques. Technomare will analyze the anchoring. Hereafter EFM will design a model in scale 1:4 and will make a financial evaluation with the assistance of suppliers, contractor and shipyard. The phase consists of:

- Optimization based on model tests and computer simulations.
- Dimensioning of a model in scale 1:4 and financial evaluation.

### Phase 4

Phase 4 is expected in the year 2001 to 2002. Possible new participants are not yet determined. Production of the model in scale 1:4. Model tests in coastal area with frequent wave heights of 5 m and thereby an expected electricity production of 30 kW. From these tests the design is optimized, a manufacturing technique is determined and a final financial evaluation will be carried our. Moreover, it is possible to test the model with 2 wing flexible windmills (30 kW) currently under development at Risø National Laboratory (Denmark). The phase consists of:

- Production of scale model (30 kW) and testing in coastal area with limited wave activity.
- Final design, manufacturing technique and economical evaluation.
- Test of windmills (30 kW).

**Phase 5**

It is expected that the final phase be conducted in the year 2003. Production of a full-scale demonstration model with an electricity production of 3 MW. Testing in the North Sea for gathering operation information in preparation for production of a fleet consisting of 25 – 150 Wave Dragon units.

- Production of full size construction (3 MW) and testing in the North Sea.
- Gathering of experiences with reference to production of a power plant consisting of 25 – 150 Wave Dragon units.

### *1.3.2 Technical areas of interest in current phase (phase 2)*

Presently the development of the Wave Dragon is in phase 2. During phase 1 only the basic ideas have been formulated. The pilot experiment in phase 4 is thus a very important step in verifying the overall concept. Before the test can be performed, however, it is necessary to consider some technical aspects formulated by the following questions:

1. Estimation of the magnitude of forces acting on the structure, especially during a storm – how can these forces be transferred through the structure and anchoring system to the sea bottom?
2. Does the geometry of the Wave Dragon (wave reflectors, ramp and basin) ensure an optimal exploitation of the wave energy?
3. How does the Wave Dragon exploit the energy in waves propagating with some randomness in the direction?
4. What is the magnitude of a continuous produced effect and the overall efficiency?

These 4 points are the main purpose of phase 2. As previously mentioned DMI contemplate making a model of the Wave Dragon in scale 1:40. DHI will thereafter carry out model tests in their offshore wave tank. These tests will mainly elucidate the behavior of the Wave Dragon under influence of waves of different sizes, the magnitude of the forces on the anchor and the magnitude of the efficiency. That is, the points 1 and 4.

## 1.4 Intention and delimitation of this report

This report is concerned with phase 2 of the development (cf. section *1.3 Scheduled phases in the development*).

With reference to a scale model test in Nissum Bredning in the Limfjord in Northern Jutland, Denmark, the main intention is to acquire some knowledge primarily on point 2 and 4 (cf. section *1.3.2 Technical areas of interest in current phase (phase 2)*. The location is chosen because phase 3 also included a scale model test conducted in inner water, for example Nissum Bredning, when the work with this report was first commenced. Later EFM dismissed the idea.

That is, this report primarily concentrates on:

- Evaluation of EFM's design of the wave reflectors and ramp, with reference to a scale model test assumed to be placed at a specific location in Nissum Bredning.

The secondary objectives are:

- Optimization of the efficiency by adjusting the geometrical shape of wave reflectors and ramp.
- Generalization of the results so they are independent of location.
- Acquiring tools which are useful in the further development of Wave Dragon.

# 2. Conditions of analysis

Before optimizing the wave reflectors and the ramp, the specific location of the Wave Dragon in Nissum Bredning and the wave conditions must be determined. Furthermore, the design of the Wave Dragon proposed by EFM must be scaled to fit the chosen position.

## 2.1 Location of the Wave Dragon

In northern Jutland the largest Danish inlet, Limfjorden, is located. At the western entrance the broad Nissum Bredning is found. Two only 1 - 2 km wide tongues of land separate the broad from the North Sea. Between the tongues Thyborøn Channel is located.

Nissum Bredning has the shape of a triangle with its summit in the eastern end and base in the western end. It is approximately 20 km long and about 15 km wide at the western end. The depth of the broad varies from about 1,0 - 4,0 m in the western half to more than 6,5 m in the eastern half. Tidal variations are neglected as the difference between mean high and low tide only amount to about 0,5 m //Kort- og matrikelstyrelsen, 1993//. Currents are assumed to be insignificant.

It is assumed that the test of the Wave Dragon is performed in the deep eastern area. The exact location of the Wave Dragon within the deep area has been chosen more or less randomly, but it has been attempted to achieve a long fetch in the western and north western directions, since the western and north western winds are strong and frequent.

**Figure 2.1** shows a map of Denmark marking Nissum Bredning and a map of Nissum Bredning marking the chosen location of the test area and the lighthouses of Vestervig, Thyborøn and Bovbjerg.

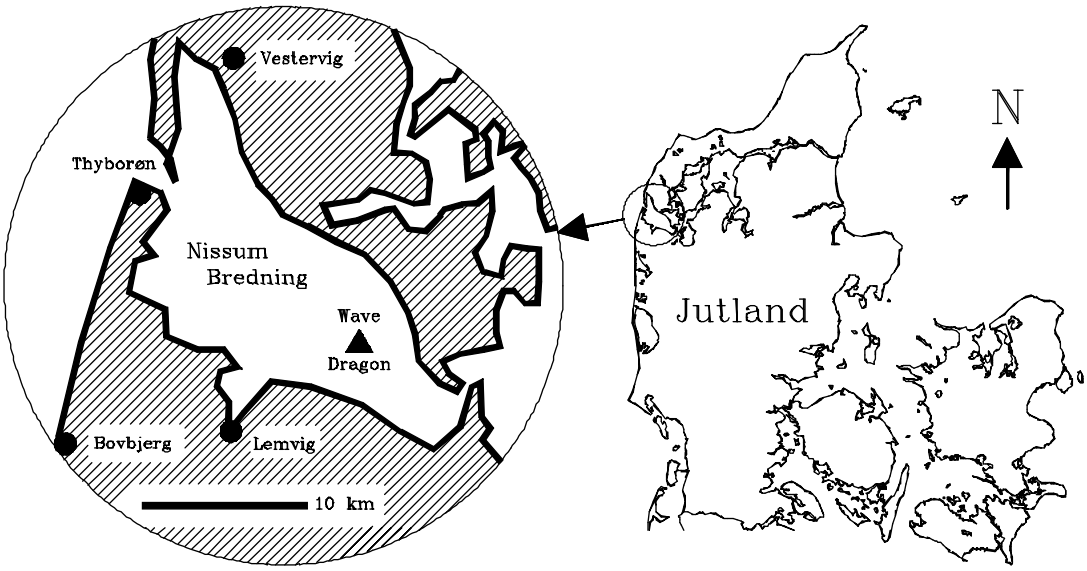


***Figure 2.1:*** *Map of Denmark marking Nissum Bredning and map of Nissum Bredning marking the chosen location of the Wave Dragon and the lighthouses of Vestervig, Thyborøn and Bovbjerg.*

At these three lighthouses of Vestervig, Thyborøn and Bovbjerg wind strength and direction have been recorded since 1872. Published recordings from 1931 to 1960 are used in the determination of the wave conditions.

## 2.2 Wave conditions

The wave conditions of Nissum Bredning are found through wind data recordings at the nearby lighthouses of Vestervig, Thyborøn and Bovbjerg. The analysis is described in appendix *A. Wave conditions*.

From the analysis it is decided only to consider 5 wave situations characterized by the wave peak period interval of [1,75 s ; 4,25 s].

Wave peak periods less than 1,75 s are ignored as they amount to about 0,5 % of the total energy. The situations disregarded in this way appear in about 30 % of the time.

Wave conditions with wave peak periods above 4,25 s only appear in about 0,2 % of the time. The situation is considered a storm condition and is therefore neglected although it contains about 5 % of the total energy. Using the Wave Dragon for energy production in this condition will entail significant extra construction expenses in order to ensure resistance against the wave forces.

Altogether the considered wave peak period interval corresponds to wave situations that occur in about 70 % of the time. In total the considered wave situations make up 94 % of the total energy.

Using the center of the wave peak period intervals the analysis is considered for periods from 2,0 to 4,0 s. This is equivalent to a significant wave height from approximately 0,2 to 1,5 m. Characteristics for the 5 wave situations are shown in **Table 2.1**.

| Wave situation | 1 | 2 | 3 | 4 | 5 |
|---|---|---|---|---|---|
| Wave peak period [s] | 2,0 | 2,5 | 3,0 | 3,5 | 4,0 |
| Significant wave height [m] | 0,20 | 0,40 | 0,80 | 1,20 | 1,50 |
| Wavelength ($h$ = 6,5 m) [m] | 6,2 | 9,7 | 14,0 | 18,6 | 23,5 |
| Mean energy flux [kJ/m/s] | 0,05 | 0,25 | 0,94 | 2,29 | 4,52 |
| Occurring probability [%] | 24 | 30 | 11 | 3 | 2 |

***Table 2.1:*** *Considered wave situations in the further analysis. The wavelengths correspond to the wave peak periods.*

The wave situations in Nissum Bredning are assumed to correspond to the JONSWAP-spectrum with a peak enhancement factor $\gamma_P = 6,5$.

## 2.3 Scaling of the Wave Dragon to fit the chosen position

The design of the Wave Dragon proposed by EFM is intended a placing in the North Sea. Since the location dealt with in this report is Nissum Bredning, which presents a different wave climate and water depth, it is necessary to scale the overall size of the Wave Dragon.

In the scaling of the Wave Dragon in the North Sea design to the Nissum Bredning design different references are possible. In **Table 2.2** three possibilities are shown with the resulting length scale. In the scaling Froudes law of scaling is used.

| Reference | North Sea | Nissum Bredning | Length scale |
|---|---|---|---|
| Mean wave energy flux [J/s/m] | $15 \cdot 10^3$ | 358 | ~ 4,5 |
| Mean wave height [m] | 2,0 | 0,34 | ~ 6 |
| Water depth [m] | 20 – 30 | 6,5 | ~ 3 – 4,5 |

***Table 2.2:*** *Length scales for scaling down the North Sea design of the Wave Dragon to the Nissum Bredning design, on the basis of different references. In the scaling Froudes law of scaling is used.*

In order to find an appropriate scale, an analysis of the movements in heave (vertical movement) and pitch (rotation around a horizontal axis) is performed. This is due to:

- Vertical movements in phase with the waves will increase the relative crest freeboard and thereby reduce overtopping.
- Pitch movements will also pitch the water level in the basin and thereby reduce the effective water depth in the basin. This increases the average rim height and thus reduces the potential energy.

The analysis is limited only to concern the basin part of the Wave Dragon. Thus it is assumed that the connection between the basin and the reflectors does not restrain the movements of the basin in heave and pitch. Moreover, the wave reflectors have not been subjects of a movement analysis.

The performed movement analysis is described in appendix *B. Analysis of wave-generated movements*. From this it is seen that the wave-generated movements of the basin part of the Wave Dragon, for a length scale of 3, are insignificant for the first 3 wave situations. For wave situations 4 and 5 the wave generated movements might be so large that they will cause a decrease in efficiency compared to a restrained basin. However, the movements are of a magnitude where it is reasonable to assume that further investigations and adjustments of the design will diminish the problem. Thus the movements are neglected and in the further work it is assumed that the construction is restrained.

Thus it is determined to use a design of the Wave Dragon based on the design proposed by EFM, scaled with a length scale of 3. In the following this design will be referred to as the Nissum Bredning design.

# 3. Overall analysis approach

To simplify the analysis procedure the Wave Dragon is split into parts. In this report the water flow is not considered from when it leaves the basin, goes through the turbines and back into the sea. On the way to the basin, the waves will encounter two main parts of the Wave Dragon, namely the wave reflectors and the ramp. These two main parts are first considered independently.

In analyzing the wave reflectors and the ramp different approaches are used. First the state of the art of the analysis methods for the two parts are presented. Then the chosen methods of approach are described.

## 3.1 Analyzing the wave reflectors

This section first gives an overview of the present level of tools and knowledge concerning determination of wave fields around a sea structure.

Finding a description for the wave field around the Wave Dragon is relatively complicated. The major problem is that the Wave Dragon is a floating structure. Even neglecting the movements still involves investigation of a semi-submerged structure. This means that the energy of the waves is partly transmitted under the structure. Moreover, the curved shape of the wave reflectors proves to be a complication.

### *3.1.1 State of the art in determination of a wave field around a sea structure*

Determination of the hydrodynamic conditions around a sea structure is very complicated even for a simple geometry of the structure. A complete mathematical description of the hydrodynamic problem is impossible, but also unnecessary for most engineering purposes.

Considering linear waves in an ideal fluid of irrotational flow the hydrodynamic problem of wave movement constitutes the boundary value problem (BVP) of solving the Laplace equation with specified boundary conditions (BC's). With simplified BC's many types of problems can be solved approximately by numerical means, e.g. using the mild slope equation.

Analytically the problem can be solved by considering the phenomena of refraction, diffraction, shoaling, reflection, transmission etc. When investigating wave fields around a sea structure the dominating phenomena are analyzed under simplified conditions while others are neglected. This lays down the guidelines for the wave field and a magnitude of the wave influence on the sea structure.

Most reliable results for complicated geometries are expected from experimental tests in a wave tank.

### *3.1.2 Description of the used approaches in analyzing the wave reflectors*

The wave reflectors will first be analyzed through simple analytical means. This approach is very primitive and a numerical model based on the Mild Slope equation is thus introduced. The latter constitutes the tool for adjusting the design of the wave reflectors. Finally, the chosen design is verified by laboratory tests. Thus the procedure is:

- Analytical consideration of the design proposed by EFM. The method is used on a simplified basis, and is therefore expected to result in a rough estimate.
- Mild slope numerical model, which is used to optimize the design of the wave reflectors in plan view.
- Experimental tests, which are used for verification of the analytical and numerical methods.

Throughout the analyses the wave height in the area near the ramp is compared with the incoming wave height. This wave height ratio will be taken as an expression of how well the wave reflectors concentrate the wave energy towards the ramp and basin.

## 3.2 Analyzing the ramp profile

This section first gives an overview of the present level of tools and knowledge concerning determination of wave overtopping.

It has not been possible to find any formula capable of calculating the overtopping of sea structures with a complicated design. The ramp of the Wave Dragon has two unusual characteristics:

- The ramp has a double curving profile. For non-breaking waves the slope angle has little influence on the overtopping discharge //Van der Meer et. al., 1994//, and it is assumed that this also applies for curvature. Though, vertical walls only have about 60 % of the overtopping discharge of sloping structures //Van der Meer et. al., 1994//.
- The draught is less than the water depth. As for the wave reflectors this must result in energy transmission under the ramp. As a wave meets a structure an overpressure is developed. A limited draught results in easier pressure equalization under the structure and thus reduces the overtopping.

Moreover for the Wave Dragon the potential energy of the overtopped water is used for electricity production and heavy overtopping is thus advantageous.

The general case of mildly sloping dikes with a draught equal to the water depth, a straight profile and little to moderate overtopping is relatively thoroughly described in the literature.

### *3.2.1 State of the art in determination of overtopping*

Overtopping is commonly dealt with in connection with the design of breakwaters, caissons, dikes etc. Usually the design criterion is an allowable degree of overtopping in order to prevent flooding and erosion. As a consequence of this the available research of overtopping is concentrated on small or moderate overtopping discharges.

Because of the complicated nature of overtopping the majority of the overtopping formulas are purely empirical. A variety of formulas have been established through dimensional analysis and verified by laboratory tests. An example is //Van der Meer et. al.,1994//:

$$\frac{q}{\sqrt{gH_s^3}} = a \exp\left(-b \frac{R_c}{H_s}\right) \qquad (3.1)$$

The advantage of this formulation is that the overtopping discharge is non-zero and finite for $R_c = 0$. This is especially convenient for heavy overtopping. Laboratory test series are used to fit the coefficients $a$ and $b$.

### *3.2.2 Description of the used approaches in analyzing the ramp profile*

The analysis of the ramp will be based on an empirical expression. As the geometry and degree of overtopping for the ramp is relatively different from the general cases which, can be found in the litterature laboratory tests are performed. Hereby a formula for predicting the overtopping is established and overtopping coefficients are determined. The procedure is:

- Laboratory tests are performed on a simple profile to determine the form and coefficients of an overtopping expression. Hereby the obtained potential energy can be found.
- Laboratory tests for investigating the influence of a profile with curvature and different slope angles (including the profile proposed by EFM). From this a design of the ramp is chosen for the following analyses.

The average amount of captured water in relation to the free crest of the ramp per time unit is taken as a measure of the functionality of the ramp.

## 3.3 Experimental verification of the composite system

After the two parts have been investigated separately it is investigated how the two separate parts function together through laboratory tests with a model of both reflectors and the basin part (the composite system).

The main purpose of the laboratory tests is to find an estimate of the efficiency during the wave situations. The average amount of captured water in relation to the crest freeboard of the ramp per time unit is taken as a measure of the functionality.

# 4. Analytical analysis of wave reflectors

In the analytical analysis of the influence of the wave reflectors on the significant wave height two considerations are made.

First superposition of elevations is considered. Then an energy consideration is made. Finally, an expected increase in average significant wave height at the exit line is found.

In the two considerations the presence and effects of the ramp are neglected. Furthermore diffraction is not considered.

## 4.1 Elevation consideration

Using linear wave theory the surface elevations of a number of waves can be superposed as the velocity potential and boundary conditions are linealized. This consideration of superposing the wave elevations is troublesome to perform analytically as the wave field is very complicated, cf. **Figure 4.1 right**. Furthermore the fact that the wave reflectors are subjected to irregular waves complicates it even more. Performing the approach on a simplified geometry results in a too inaccurate estimate on the focused wave height.

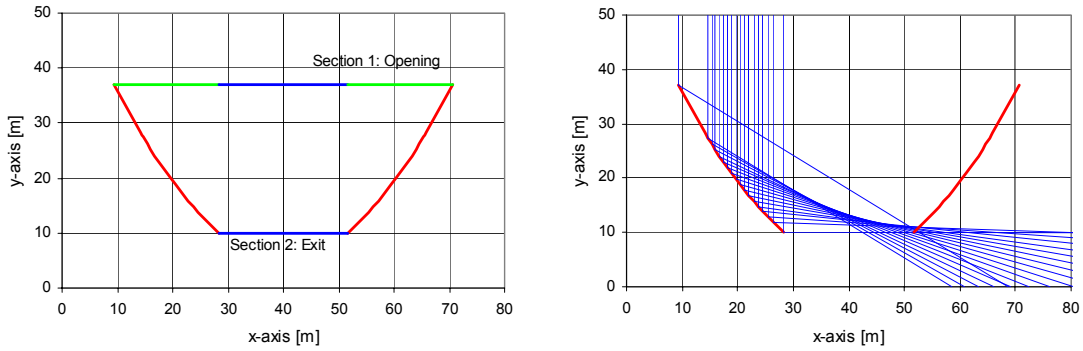


***Figure 4.1:*** *The cross-sections 1 and 2 at the opening and exit, respectively (figure to the left). On the figure to the right the reflection pattern is shown. Only the reflections of the left wave reflector are drawn. The blue reflection lines are placed between each of the elements.*

## 4.2 Energy consideration

Neglecting the transmission under the wave reflectors the mean energy flux over the exit line (cross section 2 on **Figure 4.1 left**) must be equal to the mean energy flux over the opening (cross section 1 on **Figure 4.1 left**). If this is not the case, energy will either be constantly stored or extracted from the area, which is impossible.

The transmission under the wave reflectors is taken into account by assuming that the energy entering the sides of section 1 (marked with green on **Figure 4.1 left**) is reduced according to the draught of the wave reflectors, cf. appendix *C. Transmission under the wave reflectors*. Hereby the expression for energy conservation is:

$$E_{f,middle} \cdot w_{middle} + K_{r,E} \cdot E_{f,sides} \cdot w_{sides} = E_{f,exit} \cdot w_{exit} \qquad (4.1)$$

where

*middle* represents the blue line in section 1

*sides* represents the green lines in section 1

The expression for the mean energy flux is based on a narrow banded wave spectrum, cf. appendix *A.3 Energy distribution*. Since the water depth is not changing from the opening to the exit the energy propagation velocity is constant. Thus the significant wave height at the exit is:

$$H_{s,exit} = \sqrt{1 + K_{r,E} \cdot \frac{w_{sides}}{w_{exit}}} \cdot H_{s,opening} \qquad (4.2)$$

This result is a modification of Green's Law by introduction of the transmission. It applies when changes in section are small, i.e. no reflection on the wave reflectors.

## 4.3 Conclusion on the analytical analysis of the wave reflectors

Wave energy is non-linear and therefore cannot be superposed in the general case. Superposition of energy is valid when the phases of the different superposed waves are not coupled or Green's Law applies. In case of the Wave Dragon the phases are in fact coupled (governed by the geometry of the wave reflectors).

For the design proposed by EFM the wave height ratios ($R_H = H_{s,ramp}/H_{s,opening}$) in the different wave situations are shown in **Figure 4.2**.

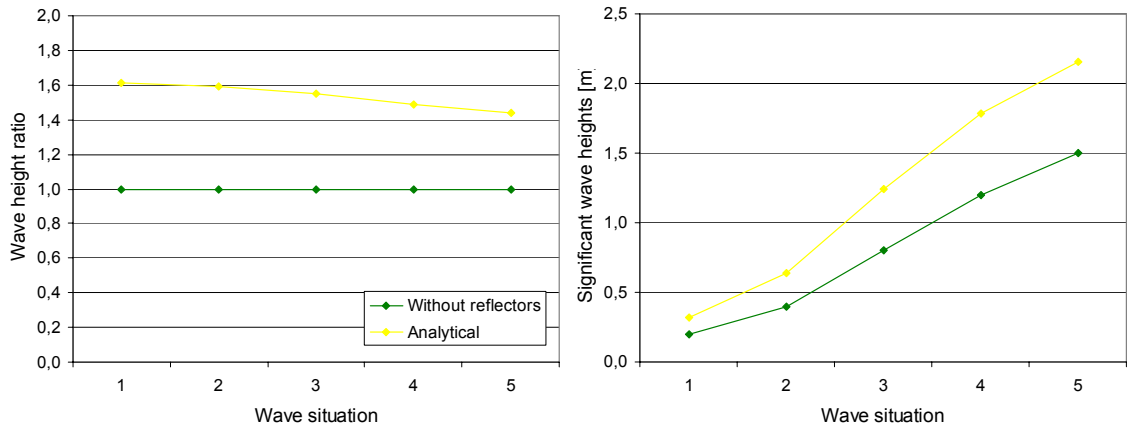


***Figure 4.2:*** *Wave height ratios calculated using the principle of energy conservation.*

# 5. Numerical analysis of wave reflectors

Before making the numerical evaluation of the wave reflectors the computer program used in the analysis is described.

## 5.1 The Mild Slope computer program

The computer program used to optimize the wave reflectors is developed by Michael Brorsen, Department of Civil Engineering, Aalborg University in 1996. The program is called MildSim, version 1.2. It is based on the time-dependent Mild Slope equation.

The MildSim program is a 2 dimensional numerical model in plan view. It applies to regular or irregular (with narrow banded spectrum), linear waves under conditions of mildly sloping bottoms.

In appendix *E. Mild Slope numerical model* the Mild Slope equation and the numerical model are described.

### *5.1.1 Description of the model used in the computer program*

The model of the Wave Dragon used in the computer program consists of boxes organized in a rectangular grid, see **Figure 5.1**. In most of the used configurations each box has a side length of 0,5 m, and the grid is 76 by 56 m. A number of cells are marked as "land", i.e. wave reflectors. Furthermore a number of boxes are marked as "sponges", i.e. boundaries that absorb energy.

The waves are generated in a line in front of the model. The generation is controlled by adding and subtracting water in the generation line and thus does not reflect energy.

The wave breaking criterion due to decrease in water depth is set at $H_{max} = 0{,}6 \cdot h$. No consideration is taken for wave breaking due to wave steepness.

In the computer model the ramp is not included. This is due to the fact that the desired wave parameters for calculating the wave overtopping are the incident wave parameters, i.e. after focusing by the wave reflectors but before they are reflected by the ramp.

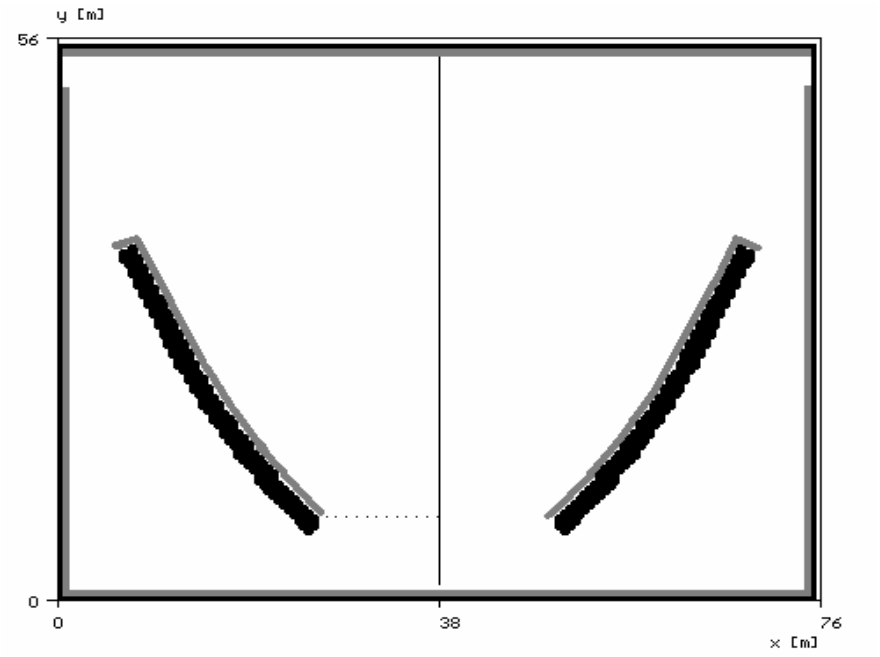


***Figure 5.1:*** *Element model used in the computer program. The black boxes are "land", the gray areas are "sponges" and the 12 black spots are measure points for determining the focused average significant wave height.*

In **Figure 5.1** the measure points used in the analysis are shown. When the numerical model is used, time series of the elevation in these 12 points are sampled for a period corresponding to 100 $T_P$'s, i. e. approximately 100 waves. The time series are calculated with a frequency of 15 Hz. Afterwards the data is subjected to a variance analysis of each time series and the average variance is found. From the average variance the average significant wave height $H_s$ is estimated. This estimate of the average significant wave height is then compared to the generated significant wave height. All model runs are conducted for a unit significant wave height, which is considered without importance as linear theory is used in modeling the waves.

## 5.2 Results of the numerical model runs

Before running the main model tests, a preliminary investigation of the modeling of the wave reflectors is performed.

Hereafter the main tests are presented. First a minor analysis is made of the importance of the starting angle of the wave reflectors. The major runs are concerned with analyzing the effect of changing the curvature of the wave reflectors.

In appendix *A. Wave conditions* 5 wave situations are found for which the design is to be evaluated. As the largest amount of wave energy is found for wave situation 3 (wave peak period of 3,0 s and significant wave height of 0,8 m), it is chosen as a representative for all wave situations. Thus in evaluating the different designs it is assumed that if situation 3 gives a high wave height ratio, this is also the case for the overall wave height ratio weighted with frequency of occurrence.

### *5.2.1 Transmission vs. absorption in modeling of the wave reflectors*

In the computer model the wave reflectors are modeled as land. By equating the reflected energy flow of the real and the model design approximate consistency is obtained. Two methods of doing this are described in appendix *E. Mild Slope numerical model*. The two methods are:

- Method 1 absorbs the energy in the sponge layers on the reflectors.
- Method 2 transmits energy through slots in the wave reflectors.

By running model tests it is found that method 2 results in a 2 % increase in wave height ratio compared to method 1. This is due to the fact that the slots permit interaction between the flow inside and outside the WRA.

Thus, since the difference in the results based on the two models is very small and the setting up of method 2 is very troublesome it is chosen to use method 1 in all of the following model runs.

### *5.2.2 Design results for starting angle investigation*

EFM has proposed a 45° starting angle for the first element (angle between the incident wave direction and the element next to the basin). This choice seems reasonable, as an increase will reflect the wave energy directly out of the wave reflection area (WRA, i.e. between the two wave reflectors), while a decrease, other things being equal, will reduce the width of the opening. Using the angle of 45° will not direct the energy reflected by the first element towards the exit, but just past it. This will though result in an increased wave height around the exit area. To further investigate the influence of the starting angle numerical model runs will be made for both 40 and 45° respectively, all other parameters being equal.

The wave conditions used in the following model runs are characterized by a wave peak period of 3,0 s and a unit significant wave height. The curvatures are set at 0,4; 0,6; 0,8; 1,0 and 1,2 for 40° and 0,8; 1,0; 1,2; 1,6 and 1,8 for 45° while the curvature-change is zero. Thus equal opening ratios are achieved for 40° and 45°.

All model runs in this investigation of the different designs are conducted with full reflection of the wave reflectors to eliminate any mistakes in the emulation of the reflection. Since the reflection is relatively high it is considered of minor importance in relation to the conclusions. The results are seen in **Table 5.1**.

| Starting angle | Opening ratio | | | | |
|---|---|---|---|---|---|
| | 2,7 | 2,6 | 2,5 | 2,4 | 2,3 |
| 40° | 1,56 | 1,57 | 1,55 | 1,50 | 1,53 |
| 45° | 1,46 | 1,59 | 1,59 | 1,48 | 1,50 |

***Table 5.1:*** *Wave height ratios as a function of opening ratio for the two systems with a starting angle of 40 and 45° respectively.*

Using this connection between wave height ratio and opening ratio shows that the starting angle for the two systems is of minor importance. Both systems have a maximum around an opening ratio of 2,5 - 2,6, with the wave height ratio 1,6. However, it seems as if a starting angle of 45° results in slightly higher wave height ratios. Thus in the following a starting angle of 45° is used for all model runs, as proposed by EFM.

### *5.2.3 Design results for curvature investigation*

Using the design scheme of appendix *D. Design scheme* the results are seen in **Figure 5.2**.

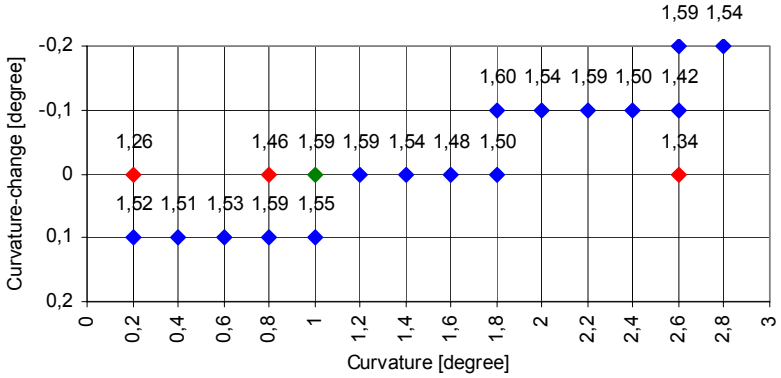


***Figure 5.2:*** *Design scheme with the results of the model runs for the varied parameters, curvature and curvature-change, for variations of 0,2° and 0,1° respectively. All runs are made for a wave peak period of 3,0 s. The numbers above the points are the respective wave height ratios.*

Considering the blue points it is seen that using the reflection patterns for designing the wave reflectors is very useful.

The amount of overtopping is not linearly proportional to the wave height. Thus in analyzing the data both the average and the variation of the 12 measure points should be considered. A large variation is preferable as this signifies locally large wave heights. The standard variation is around 20 % of the average for all the model runs. Thus in evaluation of the results it is assumed to be sufficient to consider the average of the measure points.

Expressing the curvature and curvature-change through the opening ratio and the angle ratio respectively, connections to the wave height ratio can be found. This is seen in **Figure 5.3**.

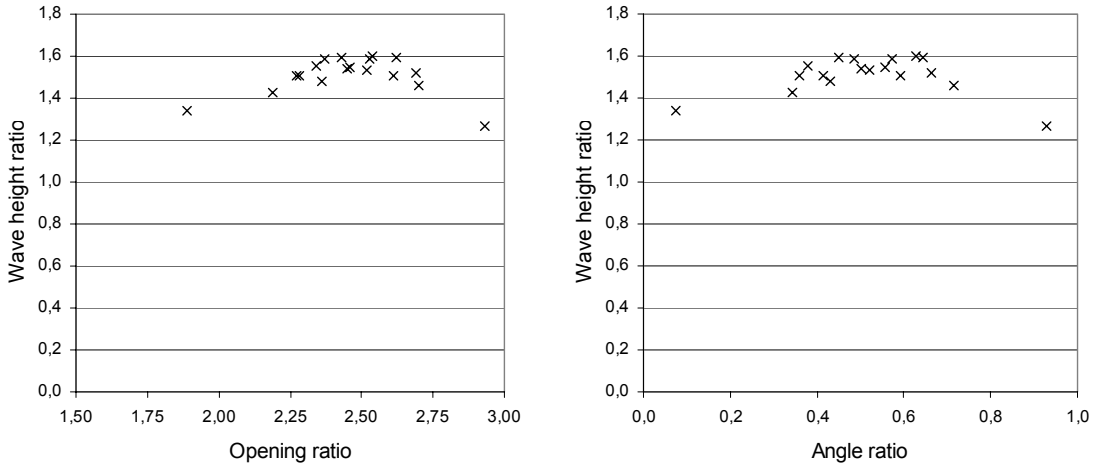


***Figure 5.3:*** *Connection between the wave height ratio and the opening ratio (to the left) and the angle ratio (to the right).*

## 5.3 Selecting an optimal design of the wave reflectors

The design of the wave reflectors has been analyzed with respect to 3 parameters, namely the starting angle, the curvature and the curvature-change (expressed through the opening and angle ratio). Through the analysis, it is evident that:

1. Keeping the same opening ratio, the wave height ratio is almost constant in the interval of 40° - 45°. Higher angles cause a high degree of reflection directly out of the WRA through the opening. Smaller values reduce the width between the wave reflectors and thus the energy flow into the WRA.
2. Within the band made from analysis of the wave reflection patterns the wave height ratio is relatively constant (cf. **Figure 5.3**). Thus no immediate advantage is gained from having a curvature-change.
3. By expressing the variables through different ratios it is apparent that the opening ratio is the most important variable and should be around 2,50. It is more advantageous with a too low than a too high opening ratio.
4. The angle ratio should be around 0,60. It is more advantageous with a too low than a too high angle ratio.

In order to maximize the amount of overtopping notice should be taken to the angle of wave attack at the ramp. Considering the reflection pattern it should be ensured that the wave propagation is as perpendicular to the ramp as possible.

Using the ramp design (plan view) proposed by EFM it is chosen to further investigate the design described by:

- Starting angle of 45°.
- Curvature of 1,2°.
- Curvature-change of 0,0°.

Thus the difference between this configuration and the design of the wave reflectors proposed by EFM is the value of the curvature. The reflection pattern for the chosen design is shown in **Figure 5.4 left** and the design proposed by EFM is shown in **Figure 5.4 right**.

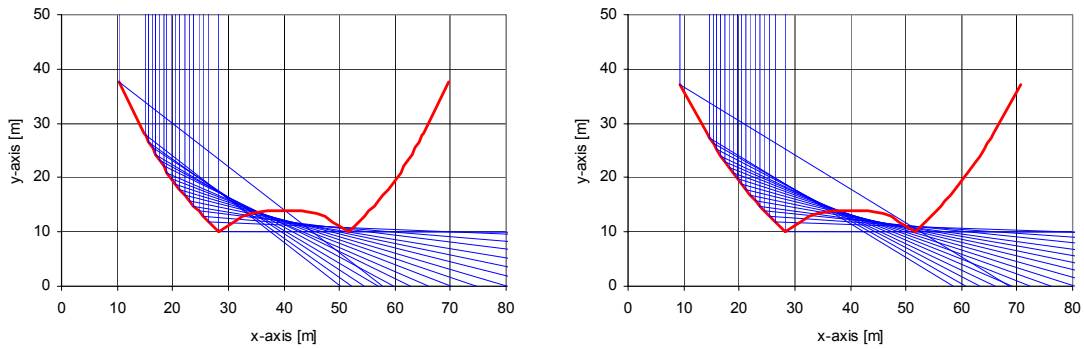


***Figure 5.4:*** *To the left the reflection pattern for the chosen design, using curvatures equal to 1,2°, is shown. Opening ratio of 2,53 and angle ratio of 0,57. To the right the reflection pattern for the design proposed by EFM, using curvatures equal to 1,0°, is shown. Opening ratio of 2,62 and angle ratio of 0,64.*

The chosen design has an opening ratio of 2,5 and an angle ratio of 0,6 (ending angle of the wave reflectors of 26°). Moreover, by choosing this design the angle of wave attack on the ramp is taken into consideration. This is the main difference from the proposed design made by EFM.

## 5.4 Investigation of the wave height ratios

The design is further investigated by exposing it to the 5 wave situations. The reflections of the wave reflectors are set according to the analysis in appendix *C. Transmission under the wave reflectors*. The results are seen in **Figure 5.5**

Compared to the model runs using full reflection of the wave reflectors, it is seen that the wave height ratio for wave situation 3 is reduced from 1,59 to 1,36 by the introduction of the reduced draught modeled as absorption in the sponge layers.

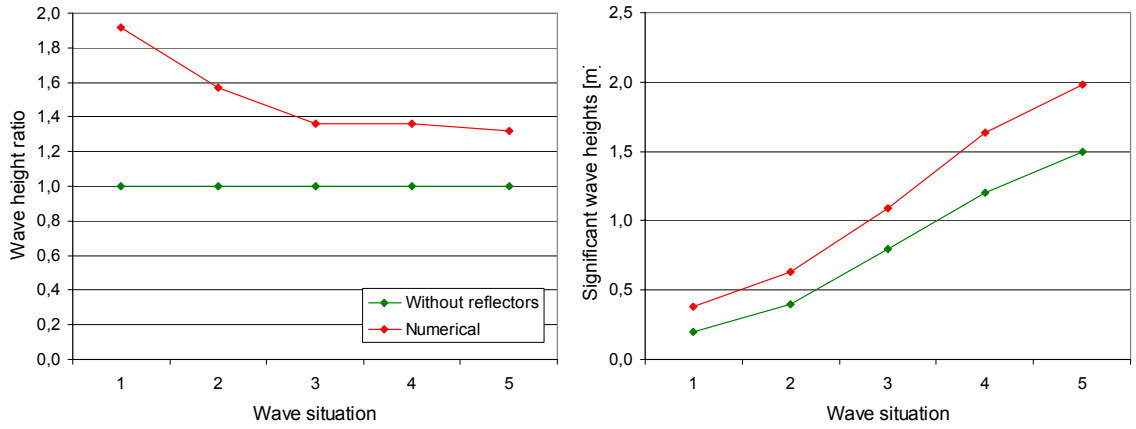


***Figure 5.5:*** *The wave height ratios and focused wave heights corresponding to the 5 wave situation found from the numerical model runs and compared to the generated wave heights.*

It is seen that the wave reflectors are most effective for the small wave situations. For wave situations 3 to 5 the effectiveness is almost constant. The reason for this is partly that the transmission under the wave reflectors retracts energy from the WRA before the energy reaches the exit line. Other reasons can be seen in the reflection patterns of the model runs, cf. next section.

## 5.5 Observations of the numerical model runs

In each of the 5 wave situations snapshot of wave fields are taken at a random time after the equilibrium state is attained. Unexpectedly the wave fields are very different, which is shown in **Figure 5.6**. Notice

that the width of the frame is 76 m, the length is 56 m and the height of the wave reflectors over MWL is 1,5 m. The changes in the wave patterns are due to a phenomenon called the Mach effect.

### The Mach effect

The angle between the wave reflector and the direction of wave propagation determines the type of reflection. In the general case of reflection on a vertical wall extending to the sea bottom reflection is undertaken with angle of incidence equal to angel of reflection. For angles of incidence below 45° two other kinds of reflection will occur:

- For angles of incidence below 45° the wave fronts close to the wall combine into one front perpendicular to the wall, which is called Mach reflection //I. A. Svendsen & I. G. Jonsson, 1994//. Still a reflected wave is present. The phenomenon can be interpreted as ordinary reflection on a fictive wall in front of the real wall. Between the walls a wave propagates with crests perpendicular to the real wall. This phenomenon will be termed partial Mach effect or partial Mach reflection.
- For angles of incidence below 20° the Mach effect results in wave propagation entirely alongside the wall with no reflected wave //NTH, page 5.30//. This phenomenon will be termed full Mach effect or full Mach reflection.

### Observations of the wave patterns

The Mach effect changes the wave patterns gradually. For small wave situation it is barely present while for the large situations it is dominating for the patterns next to the wave reflectors, i.e. partial Mach reflection.

From the wave fields of the 5 wave situations the following is generally observed:

- Judging from the crests the number of waves are decreased with the wave situations from about 5 waves for the first situation to 1 wave for the last situation. This is in qualitative accordance with the wave lengths for the wave peak periods.
- The wave fields are in agreement with the reflection pattern. The reflected waves on the wave reflectors form a 3 dimensional pattern, which of cause is most significant for the smallest wave situations because of the number of waves within the WRA.
- The Mach effect is gradually dominating the patterns next to the wave reflectors. Thus, the partial Mach effect is getting more extensive for increasing wave situations.
- Qualitative assessment shows that the increase in wave height at the exit line is largest for the smallest wave situations.

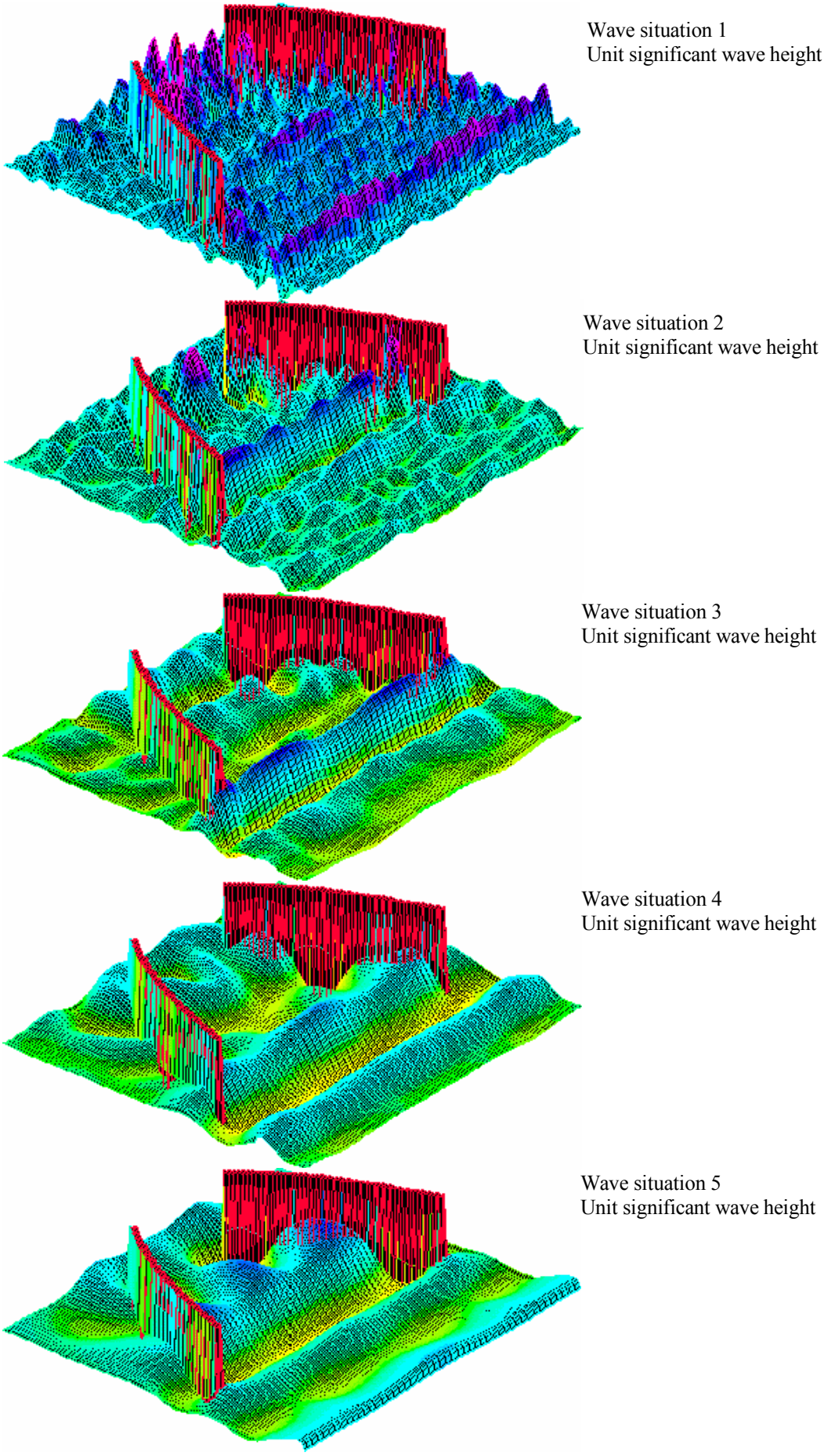


***Figure 5.6:*** *Snapshots of the 5 wave situations during model runs.*

## 5.6 Conclusion on the numerical analysis of the wave reflectors

The results from the model runs are shown in **Table 5.2**.

| Wave situation | Peak period [s] | Wave height ratio | Significant wave height [m] | | Occurring probability [%] |
|---|---|---|---|---|---|
| | | | Generated | Focused | |
| 1 | 2,0 | 1,92 | 0,20 | 0,38 | 24 |
| 2 | 2,5 | 1,57 | 0,40 | 0,63 | 30 |
| 3 | 3,0 | 1,36 | 0,80 | 1,09 | 11 |
| 4 | 3,5 | 1,36 | 1,20 | 1,63 | 3 |
| 5 | 4,0 | 1,32 | 1,50 | 1,98 | 2 |

***Table 5.2:*** *Results of the final model runs. The starting angle is 45,0°, the curvature is 1,2°, and the curvature-change is 0,0°. The reflections of the wave reflectors are set according to the analysis in appendix C.*

For use in the determination of wave overtopping of the ramp the uncertainties connected with the model runs in general is:

- In the numerical runs the modeling is encumbered with uncertainties and imperfections, e.g. 2 dimensional in plan view, modeling of the reflection, discrete steps in time and space etc.
- The sampled data used for finding the significant wave height might not be representative for the waves at the position of the ramp.

In order to eliminate these uncertainties in the estimate of the efficiency of the reflectors, the results are verified through laboratory tests. These tests are described in chapter *6. Experimental evaluation of wave reflectors*.

# 6. Experimental evaluation of wave reflectors

In this chapter laboratory tests of the wave reflectors (without presence of the basin part) are performed. As in the analytical and numerical tests the results are the wave height ratios.

## 6.1 Purpose of the tests

Laboratory tests of the wave reflectors with the shape selected on the background of the numerical analysis are performed as:

- Verification of the analytical and numerical method and thereby clarifying whether these tools are applicable.
- Determination of a more precise functionality in terms of the achieved wave height ratios.

The wave height ratios will be determined for the 5 wave situations. The comparison to the analytical and the numerical results are presented in the following chapter.

## 6.2 Configuration of the laboratory tests

The performed tests are set up in a wave tank in the Coastal Engineering Laboratory at Aalborg University.

### *6.2.1 Scaling of the laboratory tests*

For the laboratory tests described in this chapter it is chosen to scale down the Nissum Bredning design using a length scale $L_r$ = 15. This is considered to result in the most reasonable size of the model and wave fields for all 5 situations. In the scaling of the parameters Froudes law of modeling is used.

### *6.2.2 The model arrangement*

Using the length scale of 15 the entrance width of the reflectors is 4,0 m which is almost half of the width of the wave tank in the laboratory, see **Figure 6.1**. To have the option for exposing the model to 3 dimensional waves, it must be ensured that the 3 dimensional wave field covers the opening of the wave reflectors. However, the model must be at least 3 times the water depth from the wave generator, in order to ensure that the waves are fully developed before reaching the reflectors. Thus the opening of the wave reflectors is placed 1,5 m behind the wave generator, see **Figure 6.1**.

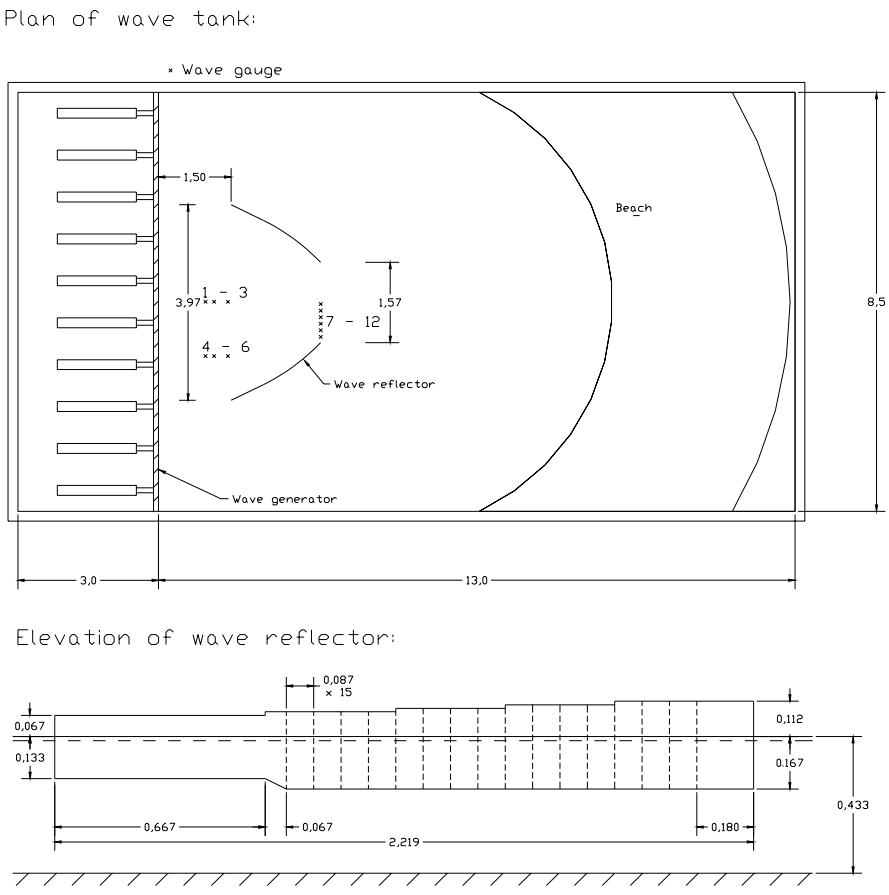


***Figure 6.1:*** *The model of the wave reflectors in the wave tank. Measures are in m.*

In order to determine the incoming wave field, 2 sets of wave gauges are placed in front of the WRA. One set is placed at the centerline (wave gauge 1 – 3, referred to as the gauges in the middle). The other set is placed in front of a reflector outside the WRA (wave gauge 4 – 6, referred to as the gauges on the side). Furthermore 6 wave gauges (wave gauge 7 - 12) are placed on the exit line of the WRA. The wave gauges are concentrated on one half of the exit line, since it is assumed that the wave field in the WRA is symmetric for the generated 2 dimensional waves. The wave elevations are recorded from each wave gauge with a sample frequency of 20 Hz and each test consists of 900 s.

### *6.2.3 Wave generation*

In all of the tests 2 dimensional irregular waves are generated. The waves are generated using a differentially amplified white noise signal so it resembles the JONSWAP-spectrum with a peak-enhancement factor $\gamma_p = 6{,}5$.

The wave parameters for the scale model are shown in **Table 6.1**.

| Wave situation | 1 | 2 | 3 | 4 | 5 |
|---|---|---|---|---|---|
| Occurring probability [%] | 24 | 30 | 11 | 3 | 2 |
| Wave peak period [s] | 0,52 | 0,65 | 0,77 | 0,90 | 1,03 |
| Wave length [m] | 0,47 | 0,65 | 0,93 | 1,24 | 1,57 |
| Incoming significant wave height [m] | 0,013 | 0,027 | 0,053 | 0,080 | 0,100 |

***Table 6.1:*** *Scaled (length scale of 1:15) wave parameters.*

## 6.3 Determination of the functionality of the wave reflectors

In determination of the functionality of the selected shape of the wave reflectors the evaluation is divided into the following steps:

- Determination of the incoming wave field.
- Determination of the wave field at the exit line.
- Calculation of the wave height ratios.

These steps are described in the following. However, first some qualitative impressions from the tests are noted.

### 6.3.1 Observations of the laboratory tests

While making the experimental tests some qualitative impressions were noted. Photos that illustrate this are presented in appendix *I.1 Photos of the wave reflectors*.

#### Observations of the wave patterns

In all of the wave situations the partial Mach effect is present, but the width of the band with crest perpendicular to the wall varies. For wave situation 1 the bands in both sides are each about $1/10^{th}$ of the width between the wave reflectors at given position. However, for wave situation 5 the full Mach effect is observed. This results in:

- For situations with partial Mach effect the wave pattern between the boundaries of the effects (in the middle area) is a superposition of a short crested and long crested wave field as expected. The area with partial Mach effect is relatively effective in providing large waves. In the middle area a short crested wave pattern (wave peaks) are positioned in an orderly fashion, i.e. the peaks reappear in the same points. Compared to the Mach area it seems relatively ineffective in regard to getting high waves. See **Figure 6.2 left** for a sketch of the wave pattern.
- For the situation with full Mach effect the wave field between the wave reflectors is long crested. A quantitative evaluation gives the impression that this phenomenon is extremely effective. The wave heights at the sides are significantly higher than in the middle area. Thus the wave reflectors act like a funnel with directly incoming waves over the entire width. See **Figure 6.2 right** for a sketch of the wave pattern.

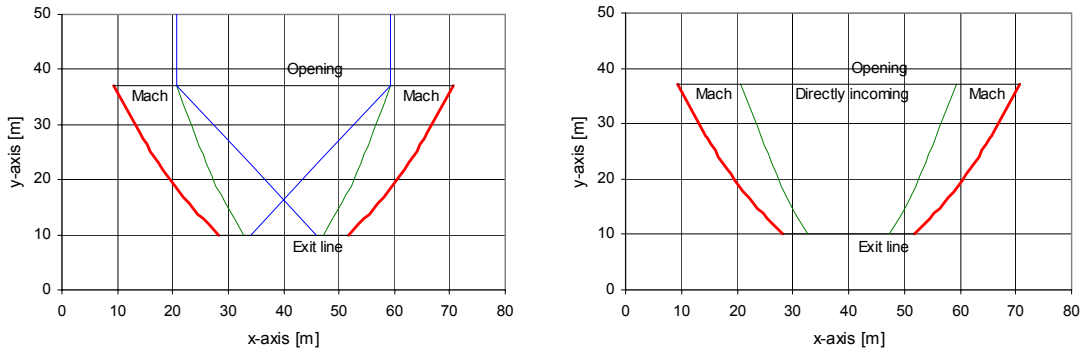


***Figure 6.2:*** *To the left the wave field for small wave situations is shown. To the right the wave pattern for the large wave situations is shown. The green lines are the fictive walls limiting the Mach effect areas. The blue lines are reflection patterns.*

For all situations diffraction is observed around the corners of the wave reflectors. This diffraction pattern is different when placing the ramp and thus constitutes a problem, as the measurements are affected by the diffraction.

#### Problems of generating waves with small wave peak periods

Difficulties connected with generating waves with small wave peak periods were encountered. Especially for wave situation 1, which has a wave peak period of 0,52 s in the tests, are encumbered with

uncertainties. The generated wave fields are dominated by unwanted scattering waves. Thus the reflection analysis, described below, is expected to give less accurate results for the wave situations with smaller periods than the ones with larger periods.

#### Wave overtopping of the wave reflectors

In the tests frequent overtopping of the wave reflectors was observed in wave situation 5 and seldom in wave situation 4. On this background it is recommended to increase the height of the wave reflectors over MWL.

### *6.3.2 Incoming wave field*

The functionality of the reflectors corresponding to the 5 wave situations is found in terms of the wave height ratios. When calculating the ratios it is crucial to determine the wave field the reflectors are subjected to in terms of significant wave heights and peak periods.

#### Peak periods

At first the measured peak periods are investigated. The peak periods are found by Fourier transformation. The deviations of the peak periods from the generated peak periods are found to be up to 10 %. This is not considered significant, since both the generation of the wave field and the analysis method are connected with uncertainties. Therefore it is considered reasonable to assume that the peak periods are not altered by the reflection. Thus, the actual wave peak period for the incoming wave field is considered equal to the input wave peak period.

#### Significant wave heights

During the test series the waves which meet the model are partly reflected. Some of these reflected waves travel back towards the wave generator, where they are partly reflected once more (re-reflected) and sent back against the model. This cycle continues during the entire test, but as the reflection is only partly, an almost steady condition will be reached, where the increase in provided energy can be neglected. This is the case for every model test. The measured waves are made up of newly generated waves superposed with re-reflected waves. Usually the reflection is limited and is thus neglected, e.g. for the experiments with the ramp profile. Though, in this test series a high degree of reflection is encountered. This is due to two reasons:

- The size of the model compared to the width of the basin is relatively large. Thus, a relatively large part of the generated waves is reflected.
- The model is placed very close to the wave generators. Thus, the reflected waves are not distributed over the entire width of the basin before reaching the model, but are concentrated in front of the model.

To determine the incoming wave field the measured waves are divided into waves moving in direction towards the model (incoming waves) and waves moving away from the model (reflected waves) and random noise. This is expressed through the reflection coefficient. Through this investigation it is assumed that the waves only move in direction perpendicular to the model, i.e. a 2 dimensional state. By observation of the wave field this is considered a reasonable assumption.

The degree of reflection is determined by use of Mansard & Funke's method using 3 wave gauges. The computer program used in the calculation is called RefCross developed by Andersen, Grønbech and Jensen, Aalborg University, 1995.

The reflection coefficients are found in two positions, namely:

- In the centerline of the ramp. It is assumed that the reflection measured in this position is a good representation of the conditions in front of the ramp, i.e. approximately the middle 40 % of the width.

- In front of one of the wave reflectors. It is assumed that the reflection measured in this position is a good representation of the conditions in front of the wave reflectors, i.e. approximately 30 % of the width on both sides.

The same distribution dictates the calculation of the average incoming significant wave height. The reflection coefficients are shown in **Figure 6.3**.

The division into two areas is a rough approximation, but is taken as a convenient alternative to a 3 dimensional reflection analysis.

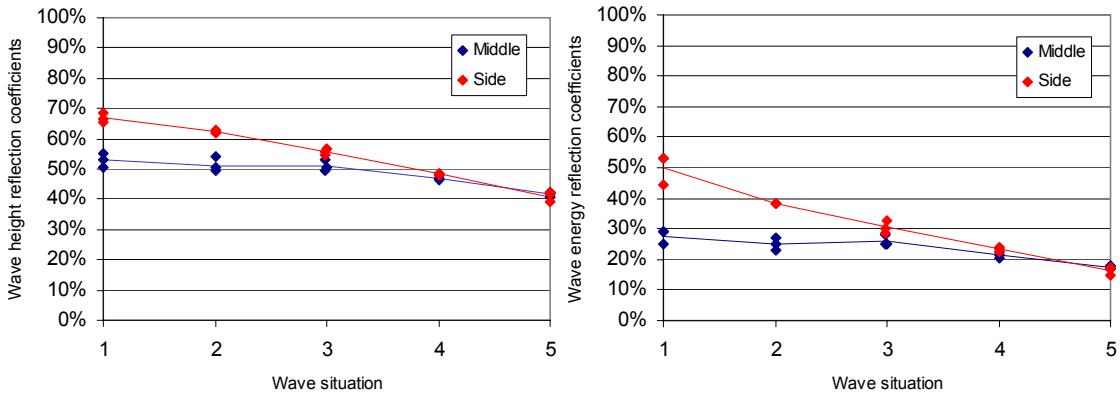


***Figure 6.3:*** *Reflection coefficients with respect to wave height and energy, to the left and the right respectively, corresponding to the 5 wave situations. The lines are the mean values while the points are the actual values.*

In **Figure 6.3** it is seen that a considerably amount of the generated energy is reflected back out of the WRA. A number of effects are connected to the nature of the reflection:

- The amount of energy transmitted under the reflectors.
- The partial or full Mach effect.
- Reflection from one wave reflector to the other.

The energy transmission under the wave reflectors explains the observed tendency of decreasing reflection coefficients for increasing wave peak period.

The change in the type of Mach effect from partial to full is the reason for the deviation from the side and the middle sections. For the large wave situations the waves are long crested of approximately equal size, while the high waves are concentrated at the wave reflectors for the small wave situations.

It is seen that the reflection coefficients are relatively high (between 15 – 50 % for energy) especially for the small wave situations. This is caused by the ending angle of 45°, which reflects the energy from one wave reflector to the other and out through the opening. This is most dominating for the small wave situations where the Mach effect is limited.

### *6.3.3 Wave field at the exit line*

As for the incoming wave field one wave peak period and one significant wave height is used to describe the wave field at the exit line. In order to determine them the wave elevations are recorded in 6 points at the exit line. Regarding the wave peak period for each point shows a deviation from the input wave peak period of up to 10 % which, as mentioned for the incoming wave field, is not considered significant. Thus the wave peak period measured at the exit line is considered equal to the input wave peak period.

In the determination of the significant wave height at the exit line it is chosen to calculate the energy by means of the variance for each measure point, and then use the mean of the wave energy in the calculation of the weighed significant wave height. This is the same procedure as in the numerical analysis.

### 6.3.4 Wave height ratios

On the basis of the significant wave height of the incoming wave field and the wave field at the exit line the wave height ratios are found for the 5 wave situations. The results are shown in **Figure 6.4**.

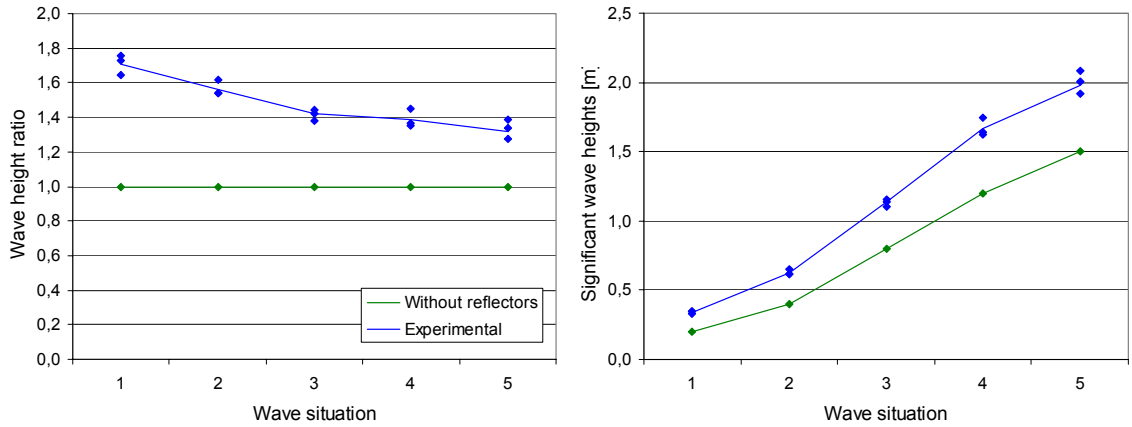


***Figure 6.4:*** *The wave height ratios and focused wave heights corresponding to the 5 wave situation found the laboratory tests and compared to the generated wave heights. The lines are the mean values while the points are the actual values.*

As shown in **Figure 6.4** the variation of the 3 tests performed in each wave situation is very limited (less than 5 %). It is seen that the small wave situations seem most effective. This is the case due to two facts:

- The transmission of energy under the wave reflectors increases for increasing periods.
- Frequent overtopping of the wave reflectors in wave situation 4 and 5.

## 6.4 Conclusions on the experimental evaluation of wave reflectors

The wave height ratios are shown in **Table 6.2**.

| Wave situation | Peak period [s] | Wave height ratio | Significant wave height [m] | | Occurring probability [%] |
|---|---|---|---|---|---|
| | | | Generated | Focused | |
| 1 | 2,0 | 1,71 | 0,20 | 0,34 | 24 |
| 2 | 2,5 | 1,56 | 0,40 | 0,62 | 30 |
| 3 | 3,0 | 1,42 | 0,80 | 1,13 | 11 |
| 4 | 3,5 | 1,39 | 1,20 | 1,67 | 3 |
| 5 | 4,0 | 1,33 | 1,50 | 2,00 | 2 |

***Table 6.2:*** *The wave height ratios based on the laboratory tests and the numerical analysis.*

The result from wave situation 1 is assessed to be misleading due to problems observed in the performed laboratory tests for small wave peak periods.

Moreover, it should be noted that the wave height ratio for wave situation 5 and partly for wave situation 4 could become slightly higher by increasing the height of the wave reflectors over MWL, since overtopping of the wave reflectors was observed for the largest wave situations in laboratory tests.

# 7. Comparing the analyses of the wave reflectors

In this chapter the analyses of the wave reflectors are evaluated. Moreover, a final result, in terms of wave height ratios, for use in the further analyses is established.

## 7.1 Wave height ratios

The analyses of the wave reflectors resulted in average increases in significant wave heights at the exit line, i.e. wave height ratios. For the 5 wave situations the results are shown in **Figure 7.1**, where they are compared to the system without reflectors.

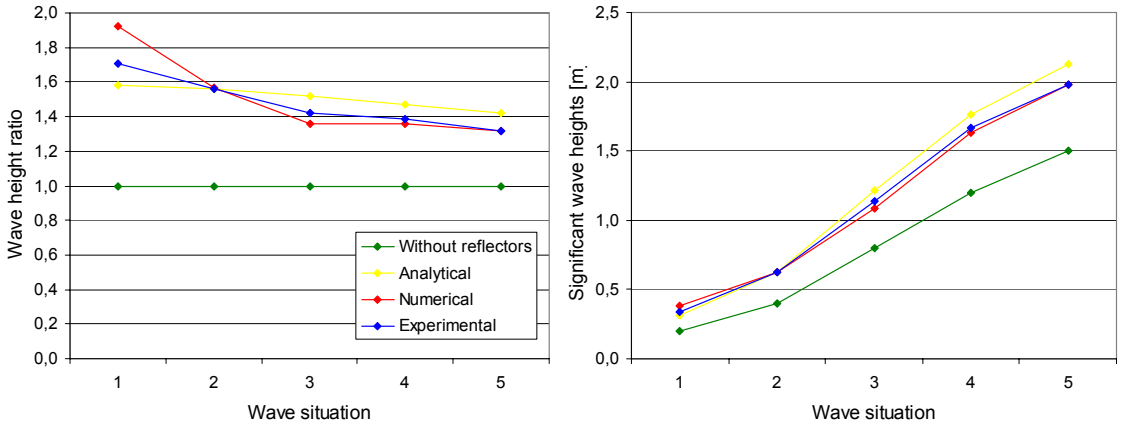


***Figure 7.1:*** *The wave height ratios and significant wave heights corresponding to the 5 wave situation found the analytical calculations, numerical analysis and the laboratory tests.*

Common for the analyses is that the wave height ratios are decreasing with increase in wave situation. The reason for this is mainly:

- The transmission increases with increasing wave peak period, and thereby with wave situation.
- For the largest wave situations frequent wave overtopping of the wave reflectors was observed in the laboratory tests.

Comparing with the analytical wave height ratios it is seen that the ratios for the numerical and experimental analyses are higher for wave situation 1 and lower for the situations 3 to 5.

For increasing wave situations the wave fields are gradually changed from being dominated by effects of partial Mach effect (displaced reflection) to being dominated of full Mach effect (no reflection). Thus the small wave situations can be described by considering superposition of reflected and non-reflected wave elevations, while for larger wave situations Green's Law is applicable implying that the wave reflectors have small changes in sections.

## 7.2 Observations of the wave fields

The most important difference in the appearing wave field for the numerical and experimental analyses is the extent of the Mach effect. Although it seems that the numerical computer program is able to model the Mach effect the degree is not as extensive as observed in the experimental tests.

Another difference is the height of the wave reflectors over MWL. In the numerical model the height is infinite while wave overtopping of the wave reflectors was observed in the experimental tests where the height is set as proposed by EFM.

## 7.3 Variation of the wave height ratios over the exit line

In order to investigate how the wave height ratios are varying over the exit line the significant wave height is calculated at each point on the exit line and related to the significant wave height of the incoming wave field. Thus the variation of the wave height ratios over the exit line in the 5 wave situations are achieved, see **Figure 7.2**.

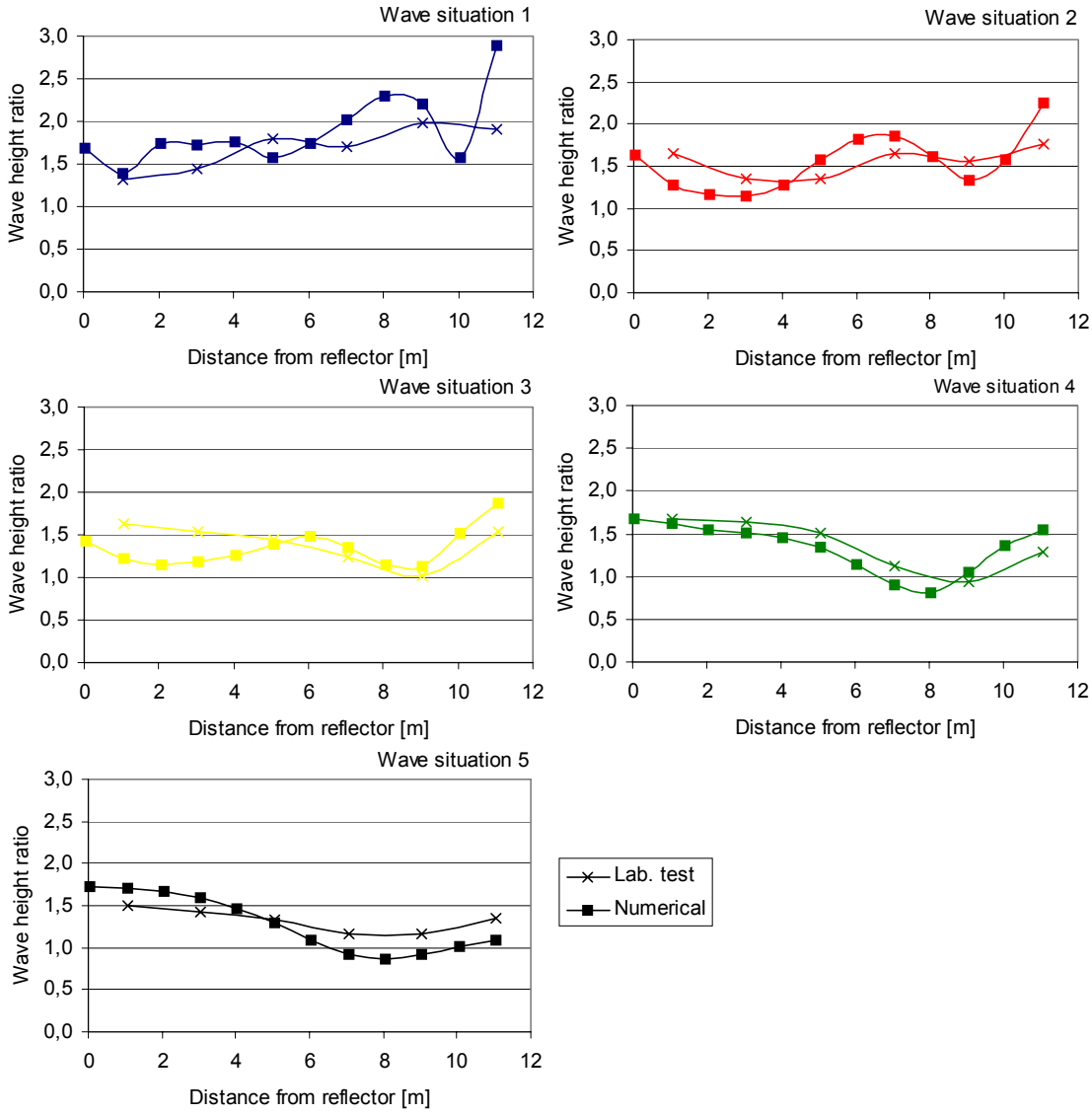


***Figure 7.2:*** *Distribution of wave height ratios over the exit line for peak periods corresponding to the 5 wave situations.*

From **Figure 7.2** it is seen that the wave height ratios generally are varying considerably over the exit line. The variation coefficients for the wave height ratios are 10 – 20 % with large variation coefficients for the small wave situations. Moreover it is seen that the variations are smaller for the laboratory tests than for the numerical analysis. This corresponds well with the fact that the Mach effect is most extensive for the laboratory tests, as the Mach effect has a tendency to distribute the energy over the entire width.

## 7.4 Analysis of the height of the wave reflectors over MWL

In the design proposed by EFM the height of the wave reflectors over MWL $h_r$ corresponds to 1,67 m in the Nissum Bredning design at the highest point. This height seems relatively low. Assuming that the wave heights are Rayleigh distributed the probability of overtopping this height $Q$ is theoretically found from:

$$H_Q = 4\sqrt{m_0}\sqrt{\tfrac{1}{2}\ln\tfrac{1}{Q}} \Leftrightarrow Q = \frac{1}{\exp\left(2\cdot\frac{H_Q^2}{H_s^2}\right)} \qquad (7.1)$$

Considering the numerical test data (without presence of the ramp) in **Figure 7.2** the wave height ratio $R_{H,sit.5,0}$ for wave situation 5 is approximately 1,7 at the wave reflectors. Moreover, usually the high waves are distributed with 2/3 of their height over MWL and 1/3 under MWL. Thus $H_Q$ and $H_s$ is found by:

$$H_Q = \tfrac{3}{2}\cdot h_r \qquad H_s = H_{s,sit.5}\cdot R_{H,sit.5,0} \qquad (7.2)$$

Inserting in ( 7.1 ) the probability of overtopping the wave reflectors for wave situation 5 is 0,15 or equivalent to every 7$^{th}$ wave. For wave situation 4 every 20$^{th}$ wave overtops, while for wave situation 3 only every 5.000$^{th}$ wave overtops.

Counting overtopping occurrences during the laboratory tests shows agreement with the calculation.

Using ( 7.1 ) the height of the wave reflectors over MWL should be set according to **Figure 7.3**.

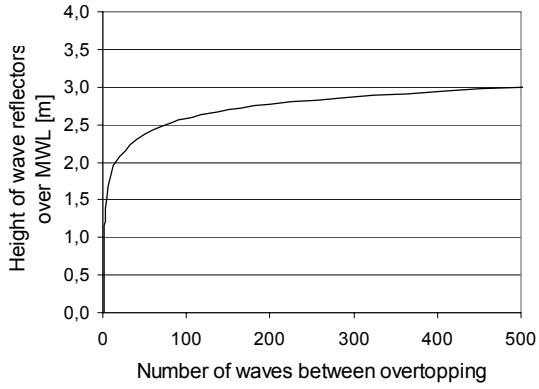


***Figure 7.3:*** *Minimum height of the wave reflectors over MWL for wave situation 5 as a function of the number of waves between overtopping.*

A reasonable height of the wave reflectors over MWL is 2,5 m as this results in overtopping for every 100$^{th}$ wave in wave situation 5.

## 7.5 Conclusions on the evaluation of the wave reflectors

For use in the following chapters the final results of the analyses of the wave reflectors are presented.

### *7.5.1 Focused wave heights*

The wave height ratios found through the analyses are used in calculation of the overtopping on the ramp. Using the ordinary means, e.g. the expression developed by Van der Meer, this means that the needed wave heights are the incoming wave heights on the ramp. That is, the wave height after focusing of the wave reflectors, but before being partly reflected by the ramp.

As the analyses have been performed only with the wave reflectors diffraction is included in the calculated wave height ratios. Placing the ramp on the exit line will diminish the diffraction.

An impression of the influence of the diffraction at the exit line is provided through the numerical model. In the model a fully absorbing wall is placed on the exit line just behind the measure points. The result is a reduction of the wave height ratios of below 5 %. This means that the diffraction is insignificant in regard to the wave height ratios.

### *7.5.2 Final results*

Generally the laboratory tests agrees well with the numerical analysis. This is taken as an indication of the fact that the energy considerations in determination of the reflection coefficients used in the numerical analysis is more exact than first assumed. Though, it should be noted that in the experimental tests the wave height ratio for wave situation 5 and partly for wave situation 4 could become slightly higher by increasing the height of the wave reflectors over MWL. This is due to the fact that frequent overtopping of the wave reflectors was observed for the largest waves in laboratory tests.

The wave height ratio distributions over the exit line shows variation coefficient of 10 – 20 %, which corresponds well to the results from the numerical analysis. Furthermore, the comparison shows that the variation of the wave height ratios have the same tendencies in the numerical analysis as in the laboratory tests for the wave situation 2 – 5, while there is larger inconsistency for wave situation 1.

Due to problems observed in the performed laboratory tests, it is chosen to use the wave height ratio from the numerical analysis for wave situation 1. However, the ratios found from the laboratory tests are used for wave situation 2 – 5 in the further work with the analysis of the ramp. The wave height ratios are shown in **Table 7.1**.

| Wave situation | Peak period [s] | Wave height ratio | Significant wave height [m] | | Occurring probability [%] |
|---|---|---|---|---|---|
| | | | Generated | Focused | |
| 1 | 2,0 | 1,92 | 0,20 | 0,38 | 24 |
| 2 | 2,5 | 1,56 | 0,40 | 0,62 | 30 |
| 3 | 3,0 | 1,42 | 0,80 | 1,13 | 11 |
| 4 | 3,5 | 1,39 | 1,20 | 1,67 | 3 |
| 5 | 4,0 | 1,32 | 1,50 | 1,98 | 2 |

***Table 7.1:*** *The wave height ratios based on the laboratory tests and the numerical analysis.*

These obtained ratios are used in the investigation of the efficiencies of the Wave Dragon described in chapter *8. Experimental evaluation of the ramp profile*.

# 8. Experimental evaluation of the ramp profile

It has not been possible to find suitable empirical expressions to evaluate a ramp profile with neither a draught different from the water depth nor a cross section with a curvature, e.g. the ramp proposed by EFM. Furthermore it is considered necessary to investigate the Van der Meer formula in regard to heavy overtopping.

On this background it is chosen to perform a series of laboratory tests. The tests are performed in the Coastal Engineering Laboratory at Aalborg University.

## 8.1 Purpose of the tests

The main purpose of these laboratory tests is to find an optimal shape of the ramp. The criterion used to determine which shape is the optimal is the amount of overtopping times the crest freeboard, i.e. the obtained potential energy in the basin.

The search for the optimal shape is divided into the following steps:

- Investigation of the applicability of the overtopping formula developed by Van der Meer.
- Determination of the influence of variation on the slope angle and curvature on the overtopping.
- Evaluation of the profile proposed by EFM on the overtopping.
- Selection of optimal ramp profile.
- Conversion of the overtopping discharge to potential energy.

## 8.2 Configuration of the experiments

In this section scaling of the Wave Dragon is described. Furthermore the conditions under which the tests were performed are described.

### *8.2.1 Scaling of the laboratory tests*

In the model tests it is chosen to use a length scale $L_r = 13$ as this results in a reasonable size of the model. In the scaling of the parameters Froude's law of modeling is used.

### *8.2.2 Model arrangement*

The model is placed in one of the wave tanks in the Coastal Engineering Laboratory at Aalborg University, see **Figure 8.1**. The tank is equipped with a computer controlled wave generator, wave gauges and a beach for wave energy absorption. A wave gauge is placed on each side of the model in order to verify the generated wave field.

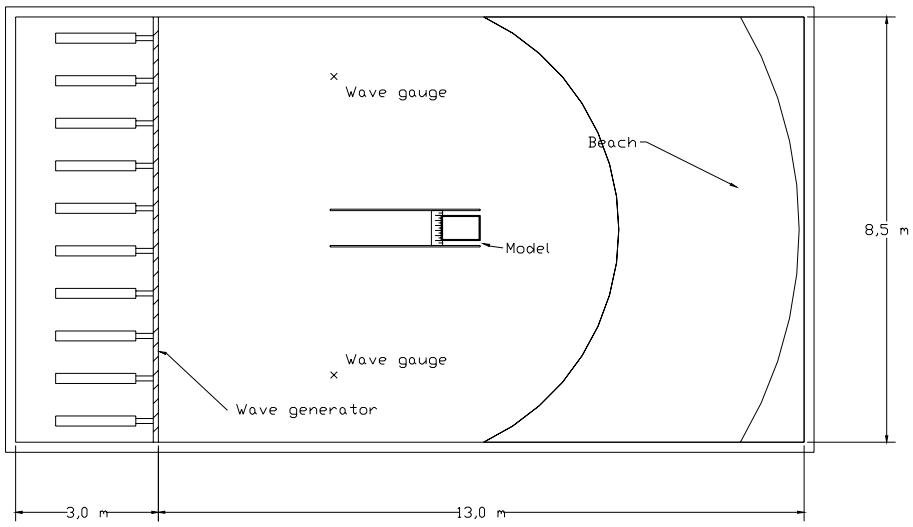


***Figure 8.1:*** *The size of the used wave tank, and the placement of the model.*

In **Figure 8.2** a sketch of the used model is shown. The model is restrained by a steel rack and is thus not floating as the real construction. This configuration is chosen since a restrained construction has also been assumed in the analyses performed so far.

On each side of the ramp and basin guiding walls are placed to ensure 2 dimensional wave motion at the ramp. In order to minimize the effects due to the presence of the guiding walls, the overtopping in the outer 0,1 m of each side is transmitted past the basin which collects the overtopped water. This means that the effective width of the tested ramp is 0,46 m in the model.

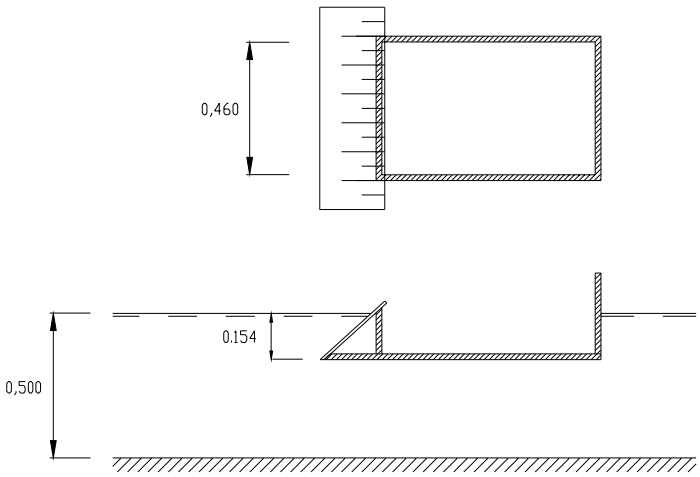


***Figure 8.2:*** *Sketch of the configuration of the model used in the laboratory. All measures are in m.*

The linear ramp shown in **Figure 8.2** is the one used in most of the test series.

### Measuring the overtopping for small discharges

For small discharges the amount of overtopped water is measured by use of a pump that pumps the water through a flow meter and back into the test tank. Furthermore the elevation, and thereby the amount of water in the basin, is recorded at the start and end of each test. Hereby the total overtopping discharge is found.

Two small pumps with meters are available. The smallest has a capacity of approximately 0,5 l/s while the other has a capacity of approximately 1,5 l/s.

**Measuring the overtopping for large discharges**

For large overtopping discharges a more troublesome approach is used. In the laboratory a flume is located next to the tank. A high capacity pump is placed in the model for pumping the overtopped water into the flume. By measuring the change in water level in the flume the overtopping discharge is found. As water is hereby retracted from the tank, the water level is kept constant by letting in water in one or both ends of the tank. The adjustments are performed continuously by monitoring the MWL of the two wave gauges. The mixing of the tank water with fresh water changes the calibration coefficients. To find the estimate for $H_s$ the test series are first run for a test where the overtopping discharge is pumped back into the tank. By storing this test and running it afterwards the wave parameters are unaffected by the change of water. The only wave gauge affected by the change of water is therefore the gauge for measuring the MWL. The tests show that the change of calibration constant is minimal and the MWL is kept within a few millimeters of accuracy.

The measuring flume has a plan area of 21 × 1,2 m and a depth of more than 1,5 m. The large pump has a capacity of 40 l/s. The overall capacity is thus limited by the amount of water which can be let into the tank. By using the two small pumps with flow meters for pumping water from the flume back into the tank and opening both water taps the capacity is about 8 - 10 l/s.

### *8.2.3 Wave generation*

In all of the tests 2 dimensional irregular waves are generated, using a differentially amplified white noise signal so it resembles the JONSWAP-spectrum with a peak enhancement factor $\gamma_P = 6{,}5$.

The wave parameters for the scale model are shown in **Table 8.1**. The wave reflectors focus the incoming significant wave height to obtain the values of a focused significant wave height at the ramp.

| Wave situation | 1 | 2 | 3 | 4 | 5 |
|---|---|---|---|---|---|
| Occurring probability [%] | 24 | 30 | 11 | 3 | 2 |
| Wave peak period [s] | 0,55 | 0,69 | 0,83 | 0,97 | 1,11 |
| Wave length [m] | 0,47 | 0,75 | 1,08 | 1,43 | 1,81 |
| Incoming significant wave height [m] | 0,015 | 0,031 | 0,062 | 0,092 | 0,115 |
| Focused significant wave height [m] | 0,030 | 0,048 | 0,087 | 0,128 | 0,152 |
| Mean energy flux [J/m/s] | 0,08 | 0,41 | 1,55 | 3,76 | 7,42 |

***Table 8.1:*** *Scaled (length scale of 1:13) wave parameters.*

All test series are run over a time period of 600 s. The generated wave peak period is very close to the input period, while some deviation is observed between the generated significant wave height and the input wave height. The deviations amounted up to 10 %.

The precision of measuring the amount of overtopping is investigated by making a number of similar test series. An inaccuracy of up to 10 % was noted.

## 8.3 Predicting the overtopping discharge

An expression for the obtained potential energy is established on the basis of an overtopping formula.

### *8.3.1 Empirical formula for calculating the potential energy*

Different overtopping formulas found by dimensional analysis are fitted to the laboratory data. Best result is obtained by using the formula developed by J. W. Van der Meer and J. P. F. M. Janssen in 1994 //Van der Meer et. al., 1994//.

From the Van der Meer formula an expression for the obtained potential energy in the basin is established, by multiplying with the crest freeboard. Taking movements of the basin part and wave overtopping volume distribution into consideration, a new parameter is introduced namely the rim height $r$, defined as the height from the MWL in the basin to the crest freeboard:

$$E_{pot,basin} = q \cdot (R_c - r) \cdot g\rho_w = a \cdot \sqrt{gH_s^3} \cdot (R_c - r) \cdot g\rho_w \cdot \exp\left(-\frac{b}{H_s} \cdot R_c \cdot \frac{1}{\gamma}\right) \quad (8.1)$$

where

$a$ and $b$ empirical coefficients.

$\gamma$ reduction factors.

Maximizing the potential energy with respect to the crest freeboard the optimal crest freeboard is found to:

$$R_{c,opt} = \frac{\gamma \cdot H_s}{b} + r \quad (8.2)$$

In the following calculations the MWL in the basin is set 0,10 m below the ramp crest freeboard, i.e. a rim height of 0,10 m. The reduction factor is set to 0,9 due to oblique wave attack (average angle of 30°).

Further information on the expression is presented in appendix *F. Potential energy based on V. Meer's formula*.

### 8.3.2 Fitting the overtopping coefficients

Generally the Van der Meer formula is not designed for the conditions of the Wave Dragon, i.e. reduced draught and heavy overtopping. Thus the overtopping coefficients fitted to the laboratory tests are significantly different from those found by Van der Meer. Furthermore it is found that the overtopping coefficients are dependent on the relationship between the significant wave height and the wave peak period. By dimensional analysis the $H_s$-$T_p$ relation that dictates the overtopping coefficients is found to:

$$T_p \sqrt{\frac{g}{H_s}} \quad (8.3)$$

The coefficients for the 5 wave situations and their approximate $H_s$-$T_p$ relations, calculated from the focused wave heights, are shown in **Table 8.2**.

| | $H_s$-$T_p$ relation | $a$ coefficient | $b$ coefficient |
|---|---|---|---|
| Wave situation 1 & 2 | 10,2 | 0,078 | 1,90 |
| Wave situation 3, 4 & 5 | 8,7 | 0,043 | 1,49 |

***Table 8.2:*** *Overtopping coefficients in Van der Meer formula for the 5 wave situations in Nissum Bredning.*

This means that the overtopping discharges cannot be directly scaled to other locations with different $H_s$-$T_p$ relation. Furthermore it is found that the overtopping coefficients are almost constant for $H_s$-$T_p$ relations between 10 and 15. For the North Sea the $H_s$-$T_p$ relation (with focused wave heights) is within this interval. Thus the overtopping coefficients for wave situation 1 & 2 are also used in the North Sea.

For further information see appendix *G. Investigation of wave overtopping.*

## 8.4 Investigation of adjustments to increase overtopping

In investigation of adjustments to increase overtopping laboratory tests have been conducted for different slope angles and curvatures of the ramp profile. None of the tests have been carried out for a constant $H_s$-$T_p$ relation. Thus a design equation for overtopping with any combination of the significant wave height and the wave peak period is established. It has the form:

$$q = c_d \cdot g \cdot T_p \cdot H_s^{2,5} \cdot (R_c + c_s)^{-1,5} \quad (8.4)$$

where

$c_d$ design overtopping coefficient. Found to $20 \cdot 10^{-3}$.

$c_s$ [m] shifted power constant for $R_c$. Found to 0,03 m.

This formula cannot be used to predict overtopping in Nissum Bredning. It only applies to the laboratory tests, as one of the coefficients is not dimensionless. No tests have been performed to determine its dependency and thereby how to scale it.

The primary tests for establishing the design equation are made for a slope angle of 40° and a straight ramp profile. The most significant adjustments for increasing the overtopping discharge are:

- The slope angle has only been investigated for angles between 35 and 60°. It is assumed that the slopes must be relatively steep to prevent wave breaking on the ramp. Slope angles between 35° and 50° do not affect the overtopping significantly, but higher values will decrease it. A slope of 60° only gives about 70 – 80 % of the overtopping of a slope of 40°.
- The influence of a ramp profile with curvature has been tested by using 4 different profiles. The tests show that a curvature does not have a significant effect. The profile proposed by EFM decreases overtopping significantly.

For further information see appendix *H. Evaluating the design of the ramp profile.*

On this background it is chosen to use a ramp profile with the following characteristics:

- Slope angle of 40°.
- No curvature.

## 8.5 Obtained potential energy

From the analyses of the ramp profile the obtained potential energy a function of the crest freeboard is found for the Van der Meer formula. The energy functions are presented for the 5 wave situations weighed with the time of occurrence. Moreover, the total energy for a fixed crest freeboard is shown. Finally the results are compared to the energy function without consideration to the rim height.

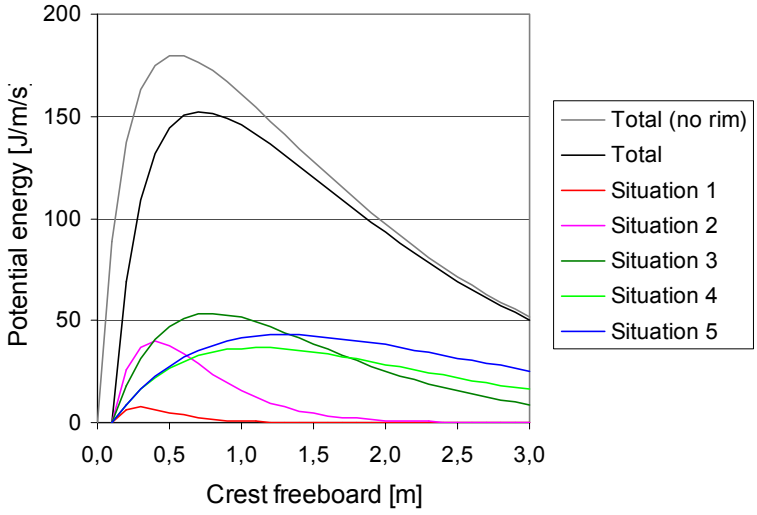


***Figure 8.3:*** *Potential energy obtained in the basin per time and width unit as a function of the crest freeboard. The colored curves are calculated using the data from the 5 wave situations (after focusing by the wave reflectors) weighed with the time of occurrence. The black curve is the sum of the colored curves, while the gray curve is the energy calculated with rim height r = 0.*

From **Figure 8.3** it is seen that neglecting the rim height result in a 16 % increase of the potential energy.

With the parameters in **Table 8.1** (scaled to Nissum Bredning design) the obtained potential energy weighed with the time of occurrence is found for the optimal crest freeboard in each wave situation. This is shown in **Table 8.3**.

| | Crest freeboard [m] | Potential energy [J/m/s] | Contribution to total [%] | Occurring probability [%] |
|---|---|---|---|---|
| Wave situation 1 | 0,28 | 8 | 4 | 24 |
| Wave situation 2 | 0,40 | 40 | 22 | 30 |
| Wave situation 3 | 0,78 | 53 | 29 | 11 |
| Wave situation 4 | 1,11 | 37 | 20 | 3 |
| Wave situation 5 | 1,31 | 43 | 24 | 2 |
| Sum | - | 180 | 100 | 70 |

***Table 8.3:*** *Optimal crest freeboard with corresponding obtained potential energy weighed with time of occurrence for the 5 wave situations.*

For simplifying the experimental tests with the composite system, it has been chosen to used a fixed crest freeboard in all wave situation.

The fixed crest freeboard of 0,71 m corresponds to the optimal fixed crest freeboard. It is seen that the maximum potential energy is reduced by 16 % by using the optimal fixed crest freeboard for all wave situations, cf. **Table 8.3** and **Table 8.4**.

| | Optimal fixed crest at 0,71 m | | Fixed crest at 0,50 m | | Occurring probability [%] |
|---|---|---|---|---|---|
| | Pot. energy [J/m/s] | Contribution [%] | Pot. energy [J/m/s] | Contribution [%] | |
| Wave situation 1 | 2 | 2 | 5 | 4 | 24 |
| Wave situation 2 | 28 | 19 | 38 | 26 | 30 |
| Wave situation 3 | 52 | 35 | 47 | 32 | 11 |
| Wave situation 4 | 33 | 22 | 27 | 18 | 3 |
| Wave situation 5 | 36 | 24 | 28 | 19 | 2 |
| Sum | 152 | 100 | 144 | 100 | 70 |

***Table 8.4:*** *Fixed crest freeboards with corresponding obtained potential energy weighed with time of occurrence for the 5 wave situations.*

On this background it might be chosen to use a crest freeboard of 0,71 m, but this analysis was not complete before designing the model used in the experimental tests of the composite system. Instead the crest freeboard was set to 0,50 m, i.e. a reduction in potential energy of 5 % (cf. **Table 8.4**) compared to the optimal fixed crest freeboard.

## 8.6 Conclusion on the evaluation of the ramp profile

As shown in **Table 8.3** the 5 wave situations only cover 70 % of the time. Thus, the overall effect is found by multiplying by 0,70. The effects are converted to the North Sea design by writing up using a length scale of 3 and overtopping coefficients corresponding to the $H_s$-$T_p$ relations for the North Sea. The resulting effects are shown in **Table 8.5**.

| | Unit | Nissum design | North Sea prototype |
|---|---|---|---|
| Effect per unit ramp width | kW/m | 0,14 | 3,1 |
| Overall effect per unit ramp width (70 %) | kW/m | 0,10 | 2,2 |
| Overall effect | kW | 2,36 | 152 |

***Table 8.5:*** *Theoretical effects for the Wave Dragon in Nissum Bredning design (1:3) and North Sea prototype for a crest freeboard of 0,50 m.*

In appendix *A.3 Energy distribution* a time averaged mean energy flux in Nissum Bredning was found to 358 J/m/s equivalent to 21 kW entering the opening. This gives an efficiency of approximately 11 %

Considering the North Sea prototype it is concluded that by changing the $H_s$-$T_p$ relations in order to fit the wave situations in the North Sea the overall effect is increased by almost 40 %.

# 9. Experimental evaluation of composite system

This chapter describes the laboratory tests performed with the composite model of the Wave Dragon, i.e. the model consisting of both the selected wave reflectors and the ramp profile.

## 9.1 Purpose of the tests

In this chapter the two parts, which until now have been dealt with separately, are analyzed in conjunction. No adjustments are carried out. The primary purpose is to determine the overall efficiency of the composite system. Hereby the tools developed in the experimental tests of the wave reflectors and ramp are verified.

## 9.2 Configuration of the tests

The performed tests are, as in the experimental ramp analysis, set up in the in the largest wave tank in the Coastal Engineering Laboratory at Aalborg University.

### *9.2.1 Scaling of the laboratory tests*

As for the model test with only the wave reflectors present a length scale of 1:15 is used.

### *9.2.2 Model arrangement*

In the set-up of the composite system the configuration of the tests with only the wave reflectors are used as starting point. But instead of the 6 wave gauges at the exit line, the model of the ramp and basin is placed in the exit area.

The model of the wave reflectors is described in chapter *6. Experimental evaluation of wave reflectors*. The placement of the entire model is shown in **Figure 9.1**.

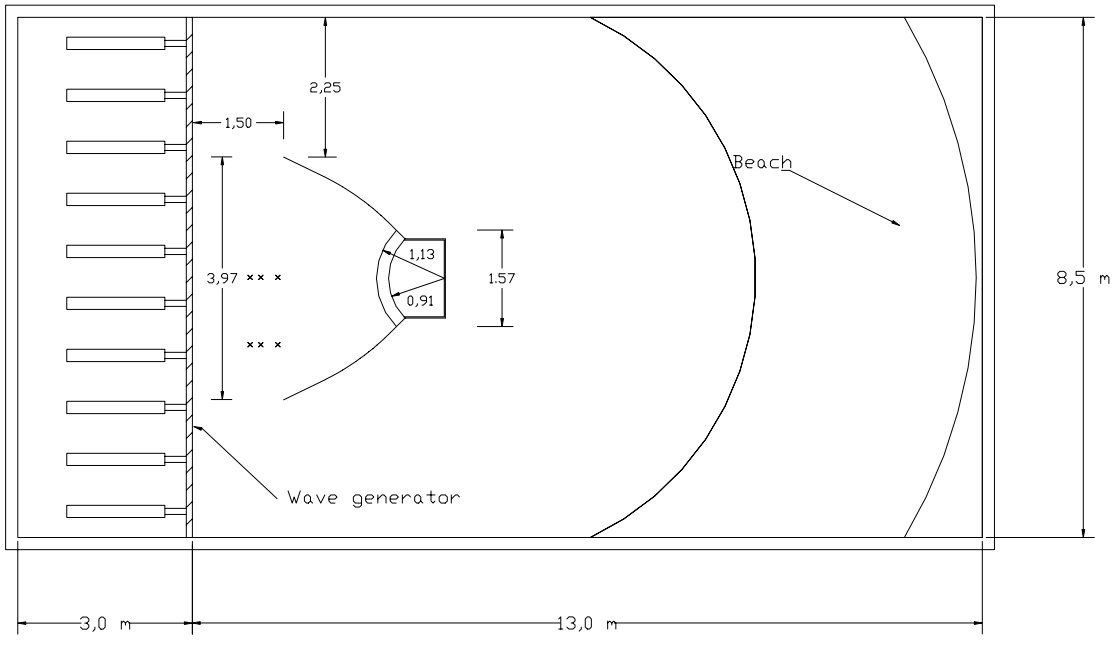


***Figure 9.1:*** *The size of the used wave tank, and the placement of the model. The x mark wave gauges used to determine the incoming wave field. All measures are in m.*

A cross section view of the basin part is shown in **Figure 9.2**. The basin part is restrained by slender columns and is therefore not a floating structure.

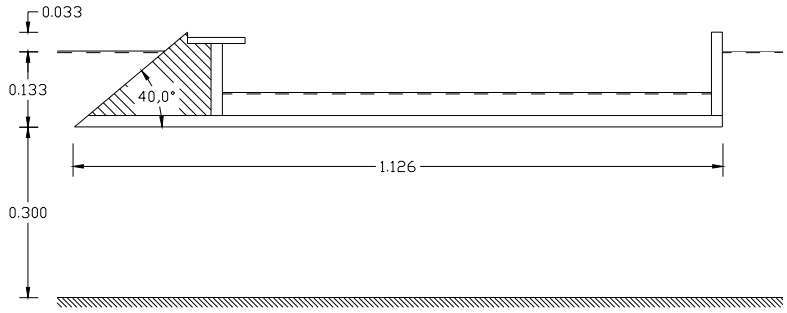


***Figure 9.2:*** *Sketch of the configuration of the model used in the laboratory. All measures are in m.*

By measuring the amount of overtopped water in the basin a measure of the obtained potential energy collected by the Wave Dragon is achieved. The measuring of the overtopped water is performed as described in chapter *8. Experimental evaluation of the ramp profile*.

In some of the tests only the half of the overtopped water was measured, but due to symmetry this is considered of minor importance.

### *9.2.3 Wave generation*

In all of the tests 2 dimensional irregular waves are generated. The waves are generated using a differentially amplified white noise signal so it resembles the JONSWAP-spectrum with a peak-enhancement factor $\gamma_P = 6{,}5$.

The tests are performed for the 5 wave situations. The wave parameters for the scale model are shown in **Table 9.1**. The full-scale parameters are shown in **Table 8.1.**

| Wave situation | 1 | 2 | 3 | 4 | 5 |
|---|---|---|---|---|---|
| Occurring probability [%] | 24 | 30 | 11 | 3 | 2 |
| Wave peak period [s] | 0,52 | 0,65 | 0,77 | 0,90 | 1,03 |
| Wave length corresponding to peak period [m] | 0,41 | 0,65 | 0,93 | 1,24 | 1,57 |
| Incoming significant wave height [m] | 0,013 | 0,027 | 0,053 | 0,080 | 0,100 |
| Mean energy flux [J/m/s] | 0,06 | 0,29 | 1,08 | 2,63 | 5,19 |

***Table 9.1:*** *Scaled (length scale of 1:15) wave parameters.*

All test series are run over a time period of 900 s. For each wave situation 3 runs are performed. This showed that precision depended on the amount of overtopping. The higher an amount of overtopping, the more precise a value. For wave situation 4 and 5 the inaccuracy in overtopping is less than 5 %.

## 9.3 Evaluation of the Wave Dragon

The generated wave peak periods have not been investigated. In the model test with only the wave reflectors the measured wave peak periods corresponded with the generated wave peak periods. It is therefore assumed that this is also the case in this experiment.

As for the experiment with the wave reflectors it is necessary to investigate the reflection for determining the incoming significant wave height. A description of the reflection phenomenon is seen in section *6.3.2 Incoming wave field*.

### *9.3.1 Observations in the laboratory tests*

While making the experimental tests some qualitative impressions were noted. These are the appearance of the wave patterns, wave overtopping of the wave reflectors and generation problems for tests with a

low wave peak period. For the 2 latter the same applies as for the experimental tests with the wave reflectors.

### Observations of the wave patterns

As for the experimental tests of the wave reflectors the Mach effect is observed. Though the extent of the effect is more prevalent:

- For situations with partial Mach effect the wave pattern between the fictive walls is a superposition of a short crested and long crested wave field. The area with partial Mach effect is relatively effective with frequent and large overtopping discharges. The water in the area with Mach effect that does not top over the ramp is directed towards the center. Hereby a crossing wave pattern is observed in front of the ramp. These transverse waves lift up the waves in the middle. Still only very little overtopping is achieved in the middle area. Most of it occurs at the centerline of the ramp.
- For the situation with full Mach effect the wave field between the wave reflectors is long crested. At the opening the crest is straight, while it becomes more and more curved as the waves approaches the exit. At the exit the crest almost has the shape of the ramp. A quantitative evaluation gives the impression that this phenomenon is extremely effective.

The shape of the ramp, and the reflection from it, seems to control the wave patterns, especially for the large wave situations. Moreover by running tests with a low wave peak period and a high significant wave height, it is concluded that the reflection has a significant influence on the degree of Mach reflection. With large wave heights, and thereby heavy overtopping resulting in low reflection, the Mach effect is very dominating.

Photos that illustrate these effects are presented in appendix *I.2 Photos of the composite system*.

## 9.3.2 Reflection and incoming wave height

The reflection is measured in two positions, namely in front of the ramp and in front of one of the wave reflectors (cf. **Figure 9.1**). The results from the middle and side measurements are assumed to represent the conditions in the mid 40 % of the width and 30 % of the width on each side respectively. The reflection coefficients for the middle and side sections are shown in **Figure 9.3**.

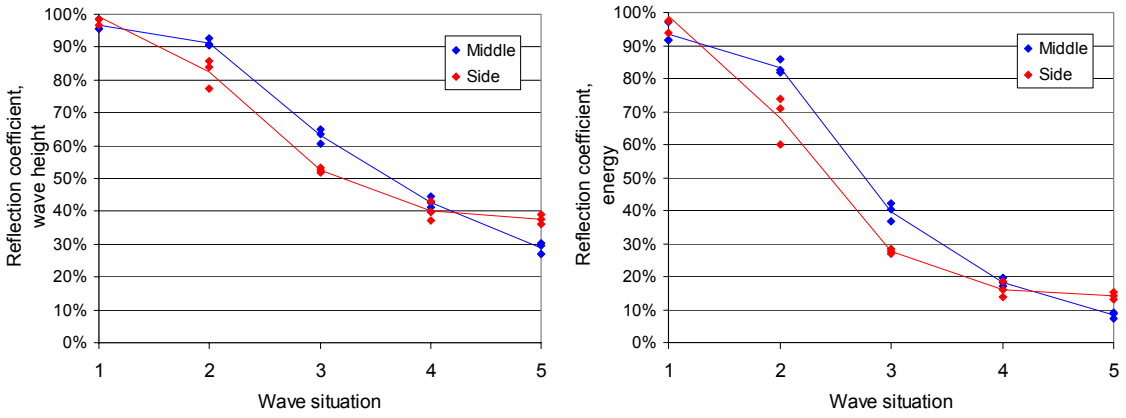


***Figure 9.3:*** *Reflection coefficients in the middle (positioned in front of the ramp) and side (positioned in front of one of the wave reflectors) corresponding to the wave peak periods of the 5 wave situations. The coefficients are shown with regard to wave height and energy to the left and right graph respectively. The lines are the mean values while the points are the actual values.*

Comparing the results in **Figure 9.3** with the reflection coefficients without the ramp (cf. section *6.3.2 Incoming wave field*, **Figure 6.3**) it is seen that the variation over the wave situations has increased. Without the ramp the reflection coefficients with respect to energy are between 15 – 25 % for the mid and

15 – 50 % for the side section. Moreover the distribution between the reflection in the mid and side section has also changed.

Of course placement of the ramp will generally increase reflection. Though, some factors will diminish the reflection:

- Transmission – as the wave peak period increases the transmission under the wave reflectors and the ramp increases. The transmission under the ramp, however, is larger because it has less draught.
- Overtopping – with increasing wave peak period, but especially with significant wave height the relative overtopping increases. As the wave energy is converted into potential energy (or heat) in the basin, less energy is of course reflected.
- Energy loss – as the significant wave height increases due to focusing, the highest waves will start breaking. Using the relationship for shallow foreshore //Van der Meer et. al., 1994// mentioned in appendix *F.3 Reduction factors* it is seen that both situations 4 and 5 will loose a significant amount of energy due to wave breaking. Moreover for wave situations 4 and 5 some of the largest waves topped over the wave reflectors.

Thus the small wave situations will generally have a high degree of reflection, while the large wave situation will dispose of the energy in the WRA by the other means, i.e. transmission or energy loss.

These phenomena are also what control the distribution of reflection over the mid and side sections. The reflection coefficients for wave situation 1 is close to 100 % but in regard to the distribution between the mid and side section, wave situation 1 is considered unreliable because of the wave generation problems for small wave periods. Thus, except for wave situation 5, all reflection coefficients at the mid section are larger than at the side section. The change is due to the fact that the ramp is heavily reflective, but for wave situation 5 the overtopping of the ramp has resulted in a diminishing of the reflection in the mid section.

The reflection coefficients also clearly imply that the crest freeboard of the ramp is too high for the small wave situations.

The measurements show that the difference in reflection in the side and mid section is relatively small. This is very fortunate as the distribution between the mid and side section will control the incoming wave height over the width. It is desirable that the waves are 2-dimensional, which will not be the case if the reflection has a large variation over the width. The incoming significant wave heights at the mid and side section are compared to the weighed significant wave height in **Figure 9.4**. The weights are 40 and 60 % for the middle and side respectively (cf. section *6.3.2 Incoming wave field*). Notice that the horizontal gridlines are the desired incoming significant wave heights.

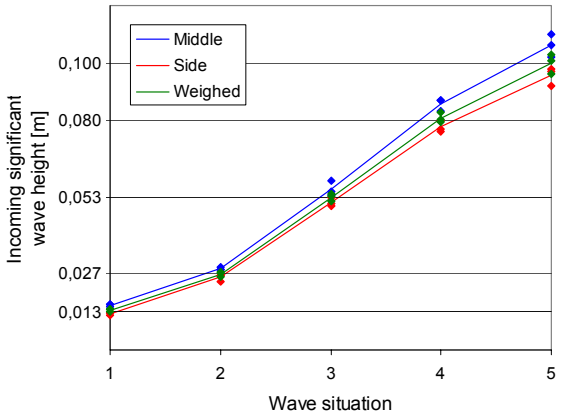


***Figure 9.4:*** *Incoming significant wave height measured in the middle (positioned in front of the ramp) and side (positioned in front of one of the wave reflectors) compared to the weighed (40 % of the middle and 60 % of the side)*

*incoming significant wave height. The horizontal gridlines are the desired incoming significant wave heights. The lines are the mean values, while the points are the actual values.*

Because of the small variation between the incoming significant wave height at the mid and side section the problem of unevenly distributed wave generation over the width is considered of minor importance.

## 9.4 Obtained potential energy

The amount of obtained potential energy is found by multiplying the experimentally found overtopping discharges with the crest freeboard (subtracted the rim height). The results for the 5 wave situations are shown in **Figure 9.5**. The energies in the graph to the left are absolute values while the energies in the graph to the right are weighed with the time of occurrence of each wave situation. In both graphs the results are compared to the expected values (cf. chapter *8. Experimental evaluation of the ramp profile*).

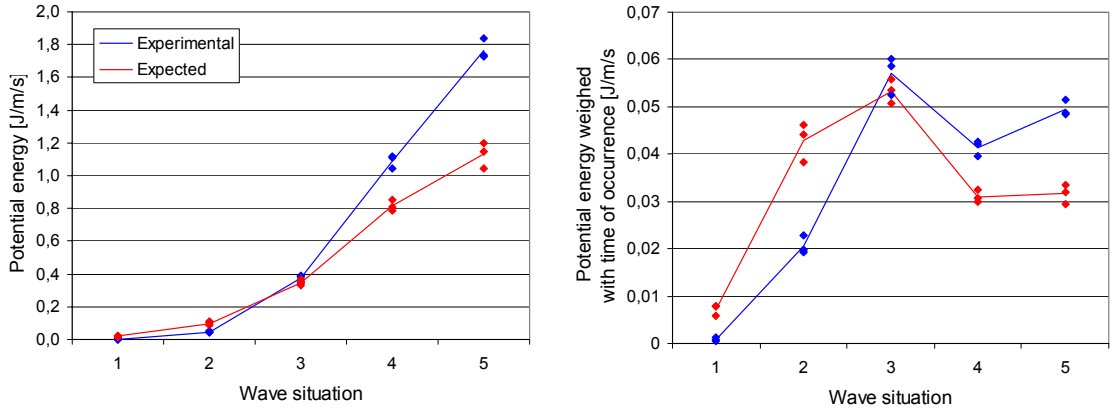


***Figure 9.5:*** *Obtained potential energy in the basin per unit width and time for the 5 wave situations. The energy found experimentally is calculated from the overtopping discharge with consideration to the rim height of 0,1/15 m. The expected amount of energy is found from the Van der Meer equation with Wave Dragon coefficients also with consideration to a rim height. The values are calculated using the significant wave height corresponding to the incoming significant wave height found in the laboratory test. The graph to the left shows the actual values while the graph to the right shows the energy weighed with the time of occurrence. The lines are the mean values, while the points are the actual values.*

The effects for the 5 wave situations scaled to the Nissum Bredning design and their respective contributions to the total energy are shown in **Table 9.2**.

| | Potential energy [J/m/s] | Contribution [%] | Occurring Probability [%] |
|---|---|---|---|
| Wave situation 1 | 1 | 0 | 24 |
| Wave situation 2 | 18 | 12 | 30 |
| Wave situation 3 | 50 | 34 | 11 |
| Wave situation 4 | 36 | 25 | 3 |
| Wave situation 5 | 44 | 29 | 2 |
| Sum | 149 | 100 | 70 |

***Table 9.2:*** *Potential energy weighed with time of occurrence.*

It is seen that wave situation 1 is of no importance, while wave situation 3 is the largest contributor to the total effect.

As shown in **Table 9.2** the 5 wave situations only cover 70 % of the time. Thus, the overall effect is found by multiplying by 0,70, cf **Table 9.3**.

| | Unit | Nissum design |
|---|---|---|
| Effect per unit ramp width | kW/m | 0,15 |
| Overall effect per unit ramp width (70%) | kW/m | 0,10 |
| Overall effect | kW | 2,43 |

***Table 9.3:*** *Effects for the Wave Dragon in the Nissum Bredning design (1:3).*

Setting the rim height at zero an effect of 3,0 kW can be achieved, i.e. 23 % higher.

Comparing the result to the expected overall effect a 3 % increase is seen. However, as shown in **Figure 9.5** the prediction for each wave situation vary significantly more. The reasons for this deviation are numerous. The ones, which are assessed to be most important, are:

- The wave height ratios used to calculate the expected effect might be inaccurate. Moreover, the wave height ratios are average increases of the significant wave heights at the opening and at the ramp, which might be a too simple measure. For wave situation 1 the numerical wave height ratio is used as the experimental is considered unreliable.
- The Wave Dragon coefficients in the Van der Meer formula are found for a cross section of the ramp profile using 2-dimensional waves. After focusing the waves are in fact short crested.
- In finding the Wave Dragon coefficients for the different wave situations the $H_s$-$T_p$ relation is approximated with an average value for wave situations 1 & 2 and situation 3, 4 & 5 respectively.
- The determination of the incoming wave is based on the two reflection coefficients at the position in front of the ramp and one of the wave reflectors respectively. Moreover, the calculation of the degree of reflection is based on 2-dimensional waves moving perpendicular to the model.

Although there are inaccuracies in both methods, the most reliable result is considered to be the experimental one.

## 9.5 Efficiencies of the Wave Dragon

From the distribution of the wave energy in Nissum Bredning the efficiencies are calculated. The results for each wave situation and overall are showed in **Figure 9.6**.

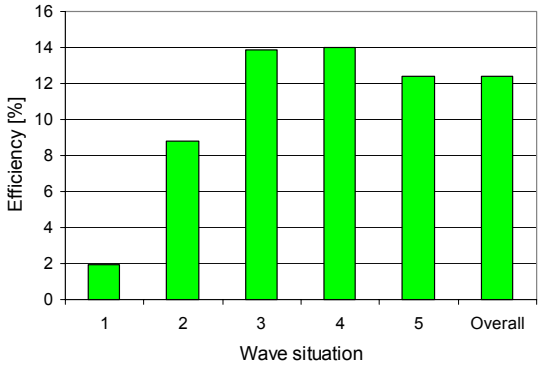


***Figure 9.6:*** *Efficiencies (the ratio between obtained potential energy and incoming energy) for the 5 wave situations and overall.*

## 9.6 Energy consideration

Considering the energy flow through the WRA it seems reasonable to set up an energy balance based on **Figure 9.7**.

It is assessed that the mean energy flux $E_f$ in the incoming and reflected waves can be found approximately from ( A.6 ).

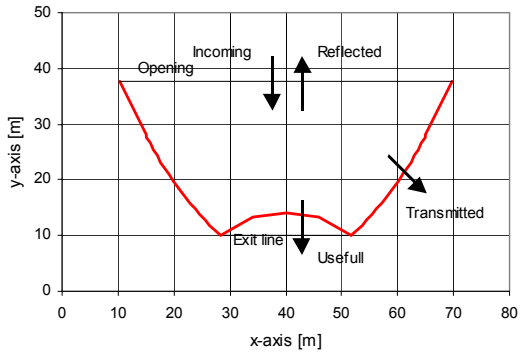


***Figure 9.7:*** *Distribution of the generated wave energy the reflectors are subjected to.*

The energy balance is:

$$E_{tot,incom.} = E_{tot,reflec.} + E_{tot,pot,basin} + E_{tot,trans.+loss} = E_{pot,out} \qquad (9.1)$$

where the total incoming energy $E_{tot,incom.}$ is found as:

$$E_{tot,incom.} = E_{f,incom.,middle} \cdot w_{ramp} + E_{f,incom.,side} \cdot w_{sides} \qquad (9.2)$$

and the total outgoing energy $E_{tot,out}$ is found as:

$$E_{tot,out} = E_{f,reflec.,middle} \cdot w_{ramp} + E_{f,reflec.,side} \cdot w_{sides} + E_{pot,basin} \cdot w_{ramp} + E_{tot,trans.+loss} \qquad (9.3)$$

All quantities are known except for the transmitted and lost energy $E_{tot,trans.+loss}$, which therefore is the balancing quantity. The distribution between transmitted and lost energy has not been measured. Instead the transmitted energy is calculated from the theoretical considerations in appendix *C. Transmission under the wave reflectors*. The lost energy comes from to contributions:

- loss in the WRA due to dissipation, wave breaking because of increasing wave height and overtopping of the wave reflectors.
- loss in the ramp/basin due to dissipation and non-exploited energy when the ramp crest freeboard is set below the optimal value.

For the 5 wave situations the energy distribution is shown in **Figure 9.8**.

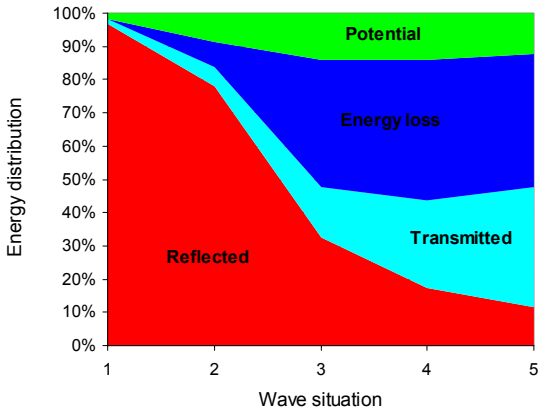


***Figure 9.8:*** *The graph shows the distribution of the incoming energy on reflected (red), transmitted (light blue), loss (dark blue) and potential energy (green) as a function of the wave peak period. The distribution between the transmitted and lost energy is found theoretically.*

Maximizing the amount of obtained potential energy is a matter of controlling the relationship between the amount of reflection and the energy loss. This is done by adjusting the crest freeboard. Considering

**Figure 9.8** it is seen that for situation 1 and 2 the reflected energy is too high due to a too high crest freeboard. Moreover, for wave situation 3 through 5 the efficiency is almost constant. This implies that the efficiency is more sensitive to adjustments of the crest freeboard for the low wave situations than for the high ones. This is in agreements with the findings in the experiment of the ramp profile, where it was found that situation 1 & 2 and situation 3, 4 & 5 are described by different overtopping coefficients.

## 9.7 Conclusion on the evaluation of the Wave Dragon

The model test of the composite system has one major cause of inaccuracy, namely the determination of the incoming significant wave height. Because of heavy reflection from both the model and the wave generator the waves must be analyzed to separate the measured wave into an incoming and a reflected wave. This is only performed in two positions, which therefore are assumed to describe the incident wave field. Moreover the analysis is only valid for 2-dimensional waves, i.e. waves which move in direction perpendicular to the model. Observing the wave field it seems that this measure is sufficiently accurate, as the waves in front of the model resemble 2-dimensional waves.

On this basis it is considered that the results from the analysis of the composite system is more accurate than the previous methods. This is quite important as the tests form the verification of the tools used in the previous chapters.

The result of the model test is an overall effect of 2,4 kW for the Nissum Bredning model. Thus the efficiency is approximately 12 %.

# 10. Summary and conclusion

The analysis of the Wave Dragon is first summarized. The used analytical, numerical and experimental tools are evaluated. Measures to optimize the efficiencies are presented and an efficiency is assessed.

## 10.1 The Wave Dragon in Nissum Bredning

In this report the overtopping converter Wave Dragon designed by EFM has been analyzed and evaluated. As compared to usual overtopping converters the Wave Dragon differs by being floating and especially by being equipped with floating pontoons for focusing the incoming waves.

The Wave Dragon is evaluated for placement in Nissum Bredning characterized by an average significant wave height of 0,34 m, an average wave peak period of 2,1 s, a water depth of 6,5 m and a time averaged mean energy flux of 358 J/m/s. For fitting these parameters the original design is scaled down using a length scale of 3.

A superficial movement analysis show that the hereby defined Nissum Bredning design has wave induced movements of a magnitude which is considered to be soluble. In the evaluation of the Wave Dragon the movements are neglected. All laboratory tests are made for a restrained structure.

## 10.2 Summary of tools used in the analysis

In this section the analytical, numerical and experimental tools are evaluated.

### *10.2.1 Methods for analyzing the wave reflectors*

The wave reflectors are evaluated by their ability to increase the average significant wave height at the exit of the WRA. This is expressed through a wave height ratio, where the value of 1 indicates no increase.

In the analytical method it is assumed, according to Green's Law, that the waves are not reflected, i.e. an energy conservation approach is applied. For a curvature of 1,2° (angle between elements) the result is a wave height ratio between 1,58 to 1,41 for the wave situations 1 through 5.

Next step is using a numerical method based on the mild slope equation. As the model is 2 dimensional (plan view) the energy transmission under the wave reflectors is modeled as absorption of energy. The degree of absorption is determined through a theoretical consideration of the energy distribution over the water depth, based on linear wave theory and a narrow banded spectrum. For a curvature of 1,2° the result of the numerical method is a wave height ratio between 1,92 and 1,32 for the wave situations 1 through 5.

In verifying the numerical results a model of the wave reflectors is investigated experimentally. Usually laboratory tests are made with a high degree of precision but due to heavy reflection of the model, the wave height ratios are determined by separating the wave fields into incoming and reflected waves. This reflection analysis is based on an assumption of 2 dimensional waves which observations support. For a curvature of 1,2° the result is wave height ratios from 1,71 to 1,32 for the wave situations 1 through 5. Due to problems in generating the wave field for situation 1 it is discarded.

All results are shown in **Figure 10.1**, where they are compared to the significant wave heights without the wave reflectors.

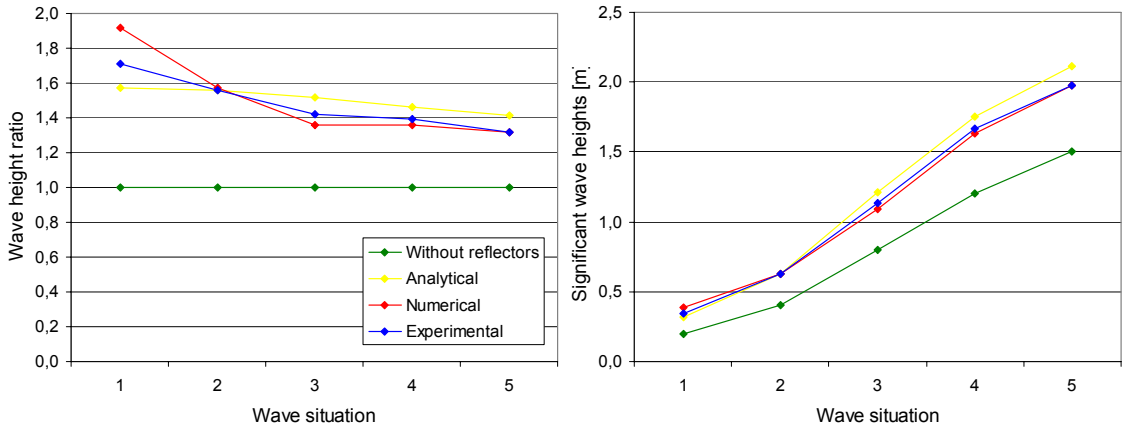


***Figure 10.1:*** *Focusing by the wave reflectors (curvature of 1,2°) expressed through wave height ratios and actual incoming wave heights for the 5 wave situations.*

Thus in general all methods are in agreement, especially the numerical and the experimental methods. It is seen that except for situation 1 and partly for situation 2, the results indicate that the energy consideration used in the analytical method is in fact applicable. This is due to the increasing influence of the Mach effect for increasing wave situation.

The deviations are due to the fact that:

- Both the analytical and numerical methods are based on the theoretically determined transmission under the wave reflectors.
- In the analytical and numerical method the wave reflectors have infinite height. Observations of the laboratory test show that the highest waves top over the wave reflectors.
- In the experimental tests the incoming wave field is determined by a reflection analysis in two points in front of the wave reflectors.

In full all three analyses substantiates each other, which makes the final result relatively reliable. For the further work it has been chosen to use the numerical ratio for wave situation 1 and the experimental ratios for wave situation 2 through 5.

### Adjustments to the EFM design

Through the numerical runs different designs are investigated for wave situation 3 with full reflection of the wave reflectors.

The wave reflectors are investigated for:

- starting angle of 40 and 45°.
- different curvatures.
- introduction of a curvature-change.

The tests show that as long as the design is reasonable the adjustments are of minimal influence. All wave height ratios are between 1,5 and 1,6. EFM has proposed a constant curvature of 1,0°. This is changed to a constant curvature of 1,2° to obtain a more perpendicular wave attack on the ramp.

## *10.2.2 Method for analyzing the ramp profile*

The ramp profile is evaluated from its ability to maximize the obtained potential energy in the basin, i.e. the amount of overtopping with consideration to the crest freeboard.

The method of analyzing the ramp profile is based on an overtopping expression developed by Van der Meer. The Van der Meer formula is not designed for the conditions of the Wave Dragon, i.e. reduced draught and heavy overtopping. Thus laboratory tests are performed. It is discovered that, for the Wave Dragon, the Van der Meer formula is only valid for a constant relationship between the significant wave height and the wave peak period.

Using the found wave height ratios and reducing the overtopping by a factor 0,9 due to oblique wave attack the Van der Meer formula (under consideration to the different $H_s$-$T_p$ relations) predicts an effect of 2,4 kW for a fixed crest freeboard of 0,5 m.

### Adjustments of the ramp profile

Through the laboratory tests alternatives to the design of a ramp with a straight slope of 40° have been investigated:

- The ramp has been investigated for slopes of 35, 45, 50 and 60°.
- The ramp has been investigated for different curvatures, e.g. the profile proposed by EFM.

The results showed that the overtopping was significantly decreased for angles of 60°, but otherwise unchanged.

Tests have been made for curvature at the bottom and top of the ramp profile, respectively. No effect is achieved. Furthermore the profile proposed by EFM has been tested. This reduces the overtopping, especially for small discharges.

The design of the profile proposed by EFM is rejected. Instead a straight profile with a slope angle of 40° is chosen.

## *10.2.3 The analysis of the composite system*

To verify the methods of analysis and to obtain a more precise efficiency of the Nissum Bredning design a laboratory test of the composite system (i.e. wave reflectors and basin part) is performed. As for the tests with the wave reflectors, the results are based on an identification of the incoming wave field, under consideration to heavy reflection of the model.

The tests have been performed for all of the 5 wave situations. The results are shown in **Figure 10.2**.

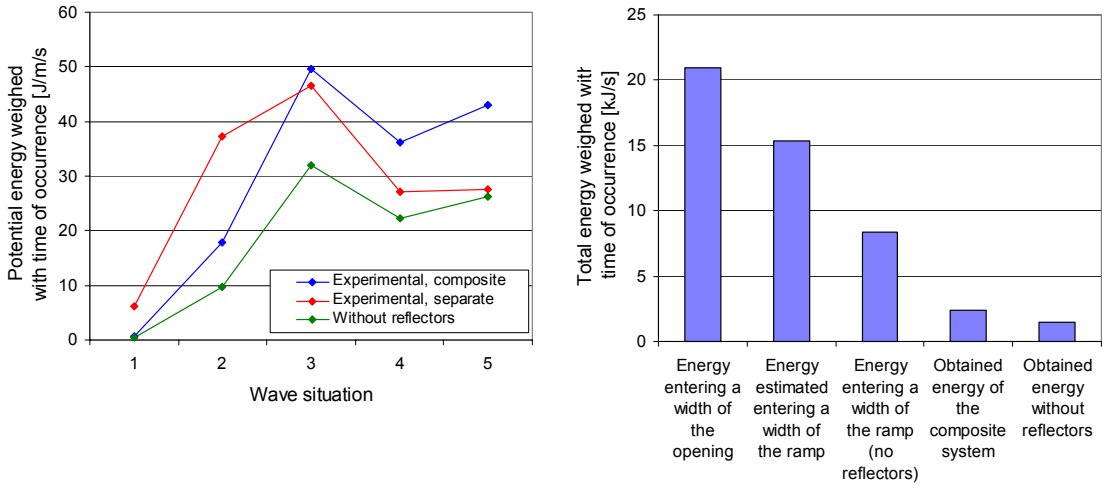


***Figure 10.2:*** *The graph to the left shows the obtained potential energy for the Wave Dragon with and without the wave reflectors, respectively. The graph to the right shows the energy in Nissum Bredning compared to the obtained energy with and without the wave reflectors. The estimate on the energy entering a width of the ramp (focused energy) is made by assuming that the ramp relatively lets the same amount of energy over, when taking oblique wave attack into consideration.*

In **Figure 10.2 right** the energy entering a width of the opening and the ramp, respectively is compared to the average obtained energy found from the experiment with the composite system and the experiment with the ramp (i.e. without wave reflectors).

From **Figure 10.2 left** it is seen that the expected obtained potential energy calculated from the wave height ratios and the Van der Meer formula is close to the results from the experimental tests with the composite system. In calculating the potential energy for the ramp (without reflectors) the coefficients are changed. Hereby the increase due to the wave reflectors is relatively limited. This only applies for the Nissum Bredning design. In the North Sea the increase is expected to be significant.

Although the overall results for the separate and composite systems are almost equal the distribution from each wave situation are different. This is assessed to be caused by:

- The Wave Dragon coefficients for the different wave situations are determined from average values of the $H_s$-$T_p$ relation for wave situation 1 & 2 and wave situation 3, 4 & 5 respectively.
- Because the overtopping is a non-linear function of the significant wave height the wave height ratios (average increases in significant wave heights) is an inaccurate measure for calculating the overtopping. Large deviations from the average, the average being the same, will result in more overtopping than a small deviation.
- The reduction in overtopping due to oblique wave attack is set to 0,9 corresponding to an average angle of 30°, which might be wrong. Observations lead to the conclusion that due to the Mach effect the angle is too low for the small wave situations and too high for the large wave situations.

From the results in **Figure 10.2 left** it can be concluded that wave situation 1 is without importance. Even with optimization it is practically needless to use the Wave Dragon during this time. This means that the Wave Dragon only needs to be operative in less than half (46 %) of the time.

## 10.3 Comparing the methods

There are 3 different methods in finding the wave height ratios, but only one way of predicting the overtopping. Comparing the results from the experiments with the composite system and the ramp (without reflectors) the effects and efficiencies are shown in **Figure 10.3**.

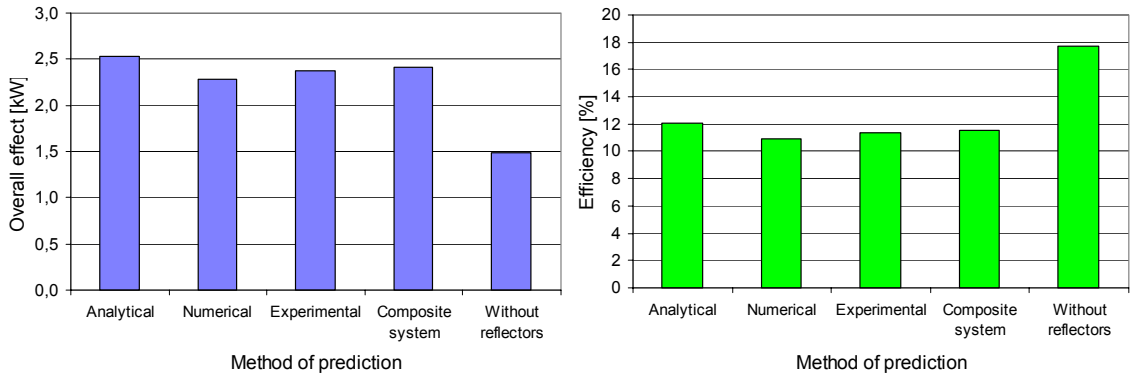


***Figure 10.3:*** *The graph to the left shows the obtained potential energy calculated in different ways and compared to the experimental tests for the composite system and the ramp (without wave reflectors). The graph to the right shows the corresponding efficiencies. The method for finding the wave height ratios are termed analytical which is found by the energy consideration, numerical which is based on the mild slope model and experimental which is from the laboratory tests. All effects are calculated for a fixed crest freeboard of 0,5 m in all wave situations.*

Although the analytical method for the wave reflectors only gives a slight deviation it can not be recommended to determine the wave height ratios by this mean only. The method is too primitive as it only applies when the wave pattern is dominated by the Mach effect. However, it is assessed that the numerical method is sufficient for determining the wave height ratios.

Notice that the efficiency for the ramp (without reflectors) is higher than for the composite system, which implies that the wave reflectors are ineffective. This is of course not completely true. It is due to the fact that the wave reflectors can not increase the overall effect by a value corresponding to the opening ratio.

## 10.4 Suggestions for improvements

The efficiency of 12 % for the composite system is considered relatively low. Some measures can be taken to increase the obtained potential energy:

- The analysis of the ramp profile showed that the optimal fixed crest freeboard is about 0,71 m. In the analysis of the composite system a fixed crest freeboard of 0,50 m was used, which lowered the obtained potential energy by approximately 5 %.
- Adjusting the crest freeboard according to the wave situations will increase the obtained potential energy. It is estimated that it hereby is possible to achieve an approximate 20 % increase.
- Increasing the height over MWL of the wave reflectors and thereby avoiding frequent overtopping of the wave reflectors for the largest waves. The exact increase in obtained potential energy has not been determined, but 10 % is estimated by increasing the overtopping of wave situation 4 and 5 with the factors 1,05 and 1,20 respectively.
- Increasing the draught of the ramp from 2,0 to 2,5 m will decrease transmission under the ramp and increase in obtained potential energy. Theoretical considerations and experimental tests indicate a 10 % increase.
- In the analysis a rim height (height from the MWL of the basin to the crest freeboard) of 0,1 m has been used. The rim is considered necessary due to movements of the Wave Dragon and unequal distributed overtopping. If the rim can be neglected by some kind of mechanism the obtained potential energy can be increased by more than 20 %.

Thus exploiting the increases of all the measures the effect can be written up by a factor of approximately 1,8. This results in an efficiency of about 22 %. This is quantity seems on the high side, especially the last point will be difficult to take advantage of. By further optimization a reasonable efficiency is assessed to approximately 18 %.

## 10.5 Generalizing the results

Transferring the Wave Dragon from Nissum Bredning to another location, e.g. the North Sea, involves scaling the wave conditions. This cannot be done directly as the following must be taken into consideration:

- the wave conditions of Nissum Bredning are described by a peak enhancement factor of 6,5 as the waves are highly fetch limited. This is not the case in the North Sea where the peak enhancement factor is around 3,3.
- the $H_s$-$T_p$ relation increases the overtopping coefficients. Hereby all wave situations are described by the same coefficients, corresponding to the low situations in Nissum Bredning. This increases the potential energy by almost 40 %.

Considering that if it is possible to achieve an efficiency of approximately 18 % in Nissum Bredning this is increased by 40 % in the North Sea. Hereby the overall efficiency is 25 %, corresponding to a net efficiency of 20 % (at 80 % efficiency of the turbines).

EFM sets the time averaged mean energy flux of the North Sea to 15 kJ/m/s. Hereby a net effect of about 550 kW is achieved. This efficiency is about 20 % smaller than expected by EFM.

## 10.6 Recommended next steps in the development

In relation to the analyses in this report it is recommended to investigate the following:

- Thoroughly investigation of the movements of the Wave Dragon in different wave situations. If the wavelength is only a fragment of the length of the Wave Dragon it is reasonable to expect that the movements are negligible. How long should this length of the Wave Dragon be?
- Overtopping discharges distributed over the time. For keeping a small rim height the overtopping should be relatively constant. Moreover the crest freeboard and the turbines must be adjusted accordingly. How large should the basin be for a relatively constant and small rim height with a given optimal crest freeboard?
- Wave motion and resonance in the basin due to wave overtopping discharges and movements of the basin part. The former and be reduced by curving the upper part of the ramp. How problematic are these movements and how are they reduced without compromising the efficiency?

In addition to this the optimizing points of section *10.4 Suggestions for improvements* and the wave forces, anchoring etc. should be investigated.

## 10.7 Concluding remarks

In the analyses of the Wave Dragon only minor adjustments have been made on the wave reflectors. Their curvature has been slightly increased and it is recommended to increase their height over MWL to avoid energy loss due to frequent overtopping.

The analysis of the ramp showed that the profile proposed by EFM is unfavorable. By using the developed profile a 20 % increase in overtopping can be achieved. Moreover, it is demonstrated that adjusting the crest freeboard to fit the occurring wave situations is advantageous.

Comparing the above systems and extrapolating to the North Sea it is demonstrated that an increase of 130 % can be achieved by equipping the Wave Dragon with the wave reflectors.

For predicting the effectiveness of the wave reflectors it is found that the numerical program is a useful tool. Moreover, for predicting the overtopping of the ramp Van der Meer's formula has been modified for use with heavy overtopping.

The experimental tests of the Wave Dragon in the Nissum Bredning design shows an overall efficiency of 12 %. Reasonable measures are assessed to increase this to approximately 18 %. Furthermore there are instances for expecting a 40 % increase for a placement in the North Sea as compared to Nissum Bredning. Thus a total overall efficiency of 25 % corresponding to an approximately 20 % net efficiency is within reach. Considering the electricity price given by EFM it seems possible to produce electricity at a cost in the vicinity of 1 dkr./kWh. This is comparable to other non-nuclear energy resources.

# References


//P. S. Andersen & T. Klindt, 1994// *Random wave propagation – based on the Mild-Slope equation*, M. Sc. graduate report in Civil Engineering, P. S. Andersen & T. Klindt, Aalborg University 1994.

//M. Brorsen, 1996// *Notat om Mild Slope ligningen*, M. Brorsen, Institut for Vand, Jord og Miljøteknik, Aalborg Universitet, December, 1996.

//Danske Meteorologisk Institut, 1971// *Klimatologiske meddelelser, Danmarks klima i vind*, Danske Meteorologisk Institut, 1971.

//EFM, 1997// Correspondence with E. Friis-Madsen, Löwenmark, 1997.

//EMU, 1997// Correspondence with H. C. Sørensen, Energy & Miljø Undersøgelser (Energy & Environmental Consultancy), 1997.

//Ingeniøren, 1997// The articles "*Wave Dragon æder bølgernes energi*" and "*Bølgekraft ude i verden*", Ingeniøren, nr. 4, 24. januar 1997.

//A. T. Ippen, 1966// *Estuary and coastline hydrodynamics*, A. T. Ippen, Ph. D., Engineering Societies Monographs, 1966.

//Kort- og matrikelstyrelsen, 1993// *Den danske havnelods,* Kort- og matrikelstyrelsen, 23. udgave, 1993, ISBN 87-7450-085-6.

//I. Langen et. al., 1979// *Dynamisk analyse av konstruksjoner*, Ivar Langen, Ragnar Sigbjörnsson, SINTEF, Avdeling for konstruksjonsteknikk, TAPIR, 1979, ISBN 82-519-0362-9.

//Löwenmark, 1995// *Building and Testing a Scale Model of the Offshore Wave Energy Converter KBL*WPD1 "Wave Dragon"*, K. B. Loewenmark I/S, Danish Hydraulic Institute, Rasmussen & Schioetz Oest A/S, Ossberger-Turbinenfabrik GmbH + Co, Biwater Hydro Power, March 1995.

//Löwenmark, 1997// *Ansøgning til Energistyrelsens udviklingsprogram for vedvarende energi m.v.*, Löwenmark, FRI, E. Friis-Madsen, Feb. 1997.

//Van der Meer et. al., 1994// *Wave run-up and wave overtopping at dikes*, Jentsje W. van der Meer, Johannes P. F. M. Janssen, article to published in ASCE Wave forces on inclined and vertical wall structures, Ed. Z. Demirbilek, 1994.

//NTH// *Bølger på dypt og grunt vann*, Institutt for Havnebyggning, Universitet i Trondheim, Norges tekniske Høgskole.

//NYTEK// *Nye fornybare energikilder*, Norges forskningsråd NYTEK.

//T. Sarpkaya & M. Isaacson, 1981// *Mechanics of Wave Forces on Offshore Structures*, T. Sarpkaya & M. Isaacson, Van Nostrand Reinhold Company, New York, 1981. ISBN 0-442-25402-4.

//Sea Power, 1992// *Sea Power AB – prospectus*, Nordic Conference Concerning Wave Energy, 8. – 9. maj 1992 in Hanstholm, Denmark.

//U. S. Army, 1977// *Shore Protection Manual*, U. S. Army Coastal Engineering Research Center, Third Edition, 1977.

//Waveλength, 1995// *Waveλength – Newsletter of the European Wave Energy Network*, Issue no. 3. Spring 1995.

# Appendix

# A. Wave conditions

The wave conditions of Nissum Bredning are found through wind data. As there are no observations from the broad itself, the wind data at the nearby lighthouses of Vestervig, Thyborøn and Bovbjerg are used. All 3 lighthouses are located within a 20 km radius. The Danish Meteorological Institute has published wind speeds in the 8 main directions (N, NE, E, SE, S, SW, W and NW) from the year 1931 to 1960 //Danske Meteorologisk Institut, 1971//. All wind data is measured according to the Beaufort's scale. No homogeneity tests have been carried out, and all measurements are subject to the influence of human estimation, both in regard to wind strength and direction. At Thyborøn there has been 32.830 observations (average of 3,0 per day), at Vestervig 32.852 observations (average of 3,0 per day) and at Bovbjerg 52.045 observations (average of 4,8 per day).

The wind velocities at a standard height of 10 m above open flat ground, equivalent to the Beaufort's scale, are converted to wave heights and wave periods at the chosen position of the Wave Dragon.

An important factor is the fetch, which is calculated from the method described in //U. S. Army, 1977//. **Figure A.1** shows a sketch of Nissum Bredning with markings of the fetch in the main directions.

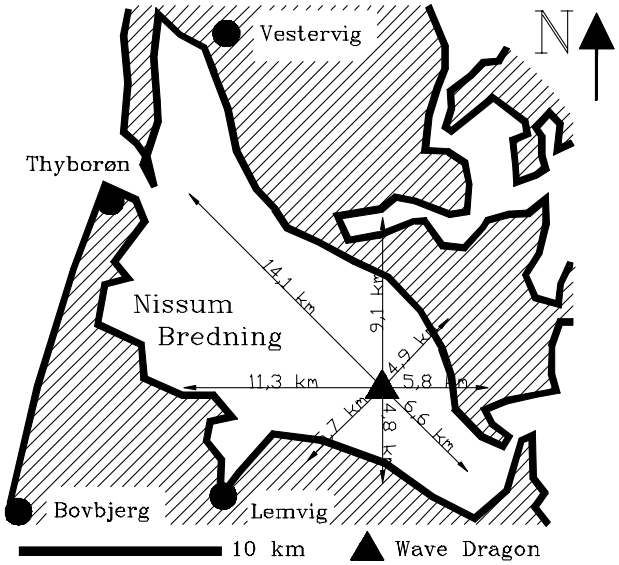


***Figure A.1:*** *Map of Nissum Bredning with markings of fetch in the main directions (N, NW, W, SW, S, SE, E and NE).*

All waves are considered fetch limited, as the time limit in the worst case with wind from NW at a velocity of 1,5 m/s is less than 5 hours. At a wind speed of only 3,3 m/s the time is about 3 hours.

The conversion of the wind velocities into significant wave heights and peak wave periods respectively is done by use of empirical expressions found from field data //U. S. Army, 1977//. Consideration is taken to whether the waves are regarded as deep or shallow water waves. In the calculations the water depth is set to 6,5 m. This is considered allowable as the areas with shallow water is in the western part, where the waves are in the beginning of their growing up.

## A.1 Distributions of significant wave heights and peak periods

The significant wave heights are divided up into appropriate intervals, and the probabilities belonging to the respective significant wave height interval are added. The result is a correlation between a significant wave height interval and the probability of encountering a significant wave height within the interval. This is shown in **Figure A.2**.

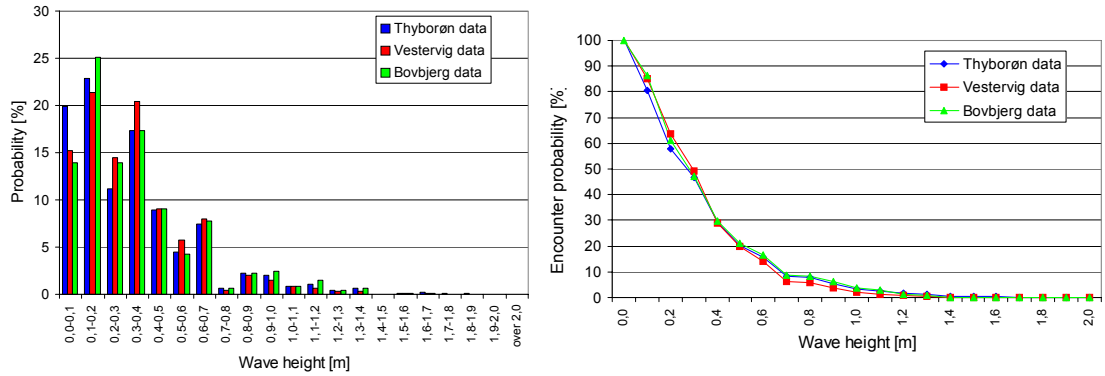


***Figure A.2:*** *Probability of having a significant wave height within the intervals (to the left) and encounter probability (to the right) at the location of the Wave Dragon. Based on wind data from Thyborøn, Vestervig and Bovbjerg lighthouses, respectively.*

From the calculations it is found that the maximum measured wind velocity during the 30-year time period is converted to a significant wave height of 1,87 m. Though, it is most likely to have a significant wave height in the interval between 0,1 and 0,2 m. The average significant wave height is 0,34 m.

The same procedure is carried out for the wave peak periods, and the result is shown in **Figure A.3**.

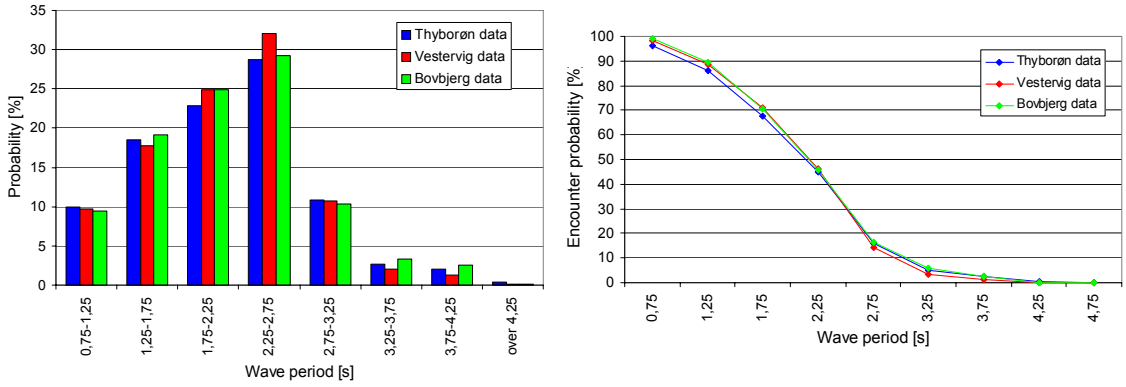


***Figure A.3:*** *Probability of having a wave peak period within the intervals (to the left) and excess probability (to the right) at the location of the Wave Dragon. Based on wind data from Thyborøn, Vestervig and Bovbjerg lighthouses, respectively.*

From the calculations it is found that maximum measured wind velocity is converted to a wave peak period of 4,6 s, equivalent to a wavelength of 29 m. Moreover a wave peak period of 2,5 s (equivalent to a wavelength of 9,7 m) is most likely with an occurrence of about 30 % of the time. The average wave peak period is 2,1 s.

A correlation between the wave peak period and the significant wave height is found from the wind data at the 3 lighthouses. This is seen in **Figure A.4**.

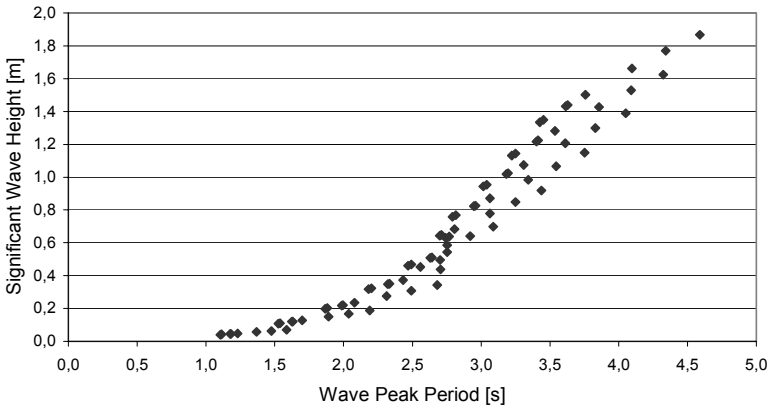


***Figure A.4:*** *Correlation between wave peak period and significant wave height at the location of the Wave Dragon. Based on wind data from Thyborøn, Vestervig and Bovbjerg lighthouses. All wave directions are included.*

The scatter is due to the difference in fetch in the 8 main directions. Furthermore there is a discontinuity at a wave peak period of 2,9 s as this is the limit between shallow water and deep water.

## A.2 Wave breaking

It is investigated at what wave height the waves start breaking.

The Stokes Wave Theory gives the limiting condition for wave breaking due to wave steepness:

$$H_{break} = 0{,}142 \cdot L_{break} \cdot \tanh\left(\frac{2\pi h_{break}}{L_{break}}\right) \qquad (A.1)$$

Calculating the wave length at the breaking point $L_{break}$ from the wave peak period, and using the constant water depth of 6,5 m, the wave height at the breaking point $H_{break}$ is above 2 $H_s$ for all situations seen in **Figure A.4**. Thus, statistically only one out of every 3.000 waves will break due to wave steepness, that is $H_{break} = H_{0,3‰}$, where $H_{0,3‰}$ is the wave with a height that is only exceeded by 0,3 ‰ of the waves. Thus wave breaking due to wave steepness is not considered to limit the wave heights.

The Solitary Wave Theory gives the limiting condition for wave breaking due to decrease in water depth:

$$H_{break} = 0{,}78 \cdot h_{break} \qquad (A.2)$$

For the water depth of 6,5 m this gives a wave height at the breaking point of 5,1 m. Thus wave breaking due to decrease in water depth is not considered to limit the wave heights.

## A.3 Energy distribution

The significant wave height and wave peak period distributions in **Figure A.2** and **Figure A.3** are combined in a mean energy flux distribution. Under the assumption of a Rayleigh distribution of the wave heights the following relation is valid:

$$H_s = 4{,}0 \cdot \sqrt{Var[\eta(t)]} \Rightarrow Var[\eta(t)] = \frac{H_s^2}{16} \qquad (A.3)$$

Thus, the energy density is found as:

$$E = Var[\eta(t)] \cdot \rho_w g = \frac{1}{16}\rho_w g H_s^2 \qquad (A.4)$$

As the energy propagates with the group velocity the mean energy flux (energy transmitted through a vertical section of unit width averaged over a wave period) is found from:

$$E_f = E \cdot c_g \qquad (A.5)$$

Approximation the group velocity for the irregular wave field with the regular expression for a period equal to the wave peak period the mean energy flux is found from:

$$E_f \cong \frac{1}{16}\rho_w g H_s^2 \cdot \frac{1}{2} c_{T_P}\left[\frac{2k_{T_P}h}{\sinh(2k_{T_P}h)}\right] \qquad (A.6)$$

where

$c_{T_P}$ [m/s] phase velocity corresponding to the wave peak period.

$k_{T_P}$ [m$^{-1}$] wave number corresponding to the wave peak period.

Thus, a mean energy flux can be found for a combination of the significant wave height and wave peak period. Using the relation between these two wave parameters (cf. **Figure A.4**) the mean energy flux is found as a function of the wave peak period, cf. **Figure A.5 left**. By multiplying the mean energy flux for each wave peak period interval with the probability of occurrence (cf. **Figure A.3 left**), the time averaged mean energy flux is found to 358 J/s/m. While the mean energy flux is an average over a wave period in a given wave condition (short time), the time averaged mean energy flux is the average of the mean energy flux over all wave conditions (long time). This distribution is shown in **Figure A.5 right**.

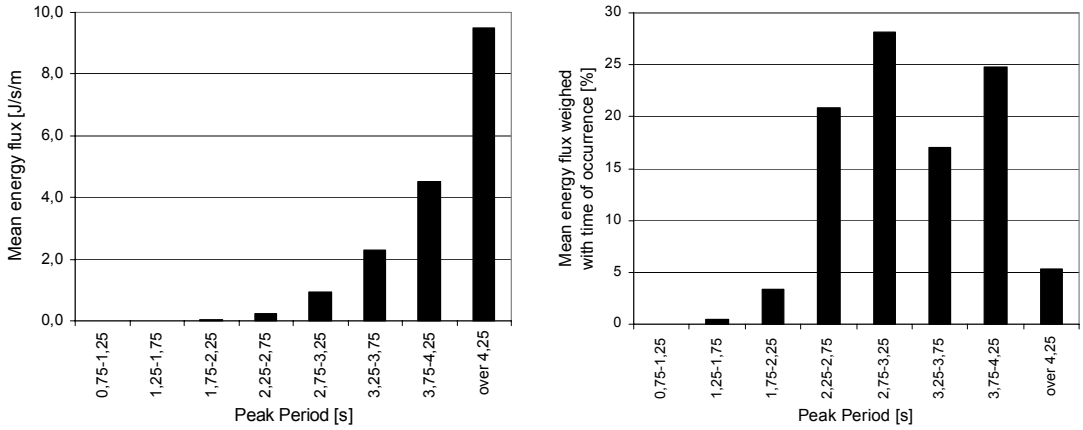


***Figure A.5:*** *Mean energy flux distributed over the wave peak period (graph to the left) and time averaged mean energy flux distributed on wave peak periods given in percentage (graph to the right). The time averaged mean energy flux is 358 J/s/m.*

Thus, it is seen that the wave conditions included in the interval from $T_p$ = [1,75 ; 4,25] make up 94 % of the mean energy flux.

# B. Analysis of wave-generated movements

In connection with determining an appropriate length scale for scaling the North Sea design of the Wave Dragon to fit the placement in Nissum Bredning, an analysis of the wave-generated movements of the basin part of the Wave Dragon is performed. This analysis is the subject of this appendix.

## B.1 The analysis approach

The analysis consists of numerical calculations of the added mass, hydrodynamic damping and forces on the floating body. A numerical solution of the thereby given equations of motions for a harmonic load, results in time series of the movements. From these time series the amplitudes of the movements can be related to the incoming wave amplitude. By performing these calculations for a number of different periods in the neighborhood of the peak periods corresponding to the occurring wave situations, response functions from wave to movement are obtained.

For the numerical calculations of the added mass, hydrodynamic damping and forces on the floating body a computer program called ShipSim is used. The program is developed by Michael Brorsen and Hans Enggrob, Department of Civil Engineering, Aalborg University, 1995. The computer program is based on potential theory, assuming that the waves at boundaries of the floating body can be described by one potential function. This potential function is made up of three separate components – one descending from the incoming waves, another from the scattered waves caused by the presence of the body, and at last a component descending from the movements of the body //T. Sarpkaya & M. Isaacson, 1981//.

The numeric solution of the equations of motions is based on Newmarks β-method //I. Langen et. al., 1979//.

## B.2 Parameters used in the movement analysis

The movement analysis is performed for a simplified version of the design of the basin proposed by EFM. Thus, the basin is modeled with horizontal sides and a reduced draught since the open grate bottom is neglected. The draught is selected to 3,3 m so it corresponds to the displacement for the used water plane area.

As input to the ShipSim program an element mesh of the basin part of the Wave Dragon is established. The mesh is shown in **Figure B.1**.

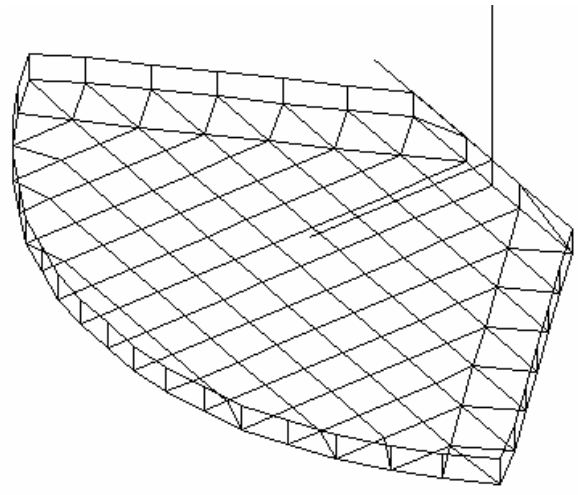

***Figure B.1:*** *The element mesh model of the basin part of the Wave Dragon used in the numerical calculations of added mass, hydrodynamic damping and forces.*

Furthermore a number of parameters are used in the analysis. These are shown in **Table B.1**.

| | | |
|---|---|---|
| Mass | $M$ [$10^3$ kg] | 7.000 |
| Area of waterplane | $A$ [$m^2$] | 2.100 |
| Moment of inertia of the cross section area in the waterplane | $I$ [$10^3$ $m^4$] | 240 |
| Mass moment of inertia of the cross section area in the waterplane | $I_m$ [$10^6$ kg $m^2$] | 500 |
| Displacement | $D$ [$m^3$] | 7.000 |
| Metacenter distance | $m_1$ [m] | 34 |

***Table B.1:*** *Parameters used in the movement analysis of the basin part of the Wave Dragon.*

The mass used in the analysis is the mass estimated by EFM, and includes 1.000 tons of water in the basin, cf. **Table 1.1**. The mass moment of inertia is based on an assumption of equally distributed mass over the area. The displacement is set to level the mass. The metacenter distance is found by using:

$$m_1 \cong \frac{I}{D} \qquad (B.1)$$

## B.3 Results of the movement analysis

By the performed analysis the response functions from waves to heave and pitch movements, respectively, are found. In **Figure B.2 left** the results are presented for the full-scale North Sea design proposed by EFM, while **Figure B.2 right** shows the results scaled with a length scale of 3 to fit Nissum Bredning. Furthermore the JONSWAP-spectrum for a typical wave period in the North Sea and Nissum Bredning respectively is shown.

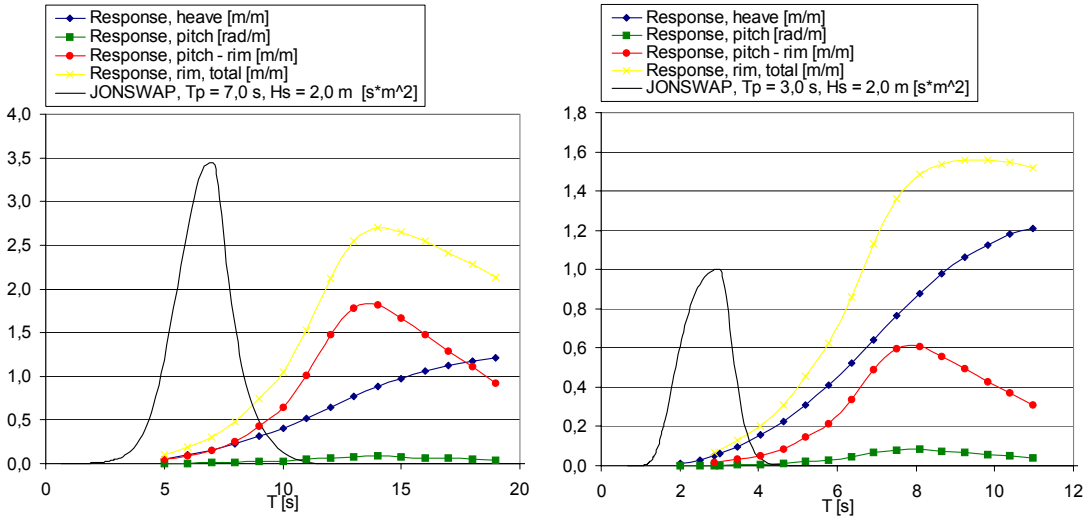


***Figure B.2:*** *Response functions from waves to heave and pitch movements (blue and green respectively). The figure to the left is the results of the analysis of the full-scale design. To the right the results are scaled corresponding to a length scale of 3. The red lines are the vertical movement of the rim of the ramp descending from pitch (the distance from center of gravity to the rim is set to 20 m in the full-scale design). The yellow lines are the sum of the red and blue lines, and thus the total vertical response at the rim of the ramp, disregarding any effects of phase shifts. The black lines represent the spectrum with a peak period corresponding to a typical wave situation.*

In addition to the response functions, the natural periods for heave ($T_{0,heave}$) and pitch ($T_{0,pitch}$) are found. This is done by solving the equations of motion for a situation without any loads, but with an initial displacement in the DOF for which the natural period is wanted. Then, the natural period is found by a zero-down crossing analysis of the calculated time series. This way the natural periods for heave and pitch shown in **Table B.2** are found.

| | North Sea design | Nissum Bredning design |
|---|---|---|
| $T_{0,heave}$ | 16,0 | 9,2 |
| $T_{0,pitch}$ | 12,3 | 7,1 |

***Table B.2:*** *Natural periods in heave and pitch in North Sea and Nissum Bredning design (length scale 3), respectively.*

These natural periods seem to agree with the response functions in **Figure B.2**. The natural periods for both heave and pitch are considered close to the peak periods of the occurring wave situations. This means that choosing the lowest of the considered length scales (3 – 6 according to **Table 2.2**) is reasonable, since a larger scale will entail that the natural periods are moved even closer to the occurring wave periods.

In the calculation of the total vertical movement at the rim shown as the yellow lines in **Figure B.2**, it is assumed that there are no phase shift between heave and pitch. Actually, the phase shift between the wave elevation and heave is –5° to 10°, while the phase shift between the wave elevation and pitch is 100° to 130° for the different wave situations. This means that the total movement of the rim is less than indicated on **Figure B.2**. Taking these phases into account the movement of the rim is found to be as shown in **Figure B.3**, where it is shown together with the wave elevation at the rim.

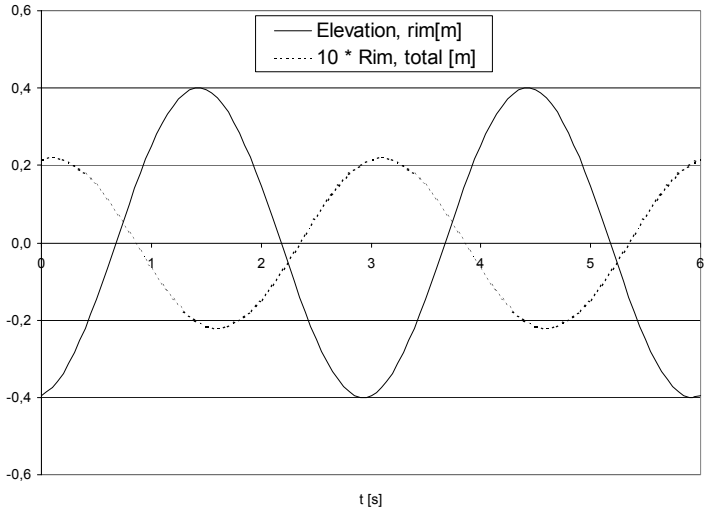


***Figure B.3:*** *Wave elevation (continuous line) and vertical response at the rim (dotted line) for the scaled design corresponding to wave situation 3, T = 3 s and H = 0,8 m. The response is exaggerated with a factor of 10.*

From **Figure B.3** it is seen that the total vertical movement of the rim is very close to be in counter phase with the wave elevation at the rim. This is considered optimal since the rim of the basin will be in the lowest level almost at the same time as a wave crest passes. Thus, the movement in fact increases the amount of water captured in the basin in this situation. For larger wave periods (and hereby wavelengths) this effect will decrease since the elevation and the total vertical movements becomes closer to be in phase. Therefore, to be on the safe side, it is decided not to take this effect into account. Thus it is desirable to minimize the movements of the rim.

In **Table B.3** the amplitudes of the responses in heave, pitch, the vertical movements of the rim descending from pitch and the total vertical movements of the rim for the 3 largest wave situations are shown.

| Wave situation | Wave peak period [s] | Wave amplitude [m] | Amplitude heave [m] | Amplitude pitch [rad] | Amplitude rim, pitch [m] | Amplitude rim, total [m] |
|---|---|---|---|---|---|---|
| 3 | 3,0 | 0,40 | 0,024 | 0,0011 | 0,008 | 0,022 |
| 4 | 3,5 | 0,60 | 0,060 | 0,0026 | 0,019 | 0,054 |
| 5 | 4,0 | 0,75 | 0,117 | 0,0051 | 0,037 | 0,095 |

***Table B.3:*** *Amplitudes of the responses in heave, pitch, the vertical movements of the rim descending from pitch and the total vertical movements of the rim.*

From **Table B.3** it is seen that both the movements in heave and the total vertical movements of the rim is small for situation 3, and situation 1 and 2 are therefore not considered. In situation 4 and 5 the movements becomes relatively large. Considering situation 5 the total vertical movements at the rim is close to 0,1 m, which means that the "effective" wave height is reduced by about 15 %, if phase shifts

between the movements and wave elevations at the rim are disregarded. This means that the wave-generated movements are significant, at least for the largest wave situation.

However, some of the used simplifications imply that the movements are overestimated. These are the following:

- The fact that the wave reflectors are connected to the basin will reduce the movements.
- The fact that all the sides of the basin are not vertical as modeled, will entail a larger added mass and thus also a reduction of the movements.
- The fact that the bottom is not modeled with open grates as in the real construction also entails a reduction of the movements. Movements will force water to pass the grates and thus function as dampers.
- Only regular waves have been considered.

How grave the overestimation of the movements is, is not investigated and should be subject to further analysis. However, this will not be done in this report.

## B.4 Conclusions on the analysis of wave generated movements

From the performed movement analysis it is seen that the wave-generated movements of the basin part of the Wave Dragon are insignificant for the first 3 wave situations. For wave situation 4 and 5 the wave generated movements might be so large that they will cause a decrease in efficiency compared to a restrained basin. However, some of the simplifications imply that the movements probably are overestimated. Furthermore the wave elevations and the movements at the rim are not in phase. Therefore it is concluded that the movements are of a magnitude where it is reasonable to assume that they can be diminished considerably by further investigations and adjustments of the design. Thus in the following analyses it is assumed that the construction is restrained. Although the reflectors have not been subjects of a movement analysis, it is assumed that they are restrained as well.

On this background it is determined to use a design of the Wave Dragon based on the design proposed by EFM, scaled with a length scale of 3. This design will in the following be referred to as the Nissum Bredning design.

# C. Transmission under the wave reflectors

As described in section *1.2 Specifications of the Wave Dragon*, the wave reflectors are floating "pontoons", and thus do not extend to the sea bottom. This results in only a partial reflection of the incoming wave energy.

The expression for the reflection coefficient as a function of the draught of the wave reflectors is found by evaluation of the energy transmission beneath a regular wave. It is assumed that all energy within the draught of the reflectors is fully reflected, while all energy beneath this point is transmitted under the wave reflectors. Experimental tests indicate that this approach gives a qualitative agreement, and for an infinite water depth there is an average difference of 15 % between theory and experiment //A. T. Ippen, 1966//.

Through a physical consideration of this theory, it is estimated that the reflection coefficients are on the high side as the theory presumes irrotational flow, i.e. no account for energy loss.

The energy flow through a vertical cross section is found by integration over depth. The mean over a wave period (the mean energy flux) is, according to linear wave theory, given as:

$$E_f = \frac{1}{16} \cdot \rho_w g H^2 c \cdot \left(1 + \frac{2kh}{\sinh 2kh}\right) = E \cdot c_g \qquad (C.1)$$

If energy flow instead is integrated over a limited draught:

$$E_{f,d}(t,d) = \int_{-d}^{0} p^+ u \, dz \Rightarrow E_{f,d}(d) = E \cdot c_g - \frac{1}{2} E \cdot c \cdot \frac{\sinh 2k(h-d) + 2kh - 2kd}{\sinh 2kh} \qquad (C.2)$$

Thus the right hand side of ( C.2 ) is the reflected mean energy flux, while the last term on the right hand side is the mean energy flux under the level *d*, i.e. the transmitted mean energy flux.

The reflection coefficient with respect to energy is defined as:

$$K_{r,E} \equiv \frac{E_{f,d}(d)}{E_f} = 1 - \frac{c}{2c_g} \cdot \frac{\sinh 2k(h-d) + 2kh - 2hd}{\sinh 2kh} \qquad (C.3)$$

The reflection coefficient with respect with wave heights is found as:

$$K_{r,H} = \sqrt{K_{r,E}} \qquad (C.4)$$

If ( C.3 ) and ( C.4 ) are applied at the chosen position of Wave Dragon with water depth of 6,5 m, **Figure C.1** is found.

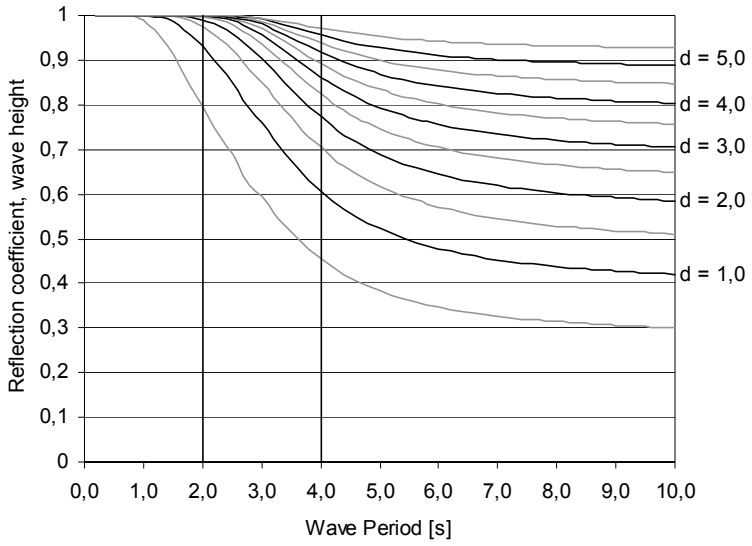


***Figure C.1:*** *Reflection coefficients with respect to wave heights at 6,5 m water depth as function of wave period for different draughts of the wave reflectors, d. Notice wave period limits 2,0 s and 4,0 s corresponding to the considered wave situations.*

EFM's proposed design for the wave reflectors has a draught of 8,0 m for the 16 sections near the basin (length of 65,0 m) and 6,0 m for the outer section (length of 30,0). Using the scale factor of 3 gives the draughts of approximately 2,5 m and 2,0 m, respectively. For the wave period area of interest, it is seen that these draughts are reasonable.

A problem arises when generating irregular waves, as they have different wave periods, but this is neglected. The reflection coefficients are chosen in accordance to the wave peak periods. The used reflection coefficients are seen in **Table C.1** for the 5 wave situations.

| | | Reflection coefficients | | | |
|---|---|---|---|---|---|
| | | Wave height coefficient $R_{r,H}$ | | Wave energy coefficient $R_{r,E}$ | |
| Wave situation | Wave period [s] | Draught: 2,0 m | Draught: 2,5 m | Draught: 2,0 m | Draught: 2,5 m |
| 1 | 2,0 | 0,99 | 1,00 | 0,98 | 0,99 |
| 2 | 2,5 | 0,96 | 0,98 | 0,92 | 0,96 |
| 3 | 3,0 | 0,90 | 0,94 | 0,82 | 0,88 |
| 4 | 3,5 | 0,84 | 0,88 | 0,70 | 0,77 |
| 5 | 4,0 | 0,77 | 0,82 | 0,60 | 0,68 |

***Table C.1:*** *Reflection coefficient with respect to wave height and wave energy in the wave period interval.*

# D. Design scheme

The ranges in which the numerical analysis will be performed are found by investigating the reflection patterns of different values of the varied parameters (starting angle, curvature and curvature-change).

In order to minimize the energy loss due to reflection out through the opening and to focus as much energy as possible, the limits of consideration are set according to the following criterions:

1. the waves should only be redirected by the wave reflectors once after which they should have a general direction towards the ramp.
2. the opening ratio and angle ratio of the wave reflectors should be as large as possible.

Furthermore it is advantageous if:

3. after the waves are redirected by a wave reflector, they should be in phase with both each other and with the waves which propagate directly towards the ramp.
4. the direction of propagation should be perpendicular to the ramp.

The reflection pattern in **Figure D.1** shows the design proposed by EFM, i.e. a constant curvature of 1,0°. Only the reflections of the left wave reflector are drawn. The blue reflection lines are placed between each of the elements.

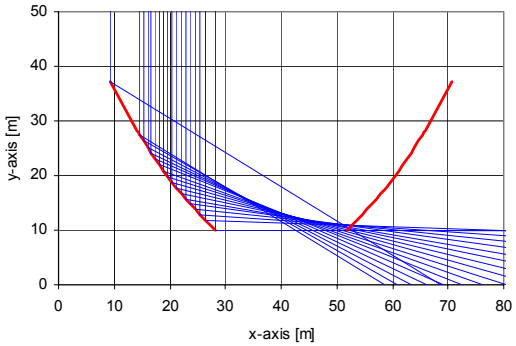


***Figure D.1:*** *The reflection pattern using a curvature equal to 1,0° as proposed by EFM. Opening ratio of 2,62 and angle ratio of 0,64.*

In **Figure D.2** two examples of designs failing the criterions are shown. The design to the left is violating criterion number 1, since much of the wave energy is reflected twice and thereafter redirected out of the WRA through the opening. The design to the right fails criterion number 2, as very little energy enters the WRA. In the model runs the validity of the criterions is rendered probable through these two examples.

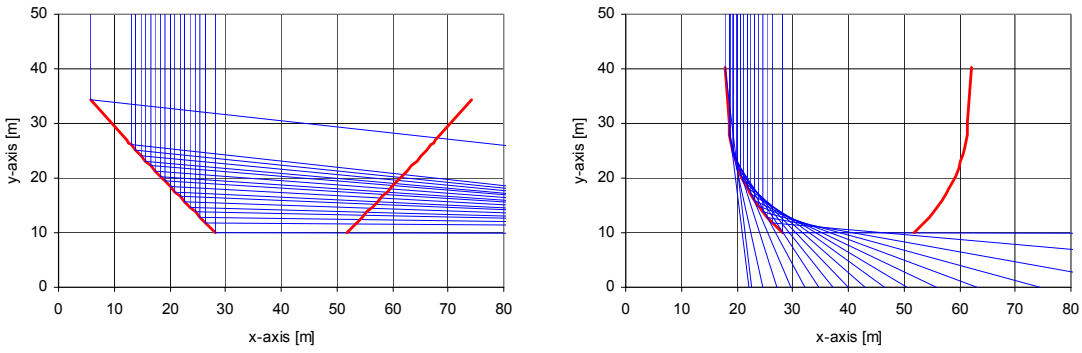


***Figure D.2:*** *The reflection patterns using curvatures equal to 0,2° (left side) and equal to 2,6° (right side). Opening ratios of 2,93 and 1,89 respectively. Angle ratios of 0,93 and 0,08 respectively.*

By rejecting patterns, which violate the first 2 criterions an area of interest can be delimited. Thus, patterns like the ones shown in **Figure D.2** are rejected, while patterns like the one in **Figure D.1** are accepted. The relevant combinations of curvature and change of curvature are illustrated in **Figure D.3**.

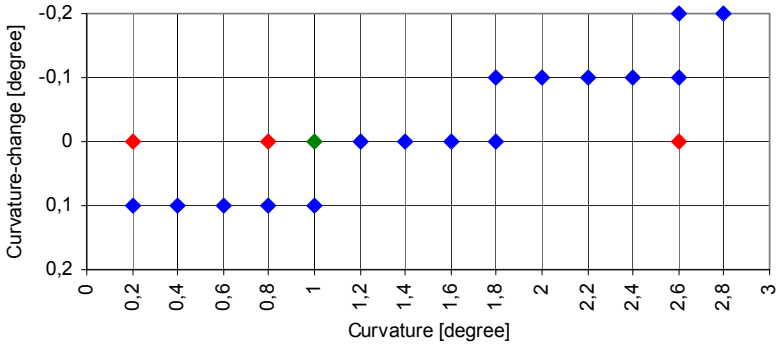


***Figure D.3:*** *Design scheme with the varied parameters, curvature and curvature-change for variations of 0,2° and 0,1° respectively. The blue spots mark the designs that fulfil the criterions of minimizing the energy loss due to either reflection out through the opening or transmission under the wave reflectors. The 2 red spots are the designs seen in* ***Figure D.2****. The green spot is the design proposed by EFM, which is seen in* ***Figure D.1****.*

Within the delimited band (blue points) the reflection pattern is further investigated with respect to the points 3 and 4.

The individual wave tracks (blue lines in **Figure D.1**) are considered in regard to angle of attack on the ramp and difference in length (and thereby phase shift compared to the directly incoming waves). It is found:

- For a constant curvature-change a higher curvature result in a more perpendicular wave attack and a low variation of the phase shifts (both between the individual reflected waves and between the reflected and directly incoming waves). This fact is of little usefulness, as the measure will vary the opening ratio, and thus the amount of energy entering the WRA, which is considered a more important factor.
- A lower curvature-change also results in a more perpendicular wave attack and a low variation of the phase shifts (both between the individual reflected waves and between the reflected and directly incoming waves). This adjustment can be done without altering the opening ratio and thus improve the effectiveness of the wave reflectors.

In average it is considered advantageous with low phase shifts between the individual reflected waves, as high phase shifts will reduce the superposed wave heights.

However, the consequence of the difference in length (and thus phase shifts) between the reflected and the directly incoming waves is dependent on their proportions compared to the wavelengths. For the considered wave situations in Nissum Bredning they are of the same magnitude. The maximum difference in lengths is ranging from 6 to 16 m for the considered designs of **Figure D.3** (blue points). The wavelengths corresponding to the wave peak periods range from 6 to 24 m for the 5 wave situations.

Thus for the largest wave situations it is considered advantageous with a low phase shifts (both between the individual reflected waves and between the reflected and directly incoming waves). This can be achieved by adjusting the curvature-change. For the lowest wave situations no general conclusion can be made.

The design scheme of **Figure D.3** and the criterions described above constitute the basis for the numerical analysis of the wave reflectors.

# E. Mild Slope numerical model

In this appendix the theoretical basis for the Mild Slope computer program used in chapter *5. Numerical analysis of wave reflectors* is described. The appendix is based on //M. Brorsen, 1996//.

## E.1 Conditions for the Mild Slope equation

Regarding the hydrodynamics it is assumed that:

- the fluid is ideal (inviscid and incompressible), i.e. no shear stresses and thus no boundary layer.
- the flow is irrotational.
- small wave steepness and wave heights, i.e. waves fulfilling $H/L << 1$ and $H/h << 1$.

Notice that there is no requirement for regular or 2-dimensional waves.

Concerning the geometry the only requirements are:

- water depth gradients are small.
- the bottom is impermeable.

## E.2 Basic equations and boundary conditions

As the fluid is irrotational, the velocity potential $\Phi$ is defined and describes the velocities $\underline{v}$ of the fluid by:

$$\underline{v} = \underline{\nabla}\Phi \qquad (E.1)$$

As the fluid is incompressible the velocity potential satisfies the Laplace equation:

$$\frac{\partial^2\Phi}{\partial x^2} + \frac{\partial^2\Phi}{\partial y^2} + \frac{\partial^2\Phi}{\partial z^2} = 0 \qquad (E.2)$$

Thus, the starting point is a boundary value problem (BVP), that is, solving the Laplace equation with some specified boundary conditions (BC), namely:

- The dynamic BC at the free surface: constant pressure at the surface.
- The kinematic BC at the free surface: a particle on the surface stays on the surface.
- The kinematic BC at the bottom: no flow through the bottom.

As the BVP is restricted to waves with small steepness and bottom slope the BC's are almost identical to the BC's of first order wave theory. The difference is that the BVP in first order wave theory is solved for constant depth and waves of constant form. Thus, for finding the Mild Slope equation the kinematic BC of first order wave theory at the bottom is solved at $z = -h(x,y)$, and the periodic BC of first order wave theory is rejected. Compared to the first order wave theory, this BVP lacks one BC, and thus the normal approach can not be undertaken. Instead an approximated separation of variables method using energy consideration is used to find the Mild Slope equation.

## E.3 Separation of variables

In solving the BVP it is assumed that the velocity potential can be separated into a function $\varphi$ which is independent of $z$, and a function $f$ which is independent of $x$ and $y$:

$$\Phi(x,y,z,t) = \varphi(x,y,t)\cdot f(z,h) \qquad (E.3)$$

The function determining the vertical variation $f(z, h)$ is approximated with the first order wave theory:

$$f(z,h) = \frac{\cosh k(h+z)}{\cosh kh} \qquad (E.4)$$

In choosing this expression a minor mistake is made, as the expression is weakly independent of $x$ and $y$ through $h(x,y)$. It is used anyway, as it is a good description of the distribution over the water depth.

Hereby it is now necessary to find a solution to the new function $\varphi$.

## E.4 Hamilton's principle

The Mild Slope equation is derivated using a principle from variational calculation called Hamilton's principle. For a mechanical system, the Lagrangian function $L$ is defined by:

$$L \equiv E_{kin} - E_{pot} \qquad (E.5)$$

Hamilton's principle states, that if the system, during the time interval $[t_1 , t_2]$, moves from one position to another, according to a function describing the so-called real movement, this will proceed in such a way that the integral:

$$\int_{t_1}^{t_2} L\,dt \qquad (E.6)$$

is stationary against small variations around this real movement. All other possible movements, caused by small variations to the real movements, but during the same time interval, are the so-called virtual movements. Hamilton's principle can be mathematically expressed by:

$$\delta \int_{t_1}^{t_2} L\,dt = 0 \qquad (E.7)$$

Physically, this means that the difference in potential and kinetic energy during a specific time is stationary to small changes in the path from two specific points. This can obviously only be upheld by the fact that only small variations are considered. Thus, the principle is a conservation of energy statement. In fact, Hamilton's principle can be interpreted as a reformulation of Newton's 2. law (N2).

As only small variations are useful the problem must lie in finding the real movements or movements very close to. This constitutes a variational problem, which is solved by knowing that ( E.7 ) is fulfilled if $L$ is the solution to the so-called Euler equation, where $L$ is a function of three independent variables $x$, $y$ and $t$, and one dependent variable $u(x, y, t)$:

$$L_u - \frac{\partial}{\partial x}\left(\frac{\partial L}{\partial u_x}\right) - \frac{\partial}{\partial y}\left(\frac{\partial L}{\partial u_y}\right) - \frac{\partial}{\partial t}\left(\frac{\partial L}{\partial u_t}\right) = 0 \qquad (E.8)$$

where the functions with subscripts are partial derivatives of the subscripts.

## E.5 Energy derivation

Before deriving the Mild Slope equation the expressions for potential and kinetic energy must be found. The potential energy in the area $A$ of a wave is:

$$E_{pot} = \int_A \left( \int_{-h}^{\eta} \rho_w g z dz \right) dA - \int_A \left( \int_{-h}^{0} \rho_w g z dz \right) dA = \int_A \left( \int_{0}^{\eta} \rho_w g z dz \right) dA = \int_A \tfrac{1}{2} \rho_w g \eta^2 dA \qquad (E.9)$$

In this expression the linearized Bernoulli equation at $z = 0$ is introduced:

$$E_{pot} = \int_A \tfrac{1}{2} \rho_w \tfrac{1}{g} \varphi_t^2 dA \qquad (E.10)$$

The kinetic energy in the area $A$ is found from:

$$E_{kin} = \int_A \left( \int_{-h}^{\eta} \tfrac{1}{2} \rho_w v^2 \, dz \right) dA \qquad (E.11)$$

For an assumed potential flow the velocity is found from:

$$v^2 = \Phi_x^2 + \Phi_y^2 + \Phi_z^2 \qquad (E.12)$$

The velocity potential is given by ( E.3 ) and ( E.4 ). The assumption of small wave steepness and wave height results in the following approximation for the kinetic energy:

$$E_{kin} = \int_A \tfrac{1}{2} \rho_w \left( (\underline{\nabla}\varphi)^2 \cdot A(kh) + \varphi^2 \cdot B(kh) \right) dA \qquad (E.13)$$

where

$$A(kh) = \tfrac{1}{2k} \tanh(kh) \left[ 1 + \tfrac{2kh}{\sinh 2kh} \right] = \tfrac{c \cdot c_g}{g} \qquad (E.14)$$

$$B(kh) = \tfrac{k}{2} \tanh(kh) \left[ 1 - \tfrac{2kh}{\sinh 2kh} \right] = \tfrac{\omega^2 - k^2 c \cdot c_g}{g} \qquad (E.15)$$

## E.6 Derivation of the Mild Slope equation

Now, Hamilton's principle can be written as:

$$\delta \int_{t_1}^{t_2} F dt = \delta \int_{t_1}^{t_2} \int_A \left( \tfrac{1}{2} \rho \left[ A(\underline{\nabla}\varphi)^2 + B\varphi^2 \right] - \tfrac{1}{2} \rho_w \tfrac{1}{g} \varphi_t^2 \right) dA \, dt = 0 \qquad (E.16)$$

This equation is fulfilled if the following expression is fulfilled in all points:

$$\delta \int_{t_1}^{t_2} G dt = \delta \int_{t_1}^{t_2} \left( A(\underline{\nabla}\varphi)^2 + B\varphi^2 - \tfrac{1}{g} \varphi_t^2 \right) dt = 0 \qquad (E.17)$$

Thus, the new Lagrangian function $G$ is equivalent to $F$ per unit of area, that is $G = F/A$.

Using the Euler equation ( E.8 ), where the function $L$ is replaced by $G$, and $u$ is replaced by $\varphi$, the result is:

$$B\varphi - \tfrac{\partial}{\partial x}\left( A\varphi_x \right) - \tfrac{\partial}{\partial y}\left( A\varphi_y \right) + \tfrac{1}{g}\varphi_{tt} = 0 \qquad (E.18)$$

Differentiation with respect to time and introducing the dynamic BC at the free surface, ( E.18 ) is rewritten as:

$$B\eta - \tfrac{\partial}{\partial x}\left( A\eta_x \right) - \tfrac{\partial}{\partial y}\left( A\eta_y \right) + \tfrac{1}{g}\eta_{tt} = 0 \qquad (E.19)$$

Both ( E.18 ) and ( E.19 ) are called the time dependent Mild Slope equation. Usually they are presented together with the dynamic BC at the free surface, and thus constitutes a two equation system:

$$\eta = -\tfrac{1}{g}\varphi_t \qquad (E.20)$$

$$\eta_t + \tfrac{\partial}{\partial x}\left( A\varphi_x \right) + \tfrac{\partial}{\partial y}\left( A\eta_y \right) - B\varphi = 0 \qquad (E.21)$$

The functions $A$ and $B$ are equations ( E.14 ) and ( E.15 ), respectively.

## E.7 Establishing the model – finite difference method

The mathematical problem described by the time dependent Mild Slope equations is impossible to solve analytically for the complex conditions in this report. Instead an approximate solution is found, by

discretization of the physical problem. Thus, the geometry is divided into a 2-dimensional grid of points with time as the 3rd dimension. It is chosen to apply the finite difference method.

First step in this process is discretization of the governing differential equations. The continuous functions $\eta$ and $\varphi$ are replaced by a finite number of values; one for each point in the grid. Thus, in the following the subscripts represents $x$,$y$-position, while the superscripts represents time $t$.

First the Mild Slope equations ( E.20 ) and ( E.21 ) are rewritten as:

$$\varphi_t = -g\eta \qquad (E.22)$$

$$\eta_t = B\varphi - A_x\varphi_x - A\varphi_{xx} - A_y\varphi_y - A\varphi_{yy} \qquad (E.23)$$

( E.22 ) and ( E.23 ) are discretized as:

$$\eta_{i,j}^{n+\frac{1}{2}} = -\frac{1}{g}\left(\varphi_t\right)_{i,j}^{n+\frac{1}{2}} \cong -\frac{1}{g}\frac{\varphi_{i,j}^{n+1}-\varphi_{i,j}^{n}}{\Delta t} \qquad (E.24)$$

$$\begin{aligned}\frac{\eta_{i,j}^{n+\frac{1}{2}}-\eta_{i,j}^{n-\frac{1}{2}}}{\Delta t} \cong\ & B_{i,j}\varphi_{i,j}^{n} \\ & -\frac{A_{i+1,j}-A_{i-1,j}}{2\Delta x}\cdot\frac{\varphi_{i+1,j}^{n}-\varphi_{i-1,j}^{n}}{2\Delta x} - A_{i,j}\frac{\varphi_{i-1,j}^{n}-2\varphi_{i,j}^{n}+\varphi_{i+1,j}^{n}}{\Delta x^2} \\ & -\frac{A_{i,j+1}-A_{i,j-1}}{2\Delta y}\cdot\frac{\varphi_{i,j+1}^{n}-\varphi_{i,j-1}^{n}}{2\Delta y} - A_{i,j}\frac{\varphi_{1,j-1}^{n}-2\varphi_{i,j}^{n}+\varphi_{i,j+1}^{n}}{\Delta y^2}\end{aligned} \qquad (E.25)$$

Notice that $n$ is an integer described by $t = n\,\Delta t$, while $i$ and $j$ are integers described by $(x, y) = (i\,\Delta x, j\,\Delta y)$.

Hereby an algorithm can be lined up, but before proceeding some preliminary considerations must be made:

- Choose time step interval $\Delta t$ and position step intervals $\Delta x$ and $\Delta y$.
- Define the geometry. In the following a square with lengths $r\,\Delta x$ and $s\,\Delta y$ is considered.

The procedure is described in the following algorithm:

1. Find $\varphi_{i,j}^{n}$ and $\eta_{i,j}^{n-\frac{1}{2}}$ at the time $n = 1$ and for all the points $(i, j) \in [0 ; r] \times [0 ; s]$. For a cold start all values are zero.
2. Next time step: $n \leftarrow n + 1$.
3. Calculation of $\eta$ for the time step $n$ in the points $(i, j) \in [1 ; r - 1] \times [1 ; s - 1]$. ( E.25 ) is rewritten to:

$$\begin{aligned}\eta_{i,j}^{n+\frac{1}{2}} = \eta_{i,j}^{n-\frac{1}{2}} + B_{i,j}^{*}\varphi_{i,j}^{n} \\ -\frac{1}{4}\left(A_{i+1,j}^{*}-A_{i-1,j}^{*}\right)\left(\varphi_{i+1,j}^{n}-\varphi_{i-1,j}^{n}\right) - A_{i,j}^{*}\left(\varphi_{i-1,j}^{n}-2\varphi_{i,j}^{n}+\varphi_{i+1,j}^{n}\right) \\ -\frac{1}{4}\left(A_{i,j+1}^{*}-A_{i,j-1}^{*}\right)\left(\varphi_{i,j+1}^{n}-\varphi_{i,j-1}^{n}\right) - A_{i,j}^{*}\left(\varphi_{i,j-1}^{n}-2\varphi_{i,j}^{n}+\varphi_{i,j+1}^{n}\right)\end{aligned} \qquad (E.26)$$

   where

$$A_{i,j}^{*} = \frac{A_{i,j}\Delta t}{\Delta x^2} = \frac{A_{i,j}\Delta t}{\Delta y^2} \text{ when } \Delta x = \Delta y \qquad (E.27)$$

$$B_{i,j}^{*} = \Delta t \cdot B_{i,j} \qquad (E.28)$$

4. Calculation of $\varphi$ for the time step $n$ in the points $(i, j) \in [0 ; r] \times [0 ; s]$. ( E.24 ) is rewritten to:

$$\varphi_{i,j}^{n+1} = \varphi_{i,j}^{n} - g \cdot \Delta t \cdot \eta_{i,j}^{n+\frac{1}{2}} \qquad (E.29)$$

5. Go to 2.

Notice that the calculation of $\eta$ only is done for the interval $(i, j) \in [1 ; r - 1] \times [1 ; s - 1]$, and thus the boundary points must be calculated in another way, namely by wave generation or reflection.

The procedure is sketched in **Figure E.1**. As it is seen, all values of $\eta$ and $\varphi$ are known at time step ½ and 1, respectively. Hereafter the calculations begin. The following example is one-dimensional, with the notation $\varphi$(position step, time step):

- The values of $\eta(i, 1½)$ is calculated from $\varphi(i - 1, 1)$, $\varphi(i, 1)$ and $\varphi(i + 1, 1)$ together with $\eta(i, ½)$.
- The value of $\varphi(i, 2)$ is calculated from $\varphi(i, 1)$ and $\eta(i, 1½)$.

Hereby the problem is clear that it is not immediately possible to calculate the new values at the boundaries (here the points at 0 and $r$ on the $x$-axis).

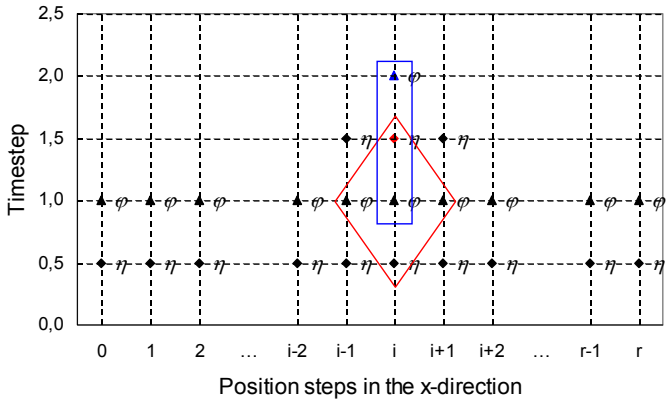


***Figure E.1:*** *Sketch for the calculation procedure of φ and η in one dimension. The red box encircle the values used to calculate the red point. The blue box encircle the values used to calculate the blue point.*

It is also seen that by having a shift in a half time step between the $\eta$- and $\varphi$-values, it is only necessary to use values one time step old in calculation of the new values.

## E.8 Wave generation

Wave generation is employed inside the boundaries by establishing a volume flux at a source. In the program the source is a line of boxes parallel to either the $x$- or $y$-axis.

Consider a source consisting of a line parallel to the $x$-axis. The wave to be generated has a phase velocity of $c$, an elevation $\eta$ and is propagating at an angle $\theta$ with the line of generation. The source is added with the volume flux $q = \eta c$ in both directions. The surface elevation $\Delta\eta$ to be added to the system in each box with the area $\Delta x\, \Delta y$ at each time step $\Delta t$ is thus:

$$\Delta\eta\, \Delta x\, \Delta y = 2c\eta\, \Delta t\, \Delta x \Rightarrow \Delta\eta = 2\frac{\Delta t}{\Delta y} c\eta \qquad (E.30)$$

The elevation from an irregular wave field is found by summation of $N$ regular waves:

$$\eta = \sum_{n=1}^{N} \frac{H_n}{2} \cos\left(\omega_n t + k_n y^* + \psi_n\right) \qquad (E.31)$$

where $\psi_n$ is a random phase shift and $y^* = y \sin\theta$.

Thus, from ( E.30 ) and ( E.31 ), $\Delta\eta$ is expressed as:

$$\Delta\eta = \frac{\Delta t}{\Delta y} \sum_{n=1}^{N} c_n H_n \cos\left(\omega_n t + k_n y^* + \psi_n\right) \qquad (E.32)$$

### *E.8.1 Irregular wave generation*

The velocity potential distribution over the water depth is assumed to be based on the first order wave theory. When using irregular waves this distribution is found from only one wave period, namely the wave carrier period (in this case set to the peak period). Thus, in generating the wave profile, an inconsistency is made when the JONSWAP spectrum is divided into a number of regular waves with different frequencies. The errors are displayed by generating regular waves with a given frequency, but with another carrier frequency (i.e. a velocity potential distribution based on another frequency). Hereby the generated wave heights and wavelengths are different from the theoretical corresponding to the given frequency. To prevent this mistake in the generation of irregular waves, wave generation calibration coefficients are multiplied to the wave heights and wavelengths.

The calibration coefficients are found by use of a test model in the MildSim program. The test model is made as a channel with full absorption in both ends, and with the same depth and element size as in the real model. Then, regular waves are generated with a frequency different from the specified carrier frequency and the hereby-obtained wave amplitudes or lengths are compared with the specified. The correction coefficient is then the ratio between the specified and the generated amplitude or length.

In finding these correction coefficients problems are encountered for frequencies lower than about 0,75 $f_P$ and frequencies higher than about 2 $f_P$. For these frequencies the model becomes unstable and these frequencies are thus neglected. The intervals are seen in **Figure E.2**, for the example $f_P$ = 0,4 s.

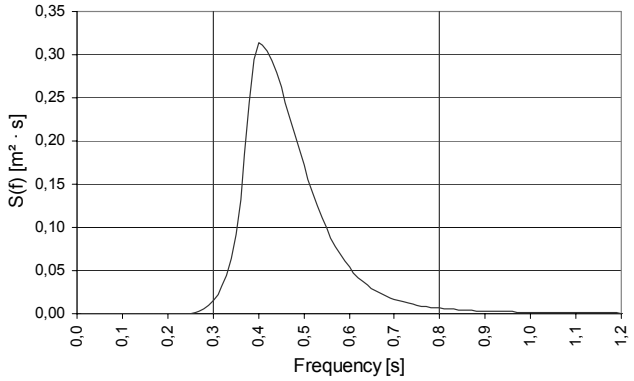


***Figure E.2:*** *JONSWAP-spectrum for a significant wave height of 1,0 m, a wave peak frequency of 0,4 s and a peak enhancement factor of 6,5. The two vertical lines are the limits for which the waves are generated in the computer program.*

From this it is seen that only a very small part of the wave energy is neglected.

## E.9 Wave reflection

Full reflection is obtained by ensuring that the flow through a boundary is zero, i.e. the gradient of the velocity potential is zero. Referring to **Figure E.1**, this is done by setting the unknown velocity potential for the boundary points, position step 0 and $r$, equal to the velocity potentials at 1 and $r - 1$, respectively.

To be able to obtain the values for all the position steps at the boundaries, all boundaries are regarded as full reflecting. If this does not consist with the reality, wave absorption is also employed.

## E.10 Wave absorption

Waves leaving the described domain are absorbed in so-called sponge layers. Mathematically a set of sponge layers is a number of position steps in front of a full reflection boundary for which factors are multiplied to both velocity potential and elevation or only the elevation.

The number of sponge layers $N$ and values of each factor $\zeta_n$ is crucial for obtaining the desired effect. The variation of the factors is described by ($1/\zeta_n$ is multiplied):

$$\zeta_n = (\zeta_{\max} - 1)\left(\frac{n}{N}\right)^P + 1 \qquad (E.33)$$

The variable $n$ is the sponge layer number and is thus an integer in the interval [0 ; $N$]. The first factor is $\zeta_1$ ($\zeta_0$ gives the value 1) while $\zeta_N$ is the factor to be multiplied to the values next to the boundary. An example of a variation is seen in **Figure E.3**.

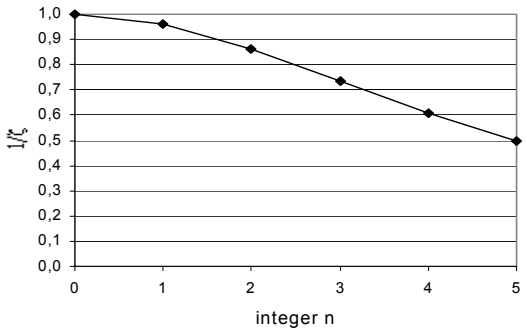


***Figure E.3:*** *Example of the variation of sponge layer factors. N = 5, $\zeta_{max}$ = 2 and P = 2. Boundary at n = 5.*

Good results are obtained with $N$ = 35 to 50, $\zeta_{max}$ = 1,3 and $P$ = 1,8. Though, in optimizing the wave reflectors only one sponge layer is used. Choosing the appropriate parameters, this gives satisfactory results.

## *E.10.1 Reflection coefficients in the computer model*

In the 2 dimensional computer model the wave reflectors are modeled as land. By equating the reflected energy flow of the original and the model design approximate consistency is obtained. Two ways of doing this is presented.

The reflection coefficients for the real system (characterized by transmission under the wave reflectors) are found theoretically in appendix *C. Transmission under the wave reflectors*, by considering the energy distribution over the water depth of a regular wave.

### Method 1: absorption

The wave reflectors in the computer model are equipped with "sponges" which absorb wave energy. Thus consistency is made by modeling the sponges in such a way that the energy that is transmitted under the wave reflectors instead is absorbed in the sponges on the wave reflectors.

The disadvantage is that there is no interaction between the waves inside the WRA and the waves propagating on the other side of the wave reflectors.

The reflection coefficients (for wave heights) used in the model are consistent with the desired within a value of ±0,01, which is unimportant compared to the uncertainties of the theory.

### Method 2: transmission

The other method is more troublesome to set up in the numerical program. In return interaction between waves on each side of the wave reflectors is made possible.

The wave reflectors are modeled with full reflection. To reduce the reflection "slots" are made in the wave reflectors according to the degree of reflection. For instance in order to obtain a 90 % reflection of wave energy (equivalent to a 95 % reflection of wave height) every $10^{th}$ element is removed.

The problem with the method is that diffraction will occur around the holes. Moreover to distribute the reduced reflection effect a very fine-meshed model is needed. This results in long calculation and setup times.

# F. Potential energy based on V. Meer's formula

Theoretical considerations are made on an overtopping formula developed by Van der Meer.

## F.1 Overtopping expression for dikes

On the background of appendix *G.1 Dimensional analysis* it is chosen to use an expression for overtopping at dikes in determination of the obtained potential energy in the basin of the Wave Dragon. The formula is developed by J. W. Van der Meer and J. P. F. M. Janssen in 1994. It applies to irregular waves.

### *F.1.1 Minimum slope of the ramp*

Two versions are available, namely for breaking and non-breaking waves, respectively. As it is the intention to convert the wave energy into potential energy in the basin of the Wave Dragon, energyloss due to breaking is to be avoided. This is done by having a steep slope of the ramp, expressed through a breaker parameter of more than 2,0.

The breaker parameter $\xi$ is defined as //Van der Meer, et. al., 1994//:

$$\xi_{op} = \frac{\tan\alpha}{\sqrt{s_{op}}} \qquad s_{op} = \frac{2\pi H_s}{gT_p^2} \tag{F.1}$$

where

$s_{op}$ wave steepness parameter

$T_p$ set to the wave peak period outside the WRA.

Thus the slope of the ramp $\alpha$ should be larger than:

$$\tan\alpha > \sqrt{s_{op}} \cdot \xi_{op} = \sqrt{\frac{8\pi H_s}{gT_p^2}} \tag{F.2}$$

For the 5 wave situations (cf. appendix *A. Wave conditions*) the minimum slope angle is about 30°.

If this is fulfilled the formula is dependent on the crest freeboard, significant wave height in the fundamental case. Reduction factors are included to describe variations from the fundamental case with respect to roughness of the dike, angle of wave attack, shallow foreshore and presence of a berm (cf. section *F.3 Reduction factors*).

### *F.1.2 Applicability of the formula*

The conditions, which must be fulfilled in order to use the formula for non-breaking waves, are not clearly defined for all parameters. Though the following requirements must be met:

- Applicability is that the ratio between the wave peak period and the mean period is between 1,1 and 1,25. Furthermore the wave peak period and the significant wave period should be almost equal.
- No application range is given for the crest freeboard. From the context of the formula it is clear that the crest freeboard over the significant wave height is useable within the range 0,5 to 4,0.
- For the overtopping discharge at least the range $10^{-5}$ to $10^{-2}$ times the square root of $g \cdot H_s^3$ is within the applicability.
- Dikes usually have slopes of the order 1:2 (equal to about 30°) or milder. Though the formula is also valid for vertical structures if a reduction factor 0,6 is multiplied to the overtopping discharge. The reduction factor for slopes between 30° and 90° is unknown.

- Expressing the slope, significant wave height and wave peak period through the breaker parameter the formula is valid for values from 2 to at least 4.

Thus considering the overtopping with respect to the Wave Dragon it is assessed to be necessary with an experimental verification, especially with respect to overtopping coefficients.

### *F.1.3 Overtopping formula for non-breaking waves*

For the ramp profile the following expression is used for determining the average overtopping discharge $q$ for non-breaking waves per unit time and width //Van der Meer et. al., 1994//:

$$q = a \cdot \sqrt{gH_s^3} \cdot \exp\left(-b \cdot \frac{R_c}{H_s} \cdot \frac{1}{\gamma}\right) \qquad (F.3)$$

where

$a$ and $b$ empirical coefficients depending on the geometry of the structure.

$\gamma$ combined reduction factors (minimum value is 0,5).

An expression proportional to the potential energy per time and width unit obtained in the basin is found from:

$$E^*_{pot,basin} = q \cdot R_c = a \cdot \sqrt{gH_s^3} \cdot R_c \exp\left(-b \frac{R_c}{H_s} \cdot \frac{1}{\gamma}\right) \qquad (F.4)$$

Maximizing the potential energy with respect to $R_c$ gives:

$$R_{c,opt} = \frac{\gamma H_s}{b} \qquad (F.5)$$

Thus the optimal $R_c$ is proportional to the significant wave height. For an optimal overtopping $q_{opt}$ the magnitude is equal to:

$$q_{opt} = a \cdot \sqrt{gH_s^3} \cdot \exp(-1) = 0{,}37 \cdot a \cdot \sqrt{gH_s^3} \qquad (F.6)$$

Using ( F.4 ), ( F.5 ) and ( F.6 ) it is seen that the maximum potential energy per unit time and width in the basin is dependent on the significant wave height:

$$E^*_{pot,basin,opt} = 0{,}37 \cdot \frac{a}{b} \cdot \gamma \cdot \sqrt{gH_s^5} \qquad (F.7)$$

Thus it is concluded that the optimal potential energy is proportional to power 5/2 of the significant wave height.

## F.2 Overtopping expression with consideration to a rim height

Taking movements of the basin part and wave overtopping volume distribution into consideration, a new parameter is introduced namely the rim height $r$, defined as the height from the MWL in the basin to the crest freeboard.

The expression ( F.3 ) giving the overtopping $q$ was introduced in section *F.1 Overtopping expression for dikes*. From this an expression proportional to the potential energy per time and width unit obtained in the basin is found. Taking a MWL in the basin that is lower than the crest freeboard into account, the result is:

$$E^*_{pot,basin} = q \cdot (R_c - r) = a \cdot \sqrt{gH_s^3} \cdot (R_c - r) \cdot \exp\left(-\frac{b}{H_s} \cdot R_c \cdot \frac{1}{\gamma}\right) \qquad (F.8)$$

Hereby the optimal crest freeboard is found to:

$$R_{c,opt} = \frac{\gamma \cdot H_s}{b} + r \qquad (F.9)$$

The maximum potential energy in the basin is:

$$E^*_{pot,basin,opt} = 0{,}37 \cdot \frac{\gamma \cdot a \cdot H_s}{b} \cdot \sqrt{g H_s^3} \cdot \exp\left(-\frac{b}{H_s} \cdot \frac{1}{\gamma} \cdot r\right) \qquad (F.10)$$

The optimal amount of potential energy obtained in the basin per unit time is found as:

$$E_{pot,basin,opt} = E^*_{pot,basin,opt} \cdot g\rho_w \cdot w_{ramp} \qquad (F.11)$$

where $E^*_{pot,basin,opt}$ is found from either ( F.7 ) or ( F.10 ).

# F.3 Reduction factors

Variations from the fundamental case with respect to roughness of the dike, angle of wave attack, shallow foreshore and presence of a berm are included through the reduction factors.

As no berm is present in front of the ramp this factor is neglected.

Notice that the reduction factors are within the exponential operator and thus are not linearly proportional with the overtopping discharge.

## *F.3.1 Roughness*

As the ramp is made of smooth concrete this is in agreement with the fundamental case. Thus, the reduction factor is 1,0 (no reduction) //Van der Meer et. al., 1994//.

## *F.3.2 Shallow foreshore*

Before calculating the overtopping for the significant wave height at the ramp, it must be ensured that the increase of the significant wave height, due to focusing by the wave reflectors, does not cause a degree of breaking waves that decreases the overtopping significantly. This is done through investigating the influence of a shallow foreshore, i.e. the increase in wave height due to focusing is equalized by a decrease in water depth.

No significant reduction of overtopping, due to wave breaking, occurs if the ratio of water depth at the toe of the structure to the significant wave height, is more than about 4 (deep foreshore), i.e. $h_{toe}/H_s \geq 4$ //Van der Meer et. al., 1994//. As the water depth at the location of the Wave Dragon is 6,5 m, this means that the wave breaking, due to focusing is unimportant for significant wave heights less than 1,6 m.

In finding the focused significant wave heights, wave height ratios are found numerically and experimentally. The wave height ratios found experimentally have of cause already taken wave breaking into account. Thus, no reduction factor is applied.

## *F.3.3 Angle of wave attack*

There are two cases of wave attack, namely short and long crested waves. In nature waves are usually short crested. Furthermore from the computer model runs and the experimental test series it has been observed that even if the waves are generated as long crested they will appear as short crested when they reach the ramp. The reduction factor for wave attack angle for short crested waves is found from //Van der Meer et. al., 1994//:

$$\gamma = 1 - 0{,}0033 \cdot \beta \qquad (F.12)$$

where

$\beta$ the angle of the wave propagation with the normal of the ramp in degrees.

Considering the reflection pattern an approximate estimate of the average angle of attack is set to about 30°. Thus, the reduction factor is 0,9.

## F.4 Overtopping coefficients

The overtopping coefficients are found from experimental results. In the article //Van der Meer et. al., 1994// the coefficients are set to 0,2 and 2,6 for *a* and *b* respectively.

The geometry of the ramp profile and the degree of overtopping are significantly different from the cases studied by Van der Meer. Thus it is considered necessary to perform laboratory tests with the ramp profile of the Wave Dragon to determine the overtopping coefficients *a* and *b*.

# G. Investigation of wave overtopping

The wave overtopping of the ramp profile is investigated in the laboratory tests and analyzed in the following.

The purpose for investigating the wave overtopping is for:

1. Predicting the overtopping of the ramp of the Wave Dragon.
2. Evaluating the adjustments for increasing overtopping.

## G.1 Dimensional analysis

In the investigation of the overtopping it is chosen to consider the overtopping as a function of the following independent parameters:

$$q = f(H_s, T_p, R_c, g) \qquad (G.1)$$

It is convenient if these parameters are made dimensionless. There are many ways of doing this. Through stepwise dimensional analysis a number of dimensionless overtopping formulas are found as functions of dimensionless parameters. The following expression is among these:

$$Q = \frac{q}{\sqrt{gH_s^3}} = f\left(\frac{R_c}{H_s}, T_p\sqrt{\frac{g}{H_s}}\right) \qquad (G.2)$$

The function $f$ is established by combining the dimensional parameters with different operators and coefficients.

Some boundary conditions must be fulfilled if the formulas are to be valid for all combinations of the significant wave height, the wave peak period and the crest freeboard, namely:

1. For a zero wave peak period or significant wave height the overtopping discharge should be zero.
2. For a zero crest freeboard the overtopping discharge should remain finite and nonzero.
3. For a large crest freeboard compared to the significant wave height the overtopping discharge should be zero.

The 3rd boundary condition is mostly important for small overtopping discharges. Thus as large overtopping amounts are desirable the second requirement is the primary boundary condition in regard to the crest freeboard.

### *G.1.1 Fitting an expression for overtopping*

Laboratory test series are used to investigate the applicability of the different formulas. The overtopping discharge $q$ is found for a variation of the crest freeboard $R_c$, wave peak period $T_p$ and significant wave height $H_s$, respectively, while the ramp slope $\alpha$ constantly is set to 40°. The parameters used in these primary test series are shown in **Table G.1**.

| Varied parameter | Significant wave height | Wave peak period | Crest freeboard |
|---|---|---|---|
| $H_s$ varied 1 | 0,034 m – 0,110 m | 0,97 s | 0,060 m |
| $H_s$ varied 2 | 0,023 m – 0,115 m | 0,97 s | 0,025 m |
| $R_c$ varied 1 | 0,062 m ± 0,001 m | 0,69 s | 0,013 m – 0,090 m |
| $R_c$ varied 2 | 0,088 m ± 0,001 m | 0,97 s | 0,013 m – 0,090 m |
| $T_p$ varied 1 | 0,054 m ± 0,001 m | 0,55 s – 1,11 s | 0,060 m |
| $T_p$ varied 2 | 0,054 m ± 0,001 m | 0,55 s – 1,11 s | 0,040 m |

***Table G.1:*** *Parameters used in the primary laboratory test series in investigating the different formulas for overtopping. All test series are made for a slope angle of 40°.*

Using the program SYSTAT 7.0 for Windows developed by SPSS Inc., 1997, the coefficients are fitted to the test series by a multiple non-linear regression based on the different overtopping formulas. For evaluating the fits the coefficient of determination $R^2$ from the method of least squares is considered.

The different formulas obtained by the dimensional analysis have been fitted. Values of $R^2$ up to 0,93 are achieved. A good fit is found for:

$$Q = \frac{q}{\sqrt{gH_s^3}} = a \cdot \exp\left(-b \cdot \frac{R_c}{H_s}\right) \qquad (G.3)$$

This formula corresponds to Van der Meer's formula. The fitted overtopping coefficients are $a$ = 0,062 and $b$ = 1,69. The fit is shown in **Figure G.1**, where it is compared to the formula using the original coefficients ($a$ = 0,2 and $b$ = 2,6).

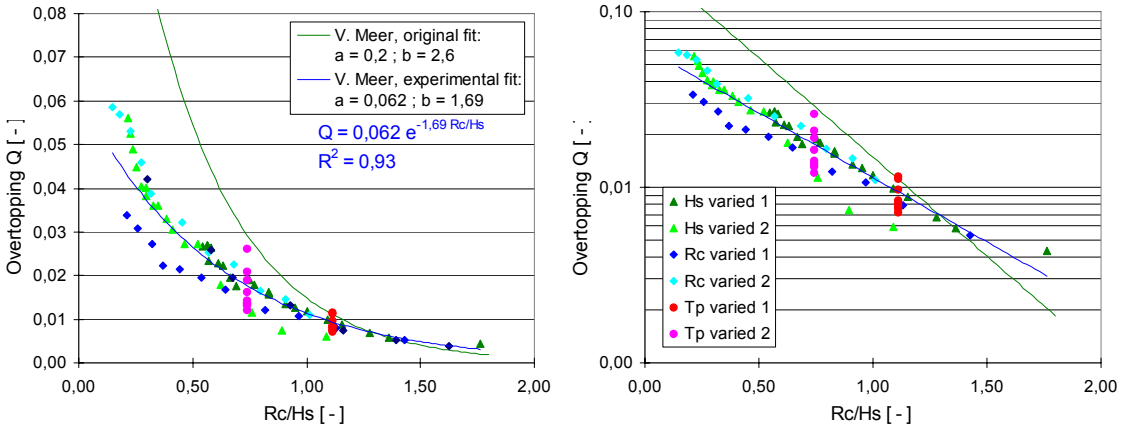


***Figure G.1:*** *Dimensionless overtopping $Q$ as a function of crest freeboard over significant wave height $R_c/H_s$. The graph to the left has linear axis while the graph to the right has a logarithmic y-axis. The parameters for the test series are shown in* ***Table G.1****. The blue line is the exponential trendline with the best fit to the points. The overtopping coefficients are $a$ = 0,062 and $b$ = 1,69. The green lines are overtopping using the coefficients $a$ = 0,2 and $b$ = 2,6 (Van der Meer, original fit). $R^2$ is the coefficient of determination from the method of least squares.*

It is concluded that Van der Meer's formula with the overtopping coefficients determined from the laboratory tests predicts the overtopping discharge with some inaccuracy. Moreover it seems like the wave peak period is in fact a dependent parameter. The reason that Van der Meer's formula does not apply precisely to the model tests is probably due to the fact that the formula is developed for a mildly sloping dike with little or moderate overtopping.

## *G.1.2 The Van der Meer formula for a fixed $H_s$-$T_p$ relation*

The Van der Meer formula is based on the fact that the significant wave height and the wave peak period are strongly correlated for wind generated waves. The problem with the fit is therefore that the relationship between the significant wave height and the wave peak period is not constant for the applied laboratory tests. This $H_s$-$T_p$ relation is described by the second dimensional parameter in ( G.2 ):

$$T_p \sqrt{\frac{g}{H_s}} \qquad (G.4)$$

The relation ( G.4 ) for the different wave situations in Nissum Bredning is shown in **Table G.2**.

| Wave situation | Dimensionless relation between $H_s$ and $T_p$ | |
|---|---|---|
| | Before focusing by wave reflectors | After focusing by wave reflectors |
| 1 | 14,0 | 10,2 |
| 2 | 12,4 | 9,9 |
| 3 | 10,5 | 8,8 |
| 4 | 10,0 | 8,5 |
| 5 | 10,2 | 8,9 |

***Table G.2:*** *Values of relation between the significant wave height and the wave peak period ( G.4 ) for the 5 wave situations in Nissum Bredning.*

In the North Sea the $H_s$-$T_p$ relation is between 13,8 and 15,7 //DS 449, 1983//.

Considering this, laboratory tests have been made for a constant $H_s$-$T_p$ relation of 8,7 ; 10,2 and 14,7. These values correspond to the test series, $R_c$ varied 1, 2 and 3, which are shown in **Figure G.2** for separate fits of Van der Meer's formula.

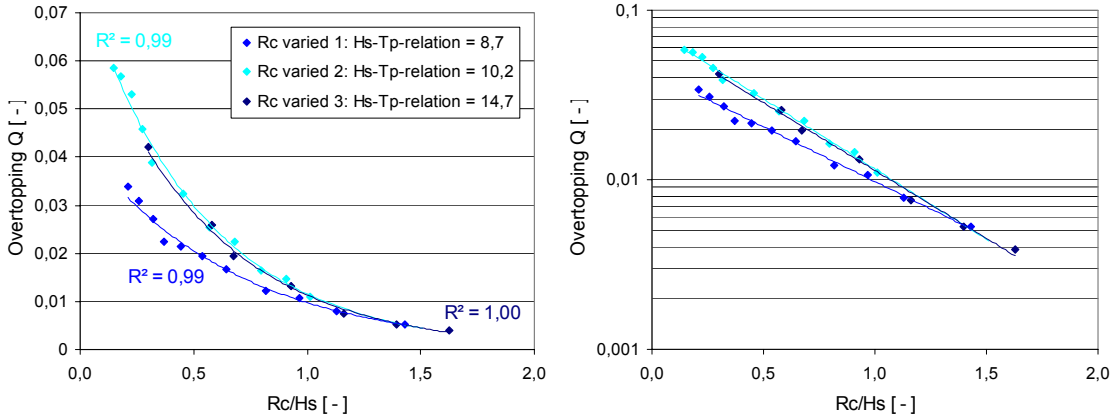


***Figure G.2:*** *Laboratory tests with a constant relationship between the significant wave height and the wave peak period. The graph to the left has linear axis while the graph to the right has a logarithmic y-axis. The parameters for the test series are shown in* ***Table G.1****. The blue lines are the exponential trendlines with the best fit to the points. The test Rc varied 3 have been made for $H_s$ = 0,043 m and $T_p$ = 0,97 m.*

The overtopping coefficients for the 3 test series corresponding to the $H_s$-$T_p$ relations are shown in **Table G.3**.

| | *a* coefficient | *b* coefficient |
|---|---|---|
| $R_c$ varied 1 | 0,043 | 1,49 |
| $R_c$ varied 2 | 0,078 | 1,90 |
| $R_c$ varied 3 | 0,072 | 1,84 |

***Table G.3:*** *Overtopping coefficients in Van der Meer formula for the 3 test series in* ***Figure G.2****.*

Thus for $H_s$-$T_p$ relations of more than 10,2 the overtopping variation is almost constant. For the Wave Dragon in Nissum Bredning the $H_s$-$T_p$ relations corresponding to the focused wave heights are used. The coefficients used in the different wave situations are based on the following test series:

- Wave situation 1 and 2: $R_c$ varied 2.
- Wave situation 3 through 5: $R_c$ varied 1.
- In the North Sea: $R_c$ varied 2.

As the coefficients for the test series $R_c$ varied 2 and 3 are almost identical, it is assumed that $R_c$ varied 2 can be used for all $H_s$-$T_p$ relations of more than 10.

## G.2 Parametric investigation

When performing the laboratory tests it was expected that the two purposes could be incorporated into one complete formula, i.e. a dimensionless and precise formula directly dependent of the crest freeboard, the significant wave height and the wave peak period.

For evaluating the measures to increase overtopping described in appendix *H. Evaluating the design of the ramp profile* it desirable to get a precise description of the overtopping. The Van der Meer formula is very precise in predicting the overtopping for a fixed $H_s$-$T_p$ relation. However, the tests for evaluation of the adjustments of the ramp profile are not performed for a fixed $H_s$-$T_p$ relation.

Using the Van der Meer formula for test series with varied $H_s$-$T_p$ relations result in an insufficient description in terms of accuracy. Instead a parametric investigation is performed in which precision is preferred to dimensionless form.

The influence of the wave peak period $T_p$, the significant wave height $H_s$ and the crest freeboard $R_c$ on the overtopping $q$ is investigated independently. Hereby a design equation for overtopping is established from:

$$q = c_d \cdot f(T_p) \cdot f(H_s) \cdot f(R_c) \qquad (G.5)$$

where

$c_d$ design overtopping coefficient.

### G.2.1 Influence of the wave peak period

Overtopping is found for a variation of the wave peak period, all other parameters being equal. The result is approximated with a linear relationship, which is shown in **Figure G.3**.

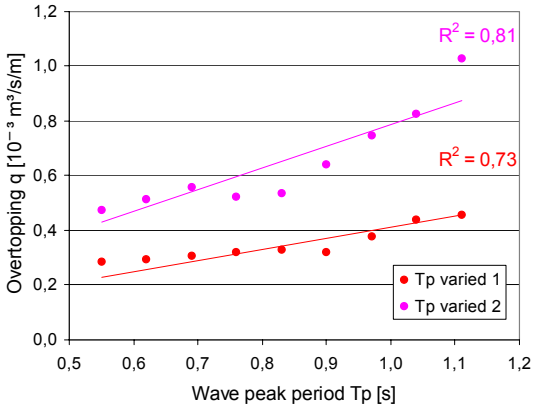


***Figure G.3:*** *Overtopping as a function of wave peak period. The trendlines intercept (0,0). The parameters for the test series are shown in* ***Table G.1****.*

Although the results are not clearly a linear relationship, it will be incorporated in the design equation for overtopping. Thus the function for the wave peak period in ( G.5 ) is:

$$f(T_p) = c_{T_p}(H_s, R_c) \cdot T_p \qquad (G.6)$$

### G.2.2 Influence of the significant wave height

Overtopping is found for a variation of the significant wave height, all other parameters being equal. The result is a rapid increase in overtopping for an increase in significant wave height. A linear relationship is found between the overtopping and the significant wave height raised to the 2,5$^{th}$ power, which is shown in **Figure G.4**.

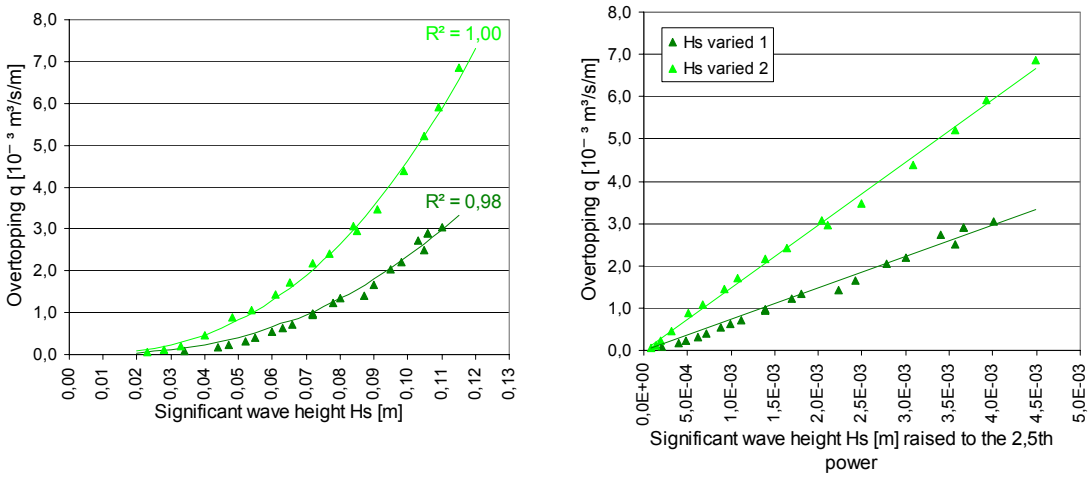


***Figure G.4:*** *Overtopping as a function of the significant wave height. The parameters for the test series are shown in* ***Table G.1****.*

Thus the function for the significant wave height period in ( G.5 ) is:

$$f(H_s) = c_{H_s}(T_p, R_c) \cdot H_s^{2,5} \qquad (G.7)$$

## G.2.3 Influence of crest freeboard

Overtopping is found for a variation of the crest freeboard, all other parameters being equal. The result is a rapid decrease in overtopping for an increase in crest freeboard. A linear relationship is found between the overtopping and the crest freeboard raised to the -1,5$^{th}$ shifted power (i.e. added a constant factor), which is shown in **Figure G.5**.

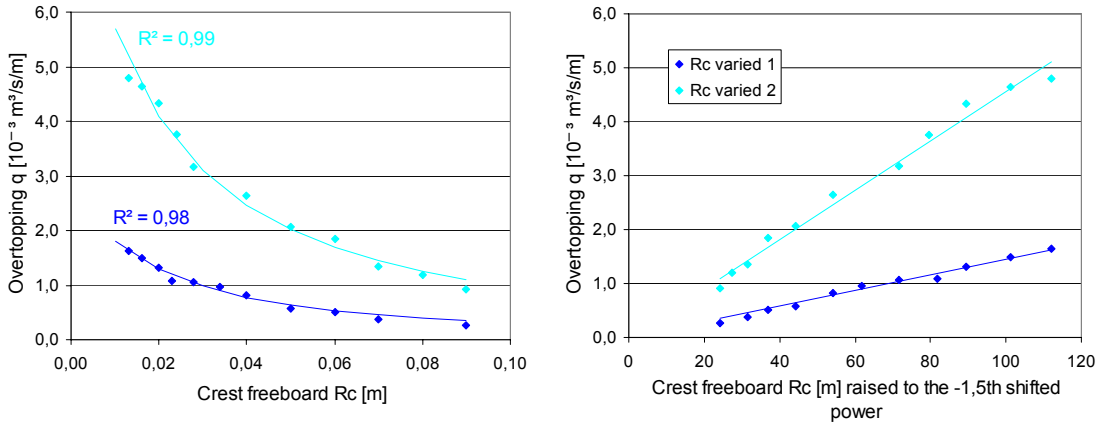


***Figure G.5:*** *Overtopping as a function of the crest freeboard. The parameters for the test series are shown in* ***Table G.1****. The shifted power constant is found to 0,03 m.*

Thus the shifted power function for the crest freeboard in ( G.5 ) is:

$$f(R_c) = c_{R_c}(T_p, H_s) \cdot (R_c + c_s)^{-1,5} \qquad (G.8)$$

where

$c_s$ [m] shifted power constant for $R_c$. Found to 0,03 m.

The consequence of the constant factor is that the overtopping discharge is nonzero for $R_c$ = 0 m, which is in agreement with the stated boundary conditions.

## *G.2.4 Design equation for overtopping discharge*

Using the relationships between overtopping and wave peak period, significant wave height and crest freeboard, respectively, a design equation for overtopping is established. It has the form:

$$q = c_d \cdot g \cdot T_p \cdot H_s^{2,5} \cdot (R_c + c_s)^{-1,5} \qquad (G.9)$$

where

$c_d$ [ - ] design overtopping coefficient. Found to $20 \cdot 10^{-3}$.

$c_s$ [m] shifted power constant for $R_c$. Found to 0,03 m.

Plotting this relationship in a graph gives the result shown in **Figure G.6**.

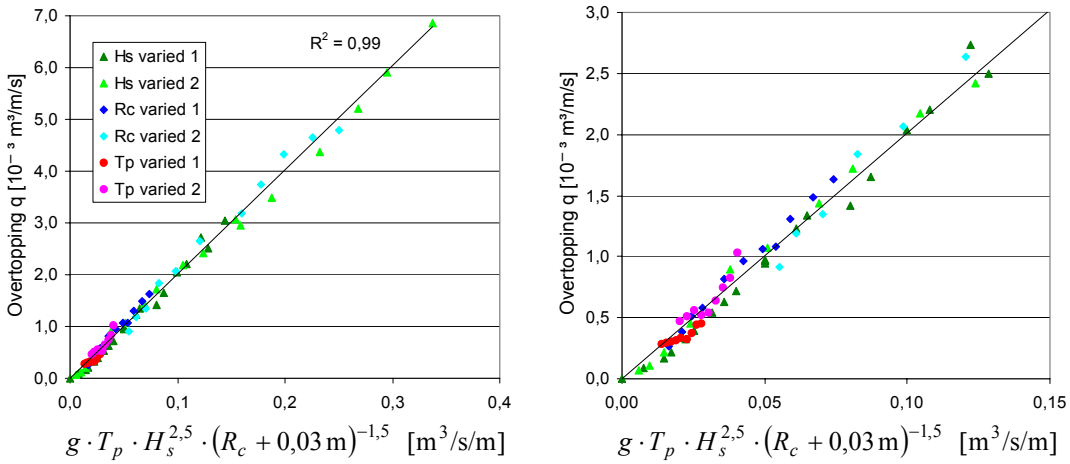


***Figure G.6:*** *Measured overtopping discharges as a function of significant wave height, wave peak period and crest freeboard. The graph to the right is a zoom of the graph to the left. The black line is the best-fitted trendline. In order for ( G.9 ) to be fulfilled the design overtopping coefficient $c_d$ has the value $20 \cdot 10^{-3}$ m. The parameters for the test series are shown in* ***Table G.1****.*

The obtained design equation ( G.9 ) is seen to fit the experimental data significantly better than Van der Meer's formula with a varied $H_s$-$T_p$ relation. Unfortunately the design equation includes a non-dimensionless coefficient $c_s$. This entails that it can not be used in other scales. However it suitable for evaluating the adjustments of the ramp profile (cf. appendix *H. Evaluating the design of the ramp profile*).

# H. Evaluating the design of the ramp profile

To increase overtopping 4 different profiles with curvature have been tested. One of the profiles is the one proposed by EFM. The profiles are shown in **Figure H.1**.

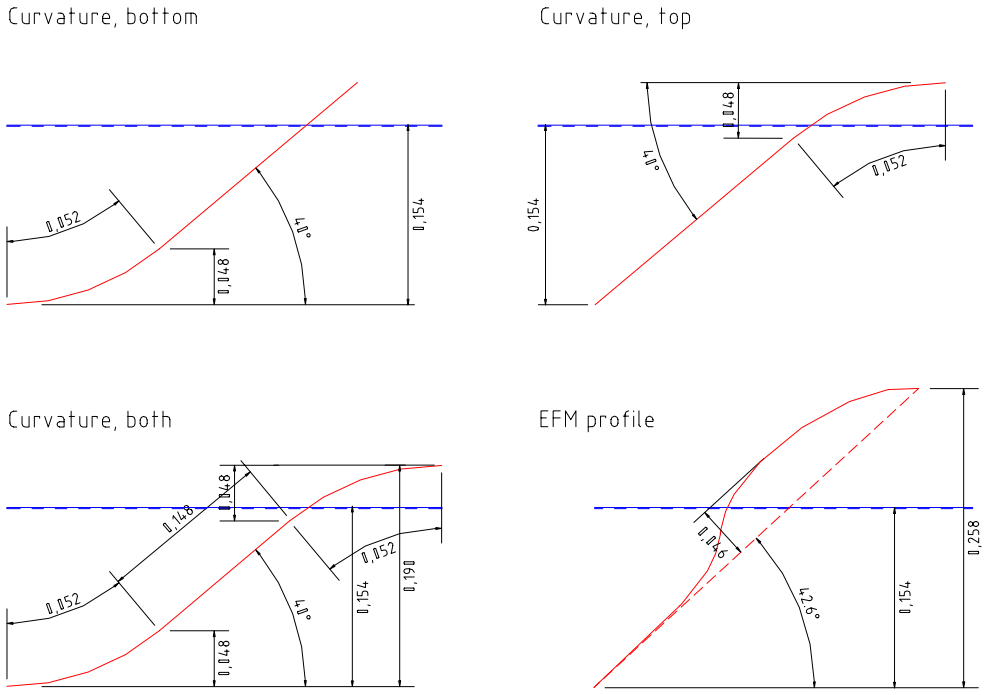


***Figure H.1:*** *Cross section sketch of the profiles with curvature used in the experimental tests. All measures are in m.*

The double curved profiles shown in **Figure H.1** must be placed as shown in the sketch while the other profiles can be used for different values of the crest freeboard.

## H.1 Evaluation of measures to increase overtopping

First the influence of the slope angle is investigated. Then an evaluation is made to clarify whether curvature of the ramp will increase the obtained overtopping.

### *H.1.1 Influence of the slope angle*

Overtopping is found for a variation of the crest freeboard and slope angle. The wave parameters used in the tests are shown in **Table H.1**.

| Slope angle | Significant wave height | Wave peak period | Crest freeboard |
|---|---|---|---|
| 35° | 0,041 – 0,087 m | 0,97 s | 0,044 m |
| 45° | 0,042 – 0,100 m | 0,97 s | 0,067 m |
| 50° | 0,053 – 0,113 m | 0,97 s | 0,096 m |
| 60° | 0,062 – 0,114 m | 0,97 s | 0,118 m |

***Table H.1:*** *Parameters used in the investigation of the slope angle.*

The previous test series are all made for a slope angle of 40°. The result is shown in **Figure H.2**.

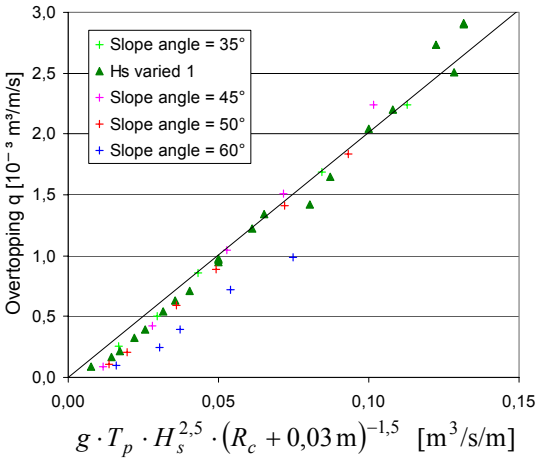


***Figure H.2:*** *Measured overtopping discharges for slope angles from 35 to 60°. Notice that the graph is a zoom corresponding to the graph to the right of* ***Figure G.6****. The black line is the trendline from this figure. The test $H_s$ varied 1 is used as reference because it has a slope angle of 40°.*

For slope angles between 35 and 50° the overtopping discharge is not significantly changed. The overtopping discharge is reduced for angles of 60°. This is due to the fact that the ramp is turning more and more into a vertical wall.

## *H.1.2 Influence of the curvature*

Overtopping is found for ramps with curvature either at the bottom, the top or both. The wave parameters used in the tests are shown in **Table G.2**.

| Profile | Significant wave height | Wave peak period | Crest freeboard |
|---|---|---|---|
| Curvature, bottom | 0,034 – 0,079 m | 0,97 s | 0,036 m |
| Curvature, top | 0,033 – 0,080 m | 0,97 s | 0,042 m |
| Curvature, both | 0,045 – 0,090 m | 0,97 s | 0,036 m |

***Table G.2:*** *Parameters used in the investigation of the curvature.*

Sketches of the profiles are shown in **Figure H.1**. The results are shown in **Figure H.3**.

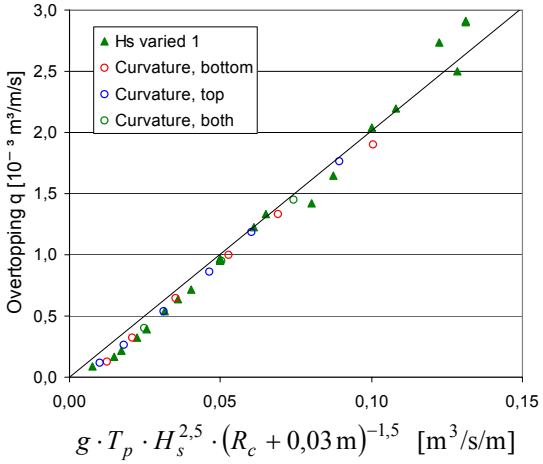


***Figure H.3:*** *Measured overtopping discharges for ramps with curvature either at the bottom, the top or both. Notice that the graph is a zoom corresponding to the graph to the right of* ***Figure G.6****. The black line is the trendline from this figure. The test $H_s$ varied 1 is used as reference because it has a straight profile.*

From the tests it is seen that changing the curvature has no effect, taking the uncertainties of the primary tests into consideration. For the profile curved at the bottom and top the tendency has been verified for a crest freeboard of 0,054 and 0,061 m, respectively all other parameters being equal.

## H.2 Evaluation of the design proposed by EFM

The profile proposed by EFM is evaluated. A sketch of the profile is shown in **Figure H.1**. The wave parameters used in the tests are shown in **Table H.3**.

| Profile | Significant wave height | Wave peak period | Crest freeboard |
|---|---|---|---|
| EFM profile 1 | 0,066 – 0,119 m | 0,97 s | 0,104 m |
| EFM profile 2 | 0,065 ± 0,001 m | 0,69 s | 0,037 – 0,100 m |

***Table H.3:*** *Parameters used in the investigation of the EFM profile.*

The result is shown in **Figure H.4**.

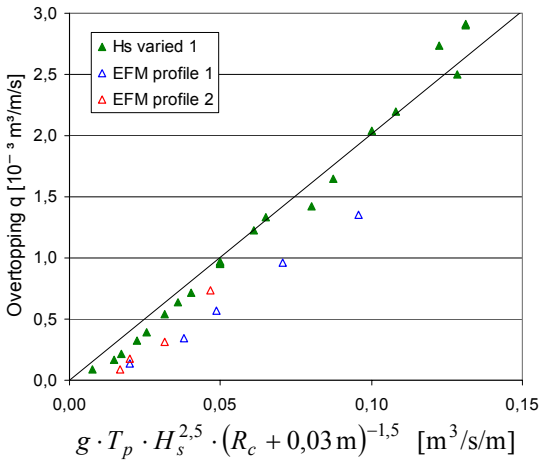


***Figure H.4:*** *Measured overtopping discharges for the profile proposed by EFM. Notice that the graph is a zoom corresponding to the graph to the right of* ***Figure G.6****. The black line is the trendline from this figure. The test $H_s$ varied 1 is used as reference because it has a straight profile.*

It is significant that the proposed profile is less effective than a straight. The problem is probably that the profile has a too steep slope angle at the middle section.

# I. Photos from the laboratory tests

## I.1 Photos of the wave reflectors

***Figure I.1:*** *Partial Mach effect present by the wave reflectors.*

***Figure I.2:*** *Diffraction around the ends of the wave reflectors are present at the exit line.*

***Figure I.3:*** *Waves reflected on the part of the wave reflectors nearest to the exit line is travelling perpendicular to the general wave propagation direction across the exit.*

***Figure I.4:*** *Overtopping of the wave reflectors occurring for a large wave situation.*

## I.2 Photos of the composite system

***Figure I.5:*** *Partial Mach effect present by the wave reflectors in a wave situation with small waves.*

***Figure I.6:*** *Full Mach effect occurring for a wave situation with large waves.*

***Figure I.7:*** *Full Mach effect by the ramp in a wave situation with large waves.*

***Figure I.8:*** *Overtopping of the wave reflectors in a wave situation with large waves.*